DESKTOP COMPUTER PROGRAMS FOR PRELIMINARY DESIGN OF TRANSONIC COMPRESSOR ROTORS

THESIS

Brian C. McDonald, Captain, USAF

AFIT/GAE/ENY/01M-06

DEPARTMENT OF THE AIR FORCE
AIR UNIVERSITY

AIR FORCE INSTITUTE OF TECHNOLOGY

Wright-Patterson Air Force Base, Ohio

The views expressed in this thesis are those of the author and do not reflect the official policy or position of the United States Air Force, Department of Defense, or the United States Government.

AFIT/GAE/ENY/01M-06

DESKTOP COMPUTER PROGRAMS FOR PRELIMINARY DESIGN OF TRANSONIC COMPRESSOR ROTORS

THESIS

Presented to the Faculty

Department of Aeronautical and Astronautical Engineering

Graduate School of Engineering and Management

Air Force Institute of Technology

Air University

Air Education and Training Command

In Partial Fulfillment of the Requirements for the

Degree of Master of Science in Aeronautical Engineering

Brian C. McDonald, B.S.

Captain, USAF

March 2001

AFIT/GAE/ENY/01M-06

DESKTOP COMPUTER PROGRAMS FOR PRELIMINARY DESIGN OF TRANSONIC COMPRESSOR ROTORS

Brian C. McDonald, B.S.

Captain, USAF

Approved:

Paul I. King	7 Mar 01
Dr. Paul I. King Committe Chairman	Date
William C. Elrod	8 Mar 2001
Dr. William C. Elrod Committee Member	Date
Montgomery C. Hughson	7 Mar '01
Maj Montgomery C. Hughson Committee Member	Date
J. Mitch Wolff	9 Mar 2001
Dr. J. Mitch Wolff Committee Member	Date

Acknowledgements

I would like to express my sincere appreciation to the individuals who assisted me in completing this thesis. I would like to thank my advisor, Dr. Paul King, whose guidance kept me from stumbling over the hurdles I encountered. I am indebted to Dr. Albin Bölcs who wrote the original source codes of the programs I worked with in this research effort. His willingness to fly from Switzerland to personally introduce his programs to me and answer my questions over e-mail were tremendous acts of kindness. I am also grateful to Mr. Dave Car who provided the TESCOM blade geometry files and the APNASA solutions that I used as benchmarks.

My very understanding wife deserves a medal for enduring the neglect she received while I labored through this process. Her love and support gave me strength. To her, I express my deepest admiration and love.

Brian C. McDonald

Table of Contents

Page

Page

List of Figures

List of Tables

List of Symbols

English Symbols

Symbol	Definition (units)
A	Flow path cross-sectional area (m^2)
A_a	Annulus area (m^2)
a	Speed of sound (m/s)
B	Flow path height (mm)
b	Streamtube thickness (mm); correction for varying inlet flow angle in deviation relation, Eq. (32)
C	Absolute velocity (m/s)
C_p	Specific heat (J/kg K)
c	Diffusion factor-based constant in K factor equation, Eq. (52)
c_m	Coefficient in subsonic off-design total loss correlation, Eq. (38)
D	Diffusion factor
D_{eq}	Equivalent diffusion factor
d	Diameter of blade maximum thickness circle (mm); diffusion factor-based constant in K factor equation, Eq. (52)
e	Shock standoff distance from blade leading edge (mm)
f	Perpendicular distance between L and the midpoint of d (mm)
h	Enthalpy (J/kg)
i	Incidence angle (deg)
j	Stagnation streamline shift near blade leading edge (mm)
K	Parabolic factor for differences in wake-momentum thickness, Eq. (51)
K_i	Correction factor in incidence angle relation, Eq. (24)
K_δ	Correction factor in deviation angle relation, Eq. (32)
L	Blade chord length (mm)
M	Mach number
M_{ref}	Blade-reference-Mach number in K factor equation, Eq. (52)
$m_{\sigma=1}$	Rate of change of deviation angle with camber angle for $\sigma = 1.0$

N	Number of blades
n	Spool rotation rate (rpm)
n	Slope factor in incidence angle relation, Eq. (24)
P	Pressure (bar)
P_{corr}	Correction factor for static pressure rise across normal shock, Eq. (57)
R	Radial height from engine centerline (mm); gas constant (J/kg K)
r	Radius (m)
s	Blade spacing (mm)
T	Temperature (K)
U	Blade speed (m/s)
u	Velocity in x-direction (m/s)
v	Velocity in y-direction (m/s)
W	Relative velocity (m/s)
w	Flow velocity (m/s)
w_{Seff}	Effective height of blade suction surface (mm), Fig. 7
X_d	Location of maximum thickness along blade chord (mm)
Z	Axial distance between station and geometric center of rotor blade (mm)

Greek Symbols

Symbol	Definition (units)
α	Angle of absolute flow from axial direction (deg)
β	Angle of relative flow from axial direction (deg or rad)
β_g	Blade stagger angle (deg)
β_m	Angle between mean camber line at blade edge and axial direction (deg)
β_{PS}	Angle between tangent to blade pressure surface at trailing edge and axial direction (deg)
Γ	Blade circulation parameter, Eq. (27)
γ	Ratio of specific heats
δ	Deviation angle (deg)
ϵ	Flow turning angle (deg)

κ	Ratio of specific heats
η	Right-running characteristic; efficiency
λ	Constant along characteristic line
μ	Constant along characteristic line
π	3.14159...
φ	Blade camber angle (deg)
Θ_*	Prandtl-Meyer expansion angle (deg)
θ	Flow deflection angle (deg); wake momentum thickness (mm)
ρ	Density (kg/m^3)
σ	Mach angle (deg); solidity - ratio of chord to spacing
ξ	Left-running characteristic
Ω	Streamtube contraction ratio
ω	Loss coefficient

Superscripts

Symbol	Definition
$( )^*$	On-design condition
$\overline{( )}$	Mean value
$\hat{( )}$	Downstream of passage shock

Subscripts

Symbol	Definition
1	Flow path station upstream of inlet guide vane
2	Flow path station between inlet guide vane and rotor
3	Flow path station downstream of rotor
c	Absolute frame; stagnation condition
e	Casing
F	Position of normal shock at entrance to blade passage
i	Hub
inc	Incompressible

is	Isentropic
J	Position of normal shock near exit of blade passage
max	Maximum
n	Axial component
p	Blade passage throat region
u	Tangential component
w	Relative frame; stagnation condition

List of Abbreviations

Abbreviation	Definition
2D	Two-Dimensional
3D	Three-Dimensional
AFB	Air Force Base
AR	Aspect Ratio
ASME	American Society of Mechanical Engineers
CFD	Computational Fluid Dynamics
CPU	Central Processing Unit
DCA	Double Circular Arc
DP	Design Point
IGV	Inlet Guide Vane
LE	Leading Edge
MCA	Multiple Circular Arc
MOC	Method-of-Characteristics
NACA	National Advisory Committee for Aeronautics
NASA	National Aeronautics and Space Administration
PC	Personal Computer
PS	Pressure Surface
Q3D	Quasi-Three-Dimensional
SS	Suction Surface
TE	Trailing Edge
TESCOM	Three-Stage Compressor

Abstract

A need exists in the field of turbomachinery for correlation-based desktop computer programs that predict the flow through transonic compressor rotors with nominal computational time and cost. In this research, modified versions of two desktop computer programs, intended for preliminary transonic compressor rotor design, BOWSHOCK and TRANSROTOR, were used to perform a parametric study on a modern compressor rotor. BOWSHOCK uses a method-of-characteristics approach to calculate exit flow properties of a supersonic streamtube through a user-defined compressor rotor. TRANSROTOR calculates flow properties at three stations in a user-defined compressor stage.

Modifications to TRANSROTOR included the incorporation of a recently published rotor loss model, advertised as suitable for analyzing modern blading concepts. The baseline and modified TRANSROTOR versions were run with two modern transonic compressor blades. Results were compared with results from a Navier-Stokes-based computational fluid dynamics (CFD) code, APNASA. A parametric study using BOWSHOCK examined the sensitivity of rotor efficiency and pressure ratio to variations in six blade parameters.

Both TRANSROTOR versions predicted rotor efficiency and pressure ratios within ten-percent of the CFD results. The baseline version predicted total pressure ratio more accurately. Computational times were under six minutes for a single 450 MHz processor. The results of the blade geometry parametric study showed that isentropic efficiency was most sensitive to stagger angle and least sensitive to blade spacing. Total pressure ratio was most sensitive to blade maximum thickness location and least sensitive to blade maximum thickness.

DESKTOP COMPUTER PROGRAMS FOR PRELIMINARY DESIGN OF TRANSONIC COMPRESSOR ROTORS

I. Introduction

1.1 Transonic Compressors

The ever-present demand for higher thrust-to-weight ratio gas turbine engines with improved fuel economy has resulted in much research being devoted to the improvement of transonic rotors in axial compressors. As used in this thesis, a transonic rotor is characterized by regions of both subsonic and supersonic relative inlet flow along the span of the blades. A compressor that contains one or more of these types of rotors is considered a transonic compressor. The use of transonic rotors within a compressor reduces the size of the compressor without a corresponding reduction in the overall pressure ratio - an ideal quality for high thrust-to-weight engines [1:1/3]. For a given level of thrust, a transonic compressor reduces fuel consumption compared to a completely subsonic compressor [2:1]. High efficiencies are achieved by mitigating the loss of stagnation pressure caused by the shock system with low supersonic relative speeds. These favorable characteristics have made transonic compressors the choice of aircraft engine designers since about 1960 [3:379].

The fluid dynamic principle upon which transonic rotors are based is that a high static pressure rise is realized when flow passes through a normal or oblique shock. Attempting to fully exploit this principle, researchers and designers have investigated compressor stages with supersonic relative inlet flow along the entire blade span. The large losses and limited range of operation associated with this type of compressor make it impractical for application in aircraft gas turbine engines. Therefore, it was concluded that the combination of high static pressure ratios from supersonic flow and flow adjustment from subsonic flow was complementary [3:379]. This is one reason why highly supersonic flow with supersonic axial velocities is generally avoided - the compressor cannot influence the upstream flow [4:194]. Additionally, compressible flow theory relating to shock waves indicates that as

the inlet flow Mach number proceeds beyond Mach 1.0, the total pressure drop across a shock becomes unacceptably large for the corresponding rise in static pressure [5:109].

The shock system of a transonic rotor is a result of blade tangential velocities greater than the local speed of sound. Since the speed of sound is a function of temperature and each stage of a compressor increases the flow temperature, most compressors only have transonic flow in the first stage. Later stages can be transonic as well if the upstream stage temperature rise is moderate and/or the blade speed is high. Generally, the hub region remains subsonic while the flow over the blade tip is in the low supersonic range. Modern transonic compressors and fans can have relative Mach numbers at the blade tip exceeding 1.6 with corresponding axial Mach numbers around 0.7 [3:379]. The maximum relative Mach number for a given compressor is typically determined by the competing design constraints of high efficiency and high pressure ratio [4:48]. Structural concerns can also arise when blade speeds become excessive.

The general shock system originates at the leading edges of the blades and consists of a passage shock and a bow shock. The passage shock intersects the suction surface (SS) of the adjacent blade. The bow shock propagates upstream from the blade leading edge (LE). The particular shock pattern that is developed by a transonic rotor is influenced by many parameters, the most significant being blade geometry, inlet Mach number, inlet flow angle, and backpressure behind the blade row [4:197]. The typical geometrical attributes of blades found in transonic compressors are discussed at length in the next section of this chapter. Clearly, the Mach number of the incoming flow has a profound influence on the shock pattern within a rotor since shock properties are a function of Mach number. The inlet flow angle determines, in part, how the rotor receives the incoming flow according to the inlet velocity diagram. The angle of the shock wave propagating from the blade LE is then specified by the θ-β-M relation of compressible flow theory. Related to this, the obliquity of the shocks is also a function of the backpressure within the stage. At low backpressures, the shocks are oblique and nearly attached to the blade LE. At high backpressures, the passage shock can be normal to the flow and appear as an extension of the bow shock, which stands off some distance from the blade LE. In reality, under no circumstances can the shock wave be attached since there is always a finite leading edge

radius; however, modeling the shock wave as attached is a good approximation for some calculations.

At the microscopic level, all losses can be attributed to viscous dissipation. It is sometimes more practical to consider losses in a macroscopic sense and examine discrete mechanisms that are present in transonic compressors. A proposed list of loss mechanisms includes blade profile drag, flow mixing, and shock waves [4:21-28]. Quantification of the total pressure loss incurred by the first two of these loss mechanisms is the subject of many correlations. A selection of these correlations is discussed in this thesis. The passage shock, which produces the desired static pressure rise, is responsible for the majority of the shock losses through the rotor. Numerous factors determine which loss mechanism is of greatest concern.

A far greater source of total pressure loss than any of these individual loss mechanisms is shock induced boundary layer separation. The location where the passage shock impinges on the suction side of the rotor blade is the primary site where a shock- boundary layer interaction occurs within a transonic rotor. When the boundary layer encounters the passage shock, it must negotiate the large, nearly instantaneous pressure gradient caused by the shock. In order to minimize losses, the boundary layer must remain attached to the blade surface despite this adverse pressure gradient. A Mach number of approximately 1.3 prior to the passage shock is generally accepted as the critical Mach number beyond which the boundary layer separates from the surface. Another location that has been identified as a large source of loss is the end wall region where the blade tip passes by the compressor casing. Many researchers assert that this is the primary source of pressure loss in axial compressors [4:58; 5:117]. The flow in this region is particularly complex due to the clearance between blade tip and casing which generates vortices. In this region, it is possible to have the combined effects of all three types of loss mechanisms. The exact flow phenomena that occur in this complex flow region are currently the subject of much research.

1.2 *Transonic Compressor Blading*

The preponderance of blade designs used in axial compressors can be grouped into four general types - double circular arc (DCA), multiple circular arc (MCA), pre-compression, and controlled diffusion. The suction and pressure surfaces of DCA-profile blades are each described by a single circular arc. DCA-profile blading is the simplest and oldest type of compressor blade design and is usually used in subsonic flows.

A more versatile version of the DCA-profile blading is the MCA-profile blading. It uses two circular arcs to describe each of the two surfaces. The defining parameters for this type of blading are chord length (L), location of maximum thickness along the chord (X_d), diameter of maximum thickness circle (d), and perpendicular distance between the blade chord and the center of the maximum thickness circle (f). Figure 1 shows the nomenclature used to define MCA-profile blades. The blade LE is on the left of Figure 1. Four circular arcs, two each from the leading and trailing edges of the chord, are drawn tangent to the maximum thickness circle to construct an MCA-profile blade.

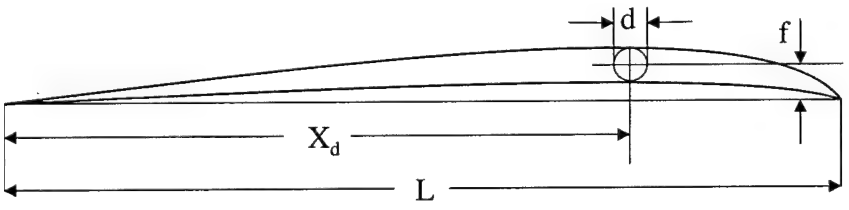

Figure 1 Geometrical Description of the Four Parameters that Define MCA- and S-profile Blades

Pre-compression blades, also called negative camber blades but referred to hereafter as S-profile blades, are a slight modification to the MCA-profile blade design. Instead of describing the portion of the suction surface that is forward of the blade maximum thickness with a circular arc, S-profile blades use a sine function. The purpose of this type of shaping is to generate a series of very weak compression waves. In this way, the Mach number of the flow between the blade LE and the passage shock is gradually reduced to lower the risk of flow separation after the shock [4:48].

Controlled diffusion blading is the most advanced and most recent type of compressor blade design. As the name implies, the surfaces of these blades are specifically designed to achieve a certain distribution of flow properties through the rotor. Computational fluid dynamics (CFD) computer codes based on a finite difference or an inverse method are used to design controlled diffusion blades for very specific applications. These two design methods are beyond the scope of this thesis.

There are certain blade characteristics that are generally regarded as beneficial to achieving compression in the transonic regime. First, a high solidity (σ), the ratio of chord length to spacing, is desirable because it helps the flow to reattach to the blade surface if separation occurs upstream. Second, a low aspect ratio (AR), the ratio of blade height to chord, is desirable. Third, a longer blade chord is beneficial because it improves both solidity and aspect ratio. A rotor with these characteristics is capable of producing a higher pressure ratio and efficiency per stage for the same blade speed than a rotor that does not have these attributes [5:211]. In addition, a high stagger angle (β_g) is typically found in transonic blading. Stagger angle is defined as the angle between the blade chord and the axial direction. Stagger angle is very influential in determining the outlet flow direction. Blade rows with high stagger angles blunt the effects of stall and exhibit better recovery characteristics than blade rows with low stagger angles. Stagger angle is particularly important when supersonic flows are involved because of the direct effect on passage area, and therefore on maximum mass flow rate [4:2]. Lastly, transonic compressor blades tend to have a small amount of camber (φ) overall, most of which is located behind the point where the passage shock impinges on the blade suction surface. Typically, the camber of the forward section of the blade is approximately two-percent of the chord length. The purpose of a low camber LE is to reduce the strength of the passage shock and lower the risk of a shock induced boundary-layer separation [6:81]. If the forward section is strongly curved, the supersonic flow accelerates through Prandtl-Meyer expansions resulting in a higher Mach number at the passage shock.

The Aero Propulsion Laboratory at Wright-Patterson Air Force Base, Ohio designed transonic compressor blades possessing these characteristics in the early 1980s as part of the Three-Stage Compressor (TESCOM) program. This program began as a preliminary

design study of a multi-stage compressor for an advanced turbofan engine. One of the objectives of the TESCOM program was to further the then-current state-of-the-art in axial compressor design [7:1]. Over the 20 years that the TESCOM program has been in existence, experimental and computational research on various generations of blades has been conducted [8]. The design of the TESCOM blades was accomplished using the UDO300M computer program. This program utilized a streamline curvature method of solution to solve the system of equations. Law provides a detailed description of the UDO300M axial compressor design program [9].

Two blade geometries from the second stage rotor of the TESCOM were selected to validate both versions of one of the desktop computer programs addressed in this thesis, TRANSROTOR. The two selected blades included a baseline design, which is referred to as the original blade geometry, and one modified geometry, which is referred to as the TM1 blade geometry. The TM1 design was given more throat margin than the original blade design in an attempt to improve rotor performance [8]. Both of these blades were descendants of the blades developed in the early years of the TESCOM program. Table 1 is a comparison of the key geometrical attributes of the two blades. Eleven streamline-

Table 1 Comparison of Original and TM1 TESCOM Compressor Blades

Blade Designation	σ	AR	L (mm)	d Hub (mm)	d Tip (mm)	φ Hub (deg)	φ Tip (deg)	β_g Hub (deg)	β_g Tip (deg)
Original	3.31	0.55	45.9	2.52	1.78	38.9	24.9	33.5	44.6
TM1	3.27	0.55	45.5	2.38	1.90	38.2	25.7	27.8	48.2

Note: The values given for σ, AR, and L are averages along the span of the blade.

defined profiles, taken at intervals along the span of each blade, were used to calculate the values shown in Table 1. The immediate availability of the blade geometry definition files and the current interest of the Compressor Aero Research Laboratory in the TESCOM program contributed to the selection of these transonic compressor blades.

1.3 Transonic Rotor Analysis Programs

A multitude of blade geometry parameters have a significant impact on compressor performance. Exhaustive parametric studies during the preliminary design phase of a

transonic rotor are extremely valuable. Despite the rapidly improving computing speed and memory of desktop computers, most computer programs designed to analyze rotating turbomachinery components run on less common, more expensive computing platforms. Additionally, overall computational time and money has not become the type of minor issue that might be expected as a result of such a competitive computer industry. This trend can be explained, for the most part, by the concurrent increase in the sophistication of CFD programs and other programs designed to analyze rotating turbomachinery. A need exists for correlation-based desktop computer programs, intended for the preliminary phase of air-breathing engine design, that provide approximate solutions in minutes for a nominal cost. The solutions from these types of programs could complement the more sophisticated programs.

This research effort focused on two computer programs, written specifically for use on desktop-based platforms, that were designed to determine the quasi-three dimensional (Q3D) flow through a transonic rotor. The titles of these computer programs were BOWSHOCK and TRANSROTOR. The source code of both programs was purchased so that they could be modified. A third computer program, INCIDUNIQUE, was also purchased. INCIDUNIQUE, a sister program to BOWSHOCK, analyzed a specific flow scenario. Since BOWSHOCK was designed to analyze the flow scenarios predominantly encountered in this research, INCIDUNIQUE was extraneous. However, discussions of INCIDUNIQUE were included in Appendix A for readers who may be interested in its capabilities.

Dr. Albin Bölcs of *École Polytechnique Fédérale de Lausanne* in Switzerland authored the original source code of these programs. The original BOWSHOCK and TRANSROTOR source codes were modified to accomplish the objectives of this thesis. The *FutureBASIC II*® programming language for *Macintosh*® computers was used to write the code. Due to the mixture of nationalities represented in the final versions of these programs, the source codes consist of English and German subroutine names, variable names, and comments. However, all screens displayed during program execution are in English.

All three programs use the method-of-characteristics (MOC) to determine the flow properties in the supersonic region at the entrance to a user-defined transonic rotor. Select correlations from the open literature determine total pressure losses. The intended use

of these theoretical and empirical programs is for preliminary examinations of prospective compressor blade geometries. The high computational speed of these limited scope, desktop computer-based analysis routines makes them well suited for blade geometry parametric studies and quick design.

BOWSHOCK is a blade-to-blade calculation of a single streamtube. The calculation is made Q3D by a user-defined streamtube contraction. Since a detached bow shock is assumed, the relative inlet Mach number must be supersonic. TRANSROTOR utilizes both blade-to-blade and throughflow calculations iteratively to automatically compute the development of up to seven streamtubes through one compressor stage. It can support fully subsonic conditions, transonic conditions, or fully supersonic conditions along the span of the rotor blade. TRANSROTOR can be run with or without an inlet guide vane (IGV) upstream of the rotor. Two different loss models were incorporated into TRANSROTOR, both were a collection of loss correlations available in the open literature. Only one version of BOWSHOCK was necessary to conduct a general blade geometry parametric study. Therefore, it was coded with one of the two validated TRANSROTOR loss models.

Having introduced the principles of transonic compressors, general transonic and TESCOM-specific blading characteristics, and the computer programs that are the primary focus of this research, the goal and objectives of this thesis can be stated.

1.4 Thesis Objectives

The goal of this thesis was to evaluate and enhance the utility of BOWSHOCK and TRANSROTOR for use in preliminary transonic rotor design. This goal was achieved after completion of four supporting objectives: algorithm documentation, alternate loss model incorporation, TRANSROTOR validation, and capability demonstration through a blade geometry parametric study using BOWSHOCK.

This research effort began by augmenting the limited documentation (Bölcs[10; 11; 12]) that accompanied the three original programs with a subroutine listing and flow diagrams of each program. A focused literature review was conducted so that a first-hand discussion of the theoretical concepts and the parameter correlations used in the programs

could be given. This information was necessary to facilitate the use and/or modification of these programs. An alternate loss model was selected from the open literature and incorporated into the original TRANSROTOR algorithm. Subsequently, the validity of both versions of TRANSROTOR was evaluated by comparing TESCOM solutions with a widely used, Navier-Stokes-based CFD program, APNASA. Finally, BOWSHOCK was used to conduct a blade geometry parametric study of an MCA-profile approximation of the TESCOM TM1 compressor blade.

1.5 Thesis Overview

This chapter introduced the topics of transonic compressors and transonic compressor blading and gave a general description of the two computer programs that were used to analyze transonic rotors. Chapter II contains in-depth discussions of select theoretical concepts distilled from the literature review. These discussions focus on calculations found in the codes. Important equations, which are not part of the loss models, are derived in Chapter II. Chapter III has two sections devoted to summarizing the capabilities, interfaces, and calculation sequence of BOWSHOCK and TRANSROTOR. Chapter IV is a summary of the research methodology - how the four thesis objectives were completed and why certain approaches were used. Chapter V presents a summary of the two different loss models incorporated into TRANSROTOR. The compilations of correlations that constitute these loss models are reviewed in detail. Chapter VI presents the results and analyses of the TRANSROTOR validation and BOWSHOCK capability demonstration objectives. Chapter VII contains the conclusions and recommendations that emerged from this research effort. The potential uses and further development areas of these computer programs are also discussed.

II. Theoretical Concepts

2.1 Through-Flow Calculation Method

The through-flow calculation method of an axial-flow compressor is based upon a meridional perspective of the flow as it passes through blade rows. Figure 4 of Chapter III is an example of a compressor stage as viewed using this perspective. This calculation method allows the spanwise distribution of flow properties to be determined at computing stations placed in the direction of the axis of rotation. For example, TRANSROTOR has three computing stations - station 1 is upstream of the IGV, station 2 is between the IGV and the rotor, and station 3 is downstream of the rotor. Through-flow calculations are usually characterized by multiple control surfaces drawn parallel to the flow path such that the span of the flow path is divided into several streamtubes. TRANSROTOR allows the user to divide the flow path into a maximum of seven streamtubes. Some assumptions are made when this approach is taken. First, the relative flow through the rotor is considered steady. Steady flow must be assumed for the path of fluid particles to be described by the streamtubes. Many authors have shown that work input by a compressor is unequivocally an unsteady phenomenon [4:10; 13; 14:8]; however, combining the steady assumption with different frames of reference for stationary and rotating blade rows has worked well for most applications. Second, the flow is assumed to be adiabatic so that there is no exchange of heat between fluid elements or across streamtube boundaries. Third, the flow is assumed to be periodic. This means that the flow properties at a given axial and radial location in a given blade passage are assumed to be the same as those in any other blade passage. With this assumption, the analysis of one representative hub-to-casing flow path can be applied to the entire annulus [15:286]. Although these three assumptions introduce some approximation error to the through-flow calculation method, they greatly simplify the analysis which increases computational speed for desktop computer programs like TRANSROTOR.

Of the many different types of through-flow calculation methods that exist, two types are pertinent to this research - simple radial equilibrium and streamline curvature. Simple radial equilibrium is based upon the fluid dynamic principle that a continuous pressure

gradient must exist in a control surface perpendicular to the axis of rotation. Any radial component of flow velocity in a control surface is assumed negligible. The general equation of simple radial equilibrium can be written as

$$\frac{\partial P}{\partial r} = \frac{\rho C_u^2}{r} \tag{1}$$

where

P = Pressure

r = radius

ρ = density

C_u = tangential component of absolute velocity

Once the static pressure is found at the mean radius of a streamtube, perhaps by an isentropic relationship with the total pressure, Equation (1) can be used to find the static pressure at the upper and lower boundaries of that streamtube. Discontinuities created by a mismatch of pressure at the boundary of adjacent streamtubes must be resolved. The thickness of the individual streamtubes is adjusted until a continuous pressure gradient is established. It is this streamtube contraction that makes a calculation Q3D.

The streamline curvature method uses an iterative process to determine the development of the streamtubes through blade rows. An initial set of streamlines is assumed and, through iteration, the paths of the streamtubes are modified to best satisfy the empirical correlations [15:286]. Projected on a meridional plane, the streamline curvature defines the radial shift of the streamtubes from blade row entrance to exit. The impact of this radial shift on compressor performance should not be underestimated. The equation for the conservation of *rothalpy* can be written as [4:7]

$$h_3 - h_2 = \frac{1}{2}(U_3^2 - U_2^2) + \frac{1}{2}(W_3^2 - W_2^2) \tag{2}$$

where

h = static enthalpy

U = blade speed

W = relative velocity

The term, $1/2(U_3^2 - U_2^2)$, in Equation (2) can be a large contributor to static enthalpy rise, and thus static pressure rise, in compressors that have a pronounced outward radial shift in the streamlines. Additionally, this term is independent of the diffusion of the flow and therefore does not contribute to losses. Axial-flow compressor designers make the most of this opportunity by using a sharply inclined hub line.

The TRANSROTOR computer program contains a combination of the simple radial equilibrium and streamline curvature through-flow calculation methods. The program attempts to establish radial equilibrium at all three stations in the stage using Equation (1). In the process of establishing radial equilibrium, the radial position of each streamline at each station is changed as necessary. For the streamline curvature portion of the calculation, the paths of all streamlines through the rotor are approximated as sine waves. In this way, the radial shift of the streamtubes through the rotor is accounted for. Fixing the shape of the paths as sine waves is a simplification of more sophisticated streamline curvature methods that allow unrestricted development of the streamtubes through the rotor.

2.2 Blade-to-Blade Calculation Method

As the name implies, blade-to-blade calculations are made in relation to the passage between adjacent blades of a rotor. The perspective of this type of calculation is given by straightening an annular cut of the blading at a given radius. The profile of the compressor blade is revealed in the blade-to-blade perspective since it is a cross-sectional view. Figure 2 of Chapter III is an example of a blade passage as viewed in the blade-to-blade perspective. This calculation method is used to determine flow properties that are a result of the blades interacting with the flow such as flow deflection, diffusion losses, and shock losses. Loss correlations usually draw upon blade properties such as stagger, solidity, chord, and camber, all of which are associated with the blade-to-blade perspective. The mass flow capacity of the blade row is an important quantity that is typically obtained from blade-to-blade calculations [4:218]. In most theoretical routines, information gained from blade-to-blade calculations made at multiple radial locations is passed on to through-flow calculations for synthesis. TRANSROTOR uses this sequence of calculations to progress toward a solu-

tion. Both BOWSHOCK and INCIDUNIQUE are only blade-to-blade calculations since they analyze the flow within one predefined streamtube.

2.2.1 Method-of-Characteristics (MOC). The MOC approach is one of many approaches for making blade-to-blade calculations. The philosophy of the MOC is to describe the supersonic flow field using a mesh of characteristic lines. Characteristic lines, also referred to as Mach lines, transport information from upstream locations where flow properties are known to downstream locations where the flow properties are calculated. The Mach number and flow direction at a given point can be determined from the information transported by the two characteristics that intersect at that point. For the simplest case, characteristic lines are found in the flow field according to the following relationship [16:312]:

$$\sin \sigma = \frac{1}{M} \tag{3}$$

where

σ = angle between characteristic line and flow direction

M = Mach number

Unlike other approaches, the use of the MOC for making blade-to-blade calculations is limited to regions of supersonic flow. The theoretical existence of this limitation is apparent in Equation (3) since a subsonic Mach number would result in an undefined angle. With such a limitation, the attempt to use the MOC to analyze a transonic rotor, which by definition has both subsonic and supersonic regions, may initially appear problematic. Indeed, only numerical methods, such as a Navier-Stokes-based CFD approach, allow regions of subsonic and supersonic flow in a mixed field to be calculated simultaneously and exactly. By dividing the flow path into discrete streamtubes and characterizing the flow in each according to the relative inlet Mach number, regions of subsonic and supersonic flow are isolated. Once isolated, the combination of a mass balance method and the MOC can be used to calculate the supersonic flow field and approximate shock position for the supersonic streamtubes [1:5/16]. The MOC-based equations used in the programs for analyzing periodic Q3D flow in a transonic rotor are developed in some detail in Bölcs[1].

An abbreviated version of this derivation is presented next for the purpose of documenting key equations that can be found in the source code.

The fundamental equation of gas dynamics for two-dimensional, irrotational flow can be written as [1:2/10]

$$(u^2 - a^2)\frac{\partial u}{\partial x} + uv(\frac{\partial v}{\partial x} + \frac{\partial u}{\partial y}) + (v^2 - a^2)\frac{\partial v}{\partial y} = 0 \tag{4}$$

where

u = velocity in x-direction

v = velocity in y-direction

a = speed of sound

Using relationships based on the flow angle (β), as well as Equation (3), Equation (4) can be transformed into a curvilinear coordinate system that involves the left running characteristic line, ξ, and the right running characteristic line, η. This transformation results in the following two equations that describe the variation of flow velocity and β along lines ξ and η:

$$\frac{\partial \beta}{\partial \eta} - \frac{\cot\sigma}{w}\frac{\partial w}{\partial \eta} = 0 \tag{5}$$

$$\frac{\partial \beta}{\partial \xi} + \frac{\cot\sigma}{w}\frac{\partial w}{\partial \xi} = 0 \tag{6}$$

where w = flow velocity ($\sqrt{u^2 + v^2}$).

By substituting Mach number-based relationships for w and σ into Equations (5) and (6) and integrating the partial differential equation, the following general solution is found:

$$\Theta_* = \mp\left(\sqrt{\frac{\gamma+1}{\gamma-1}}\tan^{-1}\sqrt{\frac{\gamma-1}{\gamma+1}(M^2-1)} - \tan^{-1}\sqrt{M^2-1}\right) \tag{7}$$

where γ = ratio of specific heats.

The geometric interpretation of the angle Θ_* is in the hodograph plane, a flow field presentation technique that is not essential for the present discussion. Equation (7) can be solved for the Mach number so that it is simply a function of Θ_*. A numerical approx-

imation of this form of Equation (7) is used by the programs to find the Mach number at consequential points in the supersonic flow field. The manner in which the value of Θ_* is determined begins by defining the values λ and μ, which are constant along the characteristic lines ξ and η, according to

$$\lambda = \frac{1}{2}(1000 - \Theta_* + \beta) \tag{8}$$

$$\mu = \frac{1}{2}(1000 - \Theta_* - \beta) \tag{9}$$

where the angles Θ_* and β are expressed in degrees. Since the Mach number and flow angle are ultimately sought at each point in the flow, it is desired to express Θ_* and β as functions of λ and μ, rather than vice versa. Equations of this form are derived by combining Equations (8) and (9) to yield

$$\Theta_* = 1000 - \lambda - \mu \tag{10}$$

$$\beta = \lambda - \mu \tag{11}$$

Again, all angles are expressed in degrees. The significance of Equations (10) and (11) is that the Mach number and flow angle at any point in the flow can be calculated with the values of λ and μ that are associated with intersecting characteristics. Equations (10) and (11) are two of the key equations that can be found in the source code.

To apply the MOC to a Q3D flow in a transonic rotor, various corrections must be made to the values of λ and μ to account for changes in streamtube thickness, radius, and total pressure. The corrections for changes in streamtube thickness are

$$\Delta\lambda_b = -\frac{1}{2}\frac{\sin\sigma\cos\beta}{\cos(\beta+\sigma)}\frac{b_2 - b_1}{\bar{b}} \tag{12}$$

$$\Delta\mu_b = -\frac{1}{2}\frac{\sin\sigma\cos\beta}{\cos(\beta-\sigma)}\frac{b_2 - b_1}{\bar{b}} \tag{13}$$

where b = streamtube thickness. The corrections for changes in radius are

$$\Delta\lambda_r = -\frac{1}{2}\frac{\sin\sigma\cos\beta}{\cos(\beta+\sigma)}\frac{r_2-r_1}{\overline{r}} \tag{14}$$

$$\Delta\mu_r = -\frac{1}{2}\frac{\sin\sigma\cos\beta}{\cos(\beta-\sigma)}\frac{r_2-r_1}{\overline{r}} \tag{15}$$

where r = radius. The corrections for changes in total pressure are

$$\Delta\lambda_{P_w} = -\frac{1}{\gamma}\frac{\sqrt{\overline{M}^2-1}}{\overline{M}^2}\ln\frac{P_{w2}}{P_{w1}} \tag{16}$$

$$\Delta\mu_{P_w} = -\frac{1}{\gamma}\frac{\sqrt{\overline{M}^2-1}}{\overline{M}^2}\ln\frac{P_{w2}}{P_{w1}} \tag{17}$$

where P_w = total pressure. The purposes of the subroutines entitled *deltalamda* and *deltamu* are to apply these corrections during flow calculations.

2.3 Efficiency and Loss

One of the most commonly used quantities that expresses the quality of a compressor is efficiency. Efficiency, in the most general sense, is the ratio of work into the ideal compressor to work into the actual compressor for a given pressure rise and mass flow. Since the actual compressor always requires more work than the ideal compressor to achieve the same pressure rise, the efficiency of the actual compressor is always less than unity or 100-percent efficient. If the ideal compressor is both adiabatic and reversible, then it is unable to alter the entropy of the flow and is called an isentropic compressor. Therefore, the isentropic efficiency of an actual compressor can be written as

$$\eta_{is} = \frac{h_{c3,is} - h_{c2}}{h_{c3} - h_{c2}} \tag{18}$$

where

η_{is} = isentropic efficiency

h_c = stagnation enthalpy

since work is equal to the rise in stagnation enthalpy through the rotor [4:35]. Isentropic efficiency is one of the three rotor performance measures that was used to validate the results from TRANSROTOR.

For the validation of the program, it is important to understand what flow phenomena are most influential in determining isentropic efficiency so that a difference from the benchmark could be traced back to the source. To this end, it is convenient to express isentropic efficiency in terms of flow properties such as temperature, pressure, and velocity. If the working fluid is assumed to be a perfect gas, then Equation (18) can be rewritten in terms of total temperatures:

$$\eta_{is} = \frac{T_{c3,is} - T_{c2}}{T_{c3} - T_{c2}} \tag{19}$$

where T_c = total temperature. Dividing through by T_{c2} and using an isentropic relationship to include the total pressure ratio, Equation (19) becomes

$$\eta_{is} = \frac{\left(\frac{P_{c3}}{P_{c2}}\right)^{\frac{\gamma-1}{\gamma}} - 1}{\frac{T_{c3}}{T_{c2}} - 1} \tag{20}$$

Equation (20) is a widely used expression for isentropic efficiency since the total pressure ratio, another important rotor performance measure, is explicitly included.

The reason an actual compressor can never be 100-percent efficient is due to losses, which can come from a variety of sources. The source of loss that received the most attention during this research is the total pressure loss associated with the rotating rotor. It is common practice to account for this type of loss as a loss coefficient (ω)

$$\omega_w = \frac{P_{w3,is} - P_{w3}}{P_{w2} - P_2} \tag{21}$$

As shown in Equation (21), the difference between the isentropic exit total pressure and the actual exit total pressure is non-dimensionalized by the inlet dynamic pressure, P_{w2}-P_2. Equation (21) is written in the relative frame since the total pressure loss occurs in the moving reference frame of the rotating compressor rotor.

Ultimately, it was desired to write an expression for isentropic efficiency that included ω_w. Revisiting Equation (20), P_{c3}/P_{c2} can be expanded to include ω_w. This author struggled to find material in the open literature that specifically addressed the relationship between the total pressure losses of a rotating rotor and total pressure ratio or isentropic efficiency. In most cases, the pressure loss coefficient was written in the absolute frame

$$\omega_c = \frac{P_{c2} - P_{c3}}{P_{c2} - P_2} \tag{22}$$

because reference was made to experimentation with stationary cascades or blade rows. Therefore, the change in frame that is required to write an equation for P_{c3}/P_{c2} that includes ω_w is rarely seen.

The mathematical procedure that this author used to write such an equation was to begin with Equation (21) and convert relative total pressures into absolute total pressures so that P_{c3}/P_{c2} could be isolated. The following three relations were used to do this:

$$\begin{aligned} P_{w3,is} &= P_{w2}\left(\frac{T_{w3}}{T_{w2}}\right)^{\frac{\gamma}{\gamma-1}} \\ P_w &= P_c\left(\frac{T_w}{T_c}\right)^{\frac{\gamma}{\gamma-1}} \\ T_w &= T_c + \frac{W^2 - C^2}{2C_p} \end{aligned}$$

where

C = absolute velocity

C_p = specific heat

After substitution, simplification, and arranging of terms, the equation for absolute total pressure ratio through a compressor rotor with losses was:

$$\frac{P_{c3}}{P_{c2}} = \frac{\left(\frac{T_{c3}}{T_{c2}} + \frac{W_3^2 - C_3^2}{T_{c2}2C_p}\right)^{\frac{\gamma}{\gamma-1}} - \omega_w\left\{\left(1 + \frac{W_2^2 - C_2^2}{T_{c2}2C_p}\right)^{\frac{\gamma}{\gamma-1}} - \left[1 + \frac{\gamma-1}{2}\left(\frac{C_2}{\sqrt{\gamma R T_2}}\right)^2\right]^{-\frac{\gamma}{\gamma-1}}\right\}}{1 + \frac{W_3^2 - C_3^2}{T_{c3}2C_p}} \tag{23}$$

where R = gas constant. Equation (23) gives P_{c3}/P_{c2} as a function of only temperatures, velocities, and the loss coefficient. The presence of C and W indicates the frame change needed to include ω_w. The significant affect of flow turning on pressure rise is implied by the C and W terms at stations 2 and 3, as well. Since isentropic efficiency and total pressure ratio were used as two of the three rotor performance measures upon which the validation of TRANSROTOR was based, Equations (20) and (23) are referred to in Chapter VI.

III. Computer Program Summaries

The sections of this chapter are summaries of the two desktop computer programs that were modified and evaluated as the primary focus of this research. The scope of the program capabilities, the user inputs, the outputs, and the general calculation sequence of each program are described. Appendix A contains the summary of the INCIDUNIQUE program that was not modified or evaluated as part of this research. Appendix B contains a listing of the subroutines called by all three programs. The subroutines are listed alphabetically with a brief description of their main purpose. Appendix C contains a flow diagram of each program. The flow diagrams show the sequence in which subroutines are called in order to arrive at a solution. Stepping through the flow diagram of a chosen program, while cross-referencing the subroutine listing, can give the viewer a detailed understanding of how these programs are coded. Chapter II discussed key theoretical concepts and equations found in these programs. Chapter V is devoted to the two loss models that differentiate the two versions of TRANSROTOR.

3.1 BOWSHOCK

For a given set of supersonic inlet conditions, this program calculates the position of a detached bow shock and determines the flow properties at the entrance and exit of a compressor rotor. The range of inlet flow velocities applicable to this scenario is bounded by subsonic flow, for which a bow shock would not exist, and supersonic flow that would cause the shock to attach. For practical purposes, the condition where the Mach number at the passage shock (M_F) exceeds approximately 1.3 could also be considered a high speed limit on inlet flow velocity due to the probability of flow separation after the shock. Calculations beyond this criterion may result in solutions based on questionable extrapolations of parameter correlations. Figure 2 depicts the type of scenario within a blade row that BOWSHOCK is designed to analyze and includes associated nomenclature. This program can analyze MCA-profile, S-profile, and xy-coordinate defined blades. If the MCA-profile or S-profile option is selected, the user must include the four defining parameters (L, X_d/L, d/L, and f/L) in the text file from which the initial user inputs are read. If the data option is selected, the xy-coordinates of points defining both blade

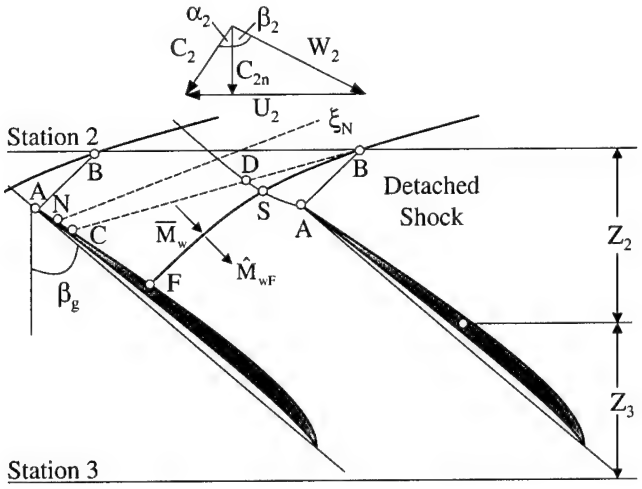

Figure 2 BOWSHOCK Flow Scenario - Blade-to-blade Perspective

surfaces must be included in the input text file. Appendix D contains examples of the required format for input text files. In addition to the blade geometry, this program allows the user to set upstream gas properties [e.g. ratio of specific heats (γ), total temperature (T_{c2}), total pressure (P_{c2}), and absolute inlet velocity (C_2)], radial height of streamtube from engine centerline at rotor inlet (R_2) and exit (R_3), streamtube thickness at rotor inlet (b_2) and exit (b_3), axial location of streamtube inlet (Z_2) and exit (Z_3) based off of the geometric center of the rotor blade, spool rotation rate (n), angle of the absolute flow from the axial direction (α_2), blade stagger angle (β_g), total number of blades (N), and rotor loss coefficient (ω_w, optional). Figure 3 presents the usage of the defined nomenclature. Once

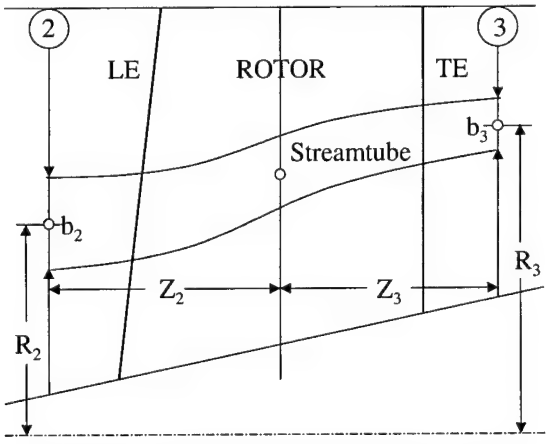

Figure 3 BOWSHOCK Flow Scenario - Meridional Perspective

the program reads the input text file containing all of this information, it echoes it back to the user in the form of an input screen. On this screen, the entries can be changed before program execution. The rotor loss coefficient is automatically computed if the default *auto* entry is left in the input box, otherwise the program uses the user-specified value.

The general calculation sequence of BOWSHOCK is described below. The minimum area through the blade passage is calculated to determine if choking conditions exist. Flow properties at station 2, the rotor entrance, are calculated. The neutral point on the profile suction surface is found. The left-running characteristic, ξ_N, begins at infinity in the inlet flow field and terminates at the neutral point. Thus, the neutral point is the point where the tangent to the surface equals the inlet flow angle. Since mass flow analyses are used to determine the evolution of the stagnation streamline and the shock position, the mass flow entering the cascade over the pitch length is calculated. An equivalent distance through which this same mass flow would pass is used to locate certain points within the rotor. Points A, B, C, and D shown in Figure 2 are subsequently found using the MOC and mass flow analyses. Point A is the sonic point on the blade LE. Point B is the point on the bow shock where the flow velocity equals Mach 1.0 after passing through the bow shock. Point C is the intersection of the blade suction surface and the left-running characteristic, ξ_{BC}, which emanates from point B. Point D is the intersection of the stagnation streamline and ξ_{BC}. The distance from the suction surface to point D is a segment of ξ_{BC} whose length equals the mass flow-based equivalent distance mentioned previously. It is known that the mass crossing the sonic line, AB, must be equal to the mass crossing the characteristic section, BD [1:5/17]. This principle is used to adjust the location of point B to balance the mass flow through the sonic lines. The Mach number at point S, before the shock on the stagnation streamline, and point F, before the shock on the blade suction surface are averaged as the incoming Mach number to the passage shock ($\overline{M}_w$). Additional points along the stagnation streamline are found using mass flow-based equivalent distances so that it is completely defined from the leading edge. Following the establishment of the stagnation streamline, the total pressure loss due to the shock wave and the critical area within the passage are calculated. Finally, profile losses are found as a function of diffusion factor (D) and the flow properties at station 3 are calculated. Inlet

and exit velocity triangles, the Mach number progression along the suction surface from the leading edge up to the passage shock, shock properties, upstream conditions, stagnation streamline conditions, and downstream conditions, as well as rotor performance measures are all displayed by this program.

3.2 TRANSROTOR

For a given set of inlet conditions, this program calculates the radial distribution of flow properties at three stations of a single-stage compressor. Station 1 is upstream of the IGV, station 2 is between the IGV and rotor, and station 3 is downstream of the rotor. Unlike BOWSHOCK, TRANSROTOR can support either subsonic or supersonic inlet conditions for each of the streamtubes. For transonic and supersonic flows, station 2 must be upstream of the shock. Entering the same flow angles at stations 1 and 2 effectively eliminates the IGV. Figure 4 depicts the compressor stage that TRANSROTOR is designed to analyze and includes associated nomenclature. Radial equilibrium

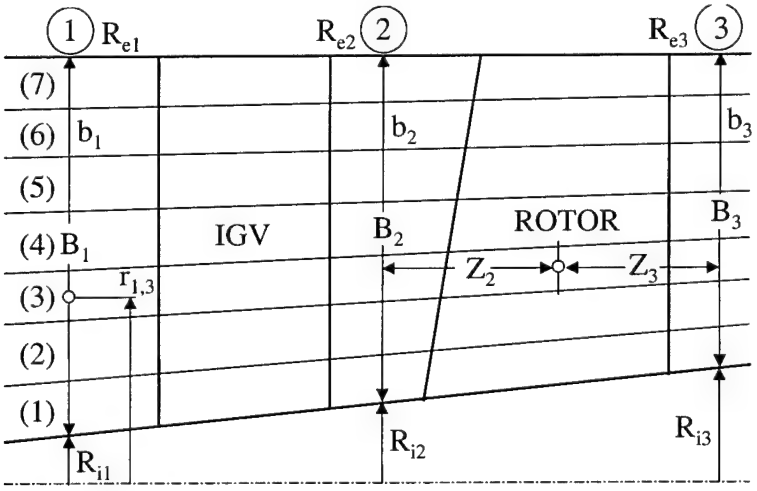

Figure 4 TRANSROTOR Compressor Stage - Meridional Perspective

of the flow between the blade rows is the method by which this program converges to a solution. The static pressure at adjoining boundaries of up to seven streamtubes must match each other within a certain tolerance for the program to consider a calculation complete. The portion of the BOWSHOCK algorithm that performs the flow analysis is

embedded, almost verbatim, into TRANSROTOR as the analysis routine for supersonic streamtubes. TRANSROTOR does not have the capability to fabricate MCA-profiles or S-profiles from the four defining parameters mentioned previously (Figure 1). Therefore, the xy-coordinates of streamline slices of the rotor blade must be included in the input text file for this program (Appendix D). Since the program assigns each profile to a streamtube, the number of streamtubes desired must equal the number of blade profiles provided. In addition to the blade geometry, this program allows the user to set many boundary conditions. The streamtube-independent inputs are γ, C_p, R, n, N, and radius of hub (R_i) and casing (R_e) at all three stations. The streamtube-dependent inputs at station 1 are total pressure (P_{c1}), total temperature (T_{c1}), axial velocity (C_{1n}), streamtube thickness normalized by flow path height (b_1/B_1), and α_1. The streamtube-dependent inputs at station 2 are α_2 and stator loss coefficient (ω_c, optional). The streamtube-dependent inputs at station 3 are β_g and ω_w (optional). Once the program reads the input text file containing all of this information, it echoes it back to the user in the form of an input screen. On this screen, the entries can be changed before program execution.

The general calculation sequence of TRANSROTOR is described below. Flow properties at station 1 are calculated by iteration until radial equilibrium is reached. Flow properties at station 2 are calculated in a similar manner, however, the presence of the IGV must be included in these calculations if an IGV is used. If *auto* is entered for the stator loss coefficient, the total pressure loss incurred by the flow passing over the stator is calculated. The majority of the computations done by TRANSROTOR determine the change in flow properties from station 2 to station 3. Beyond station 2, the relative inlet Mach number of each streamtube determines the type of analysis it will undergo. If the relative inlet Mach number is subsonic, flow deviation and diffusion losses are calculated using subsonic correlations. If the relative inlet Mach number is supersonic, TRANSROTOR invokes the same analysis routine that BOWSHOCK uses to calculate flow properties through the blade passage. Once every streamtube has been analyzed, the program checks for radial equilibrium at station 3. If the static pressures at adjoining streamtube boundaries are not within 50 Pa of each other, the streamtube thicknesses are adjusted and another analysis iteration is performed. Once radial equilibrium is reached, the final val-

ues for flow properties at station 3 are calculated. During the calculation, many screens are displayed to provide information on intermediate steps. A multitude of flow properties and performance measures are given once radial equilibrium is reached at each station. At the end, TRANSROTOR gives the user the ability to plot the radial distribution of pressure, temperature, axial velocity, Mach number, loss coefficient, and diffusion factor. Each plot shows data from all three stations so that the progression of the parameter through the stage can be seen.

IV. Methodology

To reiterate, the goal of this thesis was to evaluate and enhance the utility of BOWSHOCK and TRANSROTOR for use in preliminary transonic rotor design. This chapter recounts the actions taken to complete each of the four supporting objectives. The approaches taken and the reasoning for those approaches are stated.

4.1 Algorithm Documentation

The original source codes of INCIDUNIQUE, BOWSHOCK, and TRANSROTOR were purchased for their advertised ability to analyze a transonic compressor rotor. The speed at which these programs could calculate an approximate solution for such a complex flow and their flexibility as desktop-based programs made them particularly enticing. Growth of these programs beyond their original capabilities was envisioned. References [10], [11], and [12] accompanied the original programs. These documents provided the basics on how to run each program, explanations of each screen display, and the nomenclature used. To facilitate future development of these programs, more detailed documentation of the source code was needed. Providing this information was the essence of the first supporting objective of this thesis.

Every line of code was reviewed so that the purpose of each subroutine could be distilled and then documented. Appendix B was the result of that effort. Some subroutines were common between two or more programs. Equally important as the purpose of the subroutines was the sequence in which they were called. Every subroutine call made in each program was recorded. Nested subroutine calls were traced so that a complete flow diagram of each of the three programs could be made. Appendix C was the result of that effort. The information contained in these two appendices describe the computational framework within the programs. The general calculation sequences discussed in Chapter III were written from the knowledge gained during this portion of the research effort. Appendix B and Appendix C will be extremely helpful to future users and/or modifiers of these codes, especially for error trapping purposes.

Since these programs utilized a collection of empirical correlations to determine flow properties, the author of the source codes had to decide which correlations to use and how to apply them. Most of this engineering judgement was applied to the selection and application of a loss model. Without further documentation, users of INCIDUNIQUE, BOWSHOCK, and TRANSROTOR would be ignorant of the underlying governing equations. A focused literature review was conducted to gain first-hand knowledge of the loss correlations used in the original source codes, as well as what would become the two newly coded loss models. Chapter II and Chapter V are the primary results of that effort. They provide the additional level of detail that is essential for complete understanding of these programs.

4.2 Loss Model Selection and Incorporation

The original rotor loss model found in the source codes was loosely based on a set of correlations published by Çetin *et al.* [2]. Following the literature survey, portions of this loss model were reverted back to a form more in line with the paper upon which it was based. Some loss model modifications made by the author of the original source codes were retained as improvements to program accuracy, utility, and/or simplicity. Since the final version of this loss model still deviated from the paper, it was given the designation LM1. The LM1 loss model was one of the two loss models validated during this research.

The second, or alternate, loss model was the result of an attempt to incorporate a more recent and purportedly more accurate transonic compressor rotor loss model into the TRANSROTOR program. The 1996 two part *ASME Journal of Turbomachinery* paper by König, Hennecke, and Fottner described subsonic [17] and supersonic [6] loss models that improved upon existing correlations to enable better prediction of loss and deviation angles in modern transonic axial-flow compressors. They reported that the loss models were well suited for analyzing new blading concepts. The impression of this author was that König *et al.* offered their models for general use in predicting loss in advanced transonic compressors, regardless of whether the flow conditions were susceptible to generating their assumed two-shock system. Coincidentally, APNASA flow visualization did show a second shock in the blade passage of the TESCOM blading, although not at the trailing edge.

The advertised ability of the König *et al.* loss model to capture the effects of a two-shock system became very appealing.

This alternate loss model was given the designation LM2. This naming convention was adopted to dissociate the rotor loss models incorporated into TRANSROTOR from the papers upon which each loss model was based. Neither loss model, LM1 or LM2, strictly adhered to the sets of published correlations found in the respective references. The coded loss models were comprised of a selection of correlations found in the open literature. Additionally, some correlations were common to both loss models. Tuning of the two rotor loss models to fit specific data sets was minimized in order to preserve the general utility of the TRANSROTOR program. Most of the tuning that was done can be found in the loss prediction of supersonic streamtubes. Chapter V addresses the two loss models in great detail.

4.3 TRANSROTOR Validation

At the time TRANSROTOR was purchased, its level of accuracy was unknown. Furthermore, the original loss model was replaced by the untested LM1 and LM2 loss models. The accuracy of both versions of TRANSROTOR needed to be quantified. While TRANSROTOR had the ability to analyze a fully subsonic and a fully supersonic compressor rotor, the most interesting attribute for this research effort was its ability to analyze a transonic rotor. Additionally, only the analysis of a transonic rotor exercised all subroutines in the program. The two TESCOM blade geometries described in Chapter I had the necessary qualities to be good test specimens. Both blades were of a modern design and operated in the transonic flow regime. Extensive CFD analysis of a rotor equipped with these blades had already been accomplished using APNASA so an ample amount of data was available for comparison. The research reported in this thesis validated both versions of TRANSROTOR using the APNASA data set as the benchmark. APNASA solutions showed excellent agreement with experimental over-the-rotor pressure distributions and exit profiles for a two-stage version of the TESCOM machine [8].

TRANSROTOR validation was accomplished using two different sets of boundary conditions that consisted of flow property data extracted from the APNASA solutions.

The primary difference between the boundary conditions was their axial location. The first set of boundary conditions matched the flow properties at the inlet plane defined for the APNASA runs. The distance of this inlet plane upstream of the blade LE was equivalent to 105-percent of the average blade chord length (1.05·L). These boundary conditions were entered into TRANSROTOR as the station 1 flow properties. In this case, span-averaging of the APNASA flow properties into five representative values was inconsequential since the flow was uniform across the entire flow path. The value of axial velocity input into TRANSROTOR was adjusted to match the APNASA mass flow rate. The actual radius of the hub at the inlet plane was entered into TRANSROTOR as the radius of the hub at station 1 (R_{i1}). Similarly, the radius of the hub at stations 2 and 3 corresponded to the APNASA flow path. The radius of the casing (R_e) was also matched. Unlike the inclined hub, R_e remained constant for the entire length of the flow path under consideration. Figure 5 depicts the entire flow path as modeled for this case. This set

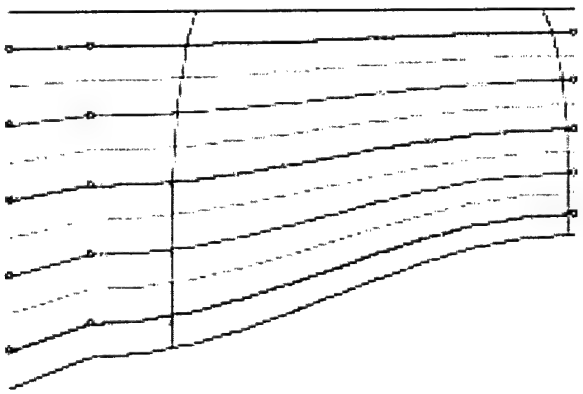

Figure 5 TRANSROTOR Flow Path Depiction when Station 1 Defined by APNASA Flow Properties 1.05·L Upstream of Blade LE

of boundary conditions was used to quantify the accuracy of TRANSROTOR when it is required to develop the flow from a location far upstream of the blade LE. This scenario simulated best the projected use of TRANSROTOR since detailed information of the flow near the blade LE will not be available for new blade geometries.

The second set of boundary conditions was based on the APNASA flow properties at an axial location that was approximately 0.15·L upstream of the blade LE. This location

was chosen by examining the pressure contours of the APNASA solutions and selecting a location that was just upstream of the detached shock. Station 2 was defined in TRANSROTOR, via Z_2, to match this axial location. R_{i2} had to be increased slightly beyond the actual radius in order to match the APNASA mass flow rate. Span-averaging of the APNASA flow properties into five representative values was necessary since viscosity had begun to distort the flow field. Since this set of boundary conditions represented the flow just upstream of the detached shock, an input technique was used to indirectly insert these conditions at station 2. The hub radius at station 1 was set equal to the hub radius at station 2. This effectively created an isentropic, straight duct that allowed the flow properties input at station 1 to be transported to station 2. Figure 6 depicts the entire flow path as modeled for this case. This set of boundary conditions was used to quantify the

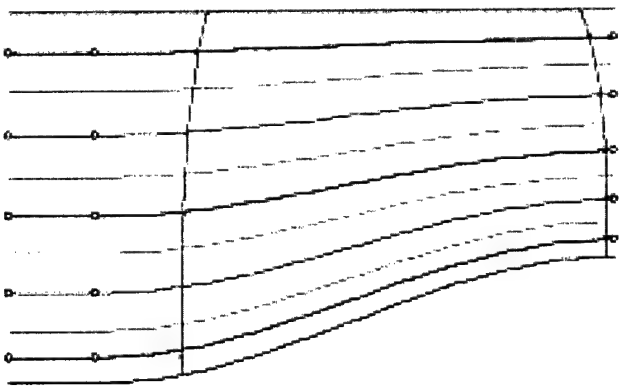

Figure 6 TRANSROTOR Flow Path Depiction when Station 2 Indirectly Defined by APNASA Flow Properties 0.15·L Upstream of Blade LE

accuracy of TRANSROTOR when it was provided greater detail of the incoming flow. It was hypothesized that these boundary conditions would produce the optimum results that could be expected from TRANSROTOR. As will be discussed in Chapter VI, the results did not prove this hypothesis to be true.

Using the flow properties at these two locations as boundary conditions allowed a comparison to be drawn that isolated the treatment of the flow between stations 1 and 2. The difference of these solutions approximated the error introduced into the calculations by the simplistic treatment of the flow path by TRANSROTOR. An understanding of the

relative magnitude of this error is important for situations in which only flow properties far upstream from the rotor are known.

In all, eight solutions were run to validate TRANSROTOR and quantify its accuracy. Each version of TRANSROTOR was used to analyze the original and TM1 blades. For each blade, both of the input techniques described above were used.

Program validation was accomplished using two methods. The first method condensed the data from these eight solutions into three values - isentropic efficiency (η_{is}), total pressure ratio (P_{c3}/P_{c2}) , and static pressure ratio (P_3/P_2). The TRANSROTOR and APNASA values of these rotor performance measures were calculated using averaged flow properties. Comparisons of these values determined the overall accuracy of both versions of TRANSROTOR and measured their response to the different blading and input techniques. While η_{is}, P_{c3}/P_{c2} , and P_3/P_2 quantified the overall performance of the compressor rotors, the spanwise distribution of flow properties provided a more detailed examination of rotor behavior. This was the second method used to validate TRANSROTOR. Effects due to local blade geometry and walls were seen using this data presentation method. The trends in the flow properties at stations 2 and 3 were compared to highlight differences in the loss models, blade geometries, and input techniques. Chapter VI presents the results of these two validation methods.

4.4 Parametric Study

A parametric study of blade geometry was completed to demonstrate the potential of these programs to be used in the preliminary design of transonic compressor rotors. The MCA-profile option available in BOWSHOCK allowed the blade geometry to be changed easily and systematically without the aid of an external program. It would have been extremely laborious to conduct a manual parametric study using TRANSROTOR since it only accepts xy-coordinate defined blade profiles. The blade geometry parameters investigated corresponded to the four defining parameters of MCA-profile blades - L, X_d/L, d/L and f/L. Two additional parameters were varied that did not affect blade geometry - β_g and N. All six of these parameters were varied by a maximum of +/-20-percent from the design point. BOWSHOCK was run at five-percent increments for each of the six

parameters. In some of the more extreme cases, BOWSHOCK was unable to converge to a solution. These cases are discussed in Chapter VI with the presentation of the results. Table 2 gives the minimum, design point, and maximum values of the parameters that were studied.

Table 2 Blade Geometry Parameters

Range	L (mm)	X_d/L	d/L	f/L	β_g (deg)	N
Minimum Value	37.31	0.523	0.04	0.054	33.00	60
Design point	46.64	0.654	0.05	0.068	40.46	74
Maximum Value	55.96	0.785	0.06	0.082	42.48	88

The design point conditions were arbitrarily chosen to be the same as those for the third streamtube from the TRANSROTOR analysis of the TM1 blade. The baseline design point geometry was an MCA-profile approximation of the TM1 blade geometry for the third streamtube. The MCA approximation may be a poor approximation of the TESCOM blading but the primary results of this parametric study were the predicted trends in performance for changes in a particular blade parameter, not the absolute performance numbers. Total pressure ratio and isentropic efficiency were used as the performance measures in this study.

V. Loss Models

This chapter contains a discussion of the two rotor loss models and one stator, or IGV, loss model that were incorporated into TRANSROTOR. The first rotor loss model to be discussed was based upon the set of correlations published in Çetin *et al.*[2]. This loss model was given the designation, LM1. The second rotor loss model to be discussed was based upon the set of correlations published in König *et al.*[6; 17]. This loss model was given the designation, LM2. A brief discussion of the IGV loss model was included at the end of this chapter for completeness. Since this research effort analyzed an isolated rotor, the TRANSROTOR subroutine that calculated losses associated with an upstream IGV was not exercised.

The two rotor loss models assume fundamentally different flow features for supersonic passage flow. The LM1 loss model presumes a single normal passage shock while the LM2 loss model presumes that a second normal shock exists near the blade trailing edge (TE). This difference begs the question of how many shocks were observed in the APNASA solution for the two blades examined in this research. While flow reacceleration after the leading edge shock was predicted by APNASA resulting in a second shock, the location of the second shock within the blade passage was well forward of the trailing edge. Because the actual shock pattern generated by these blades did not exactly match the premise of either loss model, two loss model versions of TRANSROTOR were evaluated.

5.1 Calculating Loss by Correlation

Both loss models use a common approach to calculating the losses in a transonic rotor by correlation. Streamtubes are grouped by subsonic or supersonic relative inlet flow. For subsonic streamtubes, key on-design parameters, which occur only at the minimum loss condition, are computed as a reference point for determining how far off-design the rotor is operating. The minimum loss incidence angle (i^*), diffusion factor (D) or equivalent diffusion factor (D_{eq}), on-design deviation angle (δ^*), and on-design loss coefficient (ω^*) are the key parameters that are used to define the on-design state. Off-design correlations, which draw upon the on-design parameters, are used to determine the total loss attributed to

subsonic streamtubes. For supersonic streamtubes, the presence of shock waves introduces additional sources of loss. Therefore, correlations are used to determine the shock loss as well as the other types of losses. The total loss attributed to supersonic streamtubes is based upon the summation of two loss coefficients.

5.2 The LM1 Loss Model

Çetin, Hirsch, Serovy, and Üçer reported the results of their 1989 study to evaluate on-design and off-design loss correlations using transonic compressor test data in Çetin *et al.*[2]. Eight data sets from testing axial flow compressors designed in the 1970s were compiled and analyzed. Hub radii ranged between 63 mm and 75 mm and tip radii ranged between 125 mm and 205 mm. All of the investigated compressors used MCA- or DCA-type blades. The result of this research was a set of correlations that were recommended for performance prediction of transonic compressors. Some correlations were accepted by Çetin *et al.* as originally published, while others were modified to better fit the test data. The following is a summary of the recommended correlations. For those cases where the recommended correlation was not used in the LM1 loss model, the replacement correlation is discussed.

5.2.1 Loss Correlations for Subsonic Flow.

5.2.1.1 On-Design. For predicting the minimum loss incidence angle, Çetin *et al.* began with a correlation presented in the 1965 NASA SP-36 Report [18:234]. The same correlation can also be found in a 1960 *ASME Journal of Basic Engineering* paper by Lieblein [19:578]. It was derived from two-dimensional (2D), subsonic cascades consisting of ten-percent thick NACA 65-(A_{10})-series blades. Equation (24) is the basic correlation:

$$i^*_{2D} = (K_i)_{sh}(K_i)_t(i_0)_{10} + n\varphi \tag{24}$$

where

$(K_i)_{sh}$ = correction for thickness distribution
$(K_i)_t$ = correction for maximum blade thickness

$(i_0)_{10}$ = zero-camber incidence angle for ten-percent thick 65-series blades

n = slope factor

φ = blade camber angle

For the LM1 loss model, a value of 1.0 was used for the $(K_i)_{sh}$ term. The same value was used for this term by König *et al.* for more advanced blade designs [17:78]. The value of $(K_i)_t$ was simply a function of d/L. The remaining two factors of Equation (24), $(i_0)_{10}$ and n, were functions of β_2 and σ. Due to the solidity of the TESCOM rotors far exceeding the published range, the behavior of the numerical representations of these two-variable functions had to be examined. While the $(i_0)_{10}$ relation behaved well when extrapolated to high values of solidity ($\sigma > 3.0$), the maximum value for n had to be limited to 2.4 to avoid large numerical error caused by erroneous extrapolation. The subroutine entitled *minlossinc* calculates the value of i^* according to Equation (24).

Çetin *et al.* suggested that inlet Mach number corrections be applied to i^*_{2D} based on blade type (DCA or MCA). The MCA blade profile correction

$$i^*_{cor} = i^*_{2D} + 5.738 + 1.3016 M_{w2} \tag{25}$$

was initially incorporated in the LM1 loss model. However, this correction made i^*_{cor} excessively high so the correction was omitted. König *et al.* justified the exclusion of this correction on the basis that the Mach effects could not be proven for their cascade data [17:78].

The on-design total loss prediction method for axial-flow compressors given by Koch and Smith in 1976 [20] was cited by Çetin *et al.* as the most satisfactory predictor of transonic cascade design loss [2:4]. Çetin *et al.* noted that this method is quite comprehensive, accounting for a multitude of parameters including blade surface roughness. The Koch and Smith derived equivalent diffusion factor was incorporated into the subsonic portion of the LM1 loss model. An alternative method for calculating the on-design loss coefficient based on equivalent diffusion factor (D^*_{eq}) was used to reduce computational complexity at

the potential expense of a small amount of accuracy. The following is a summary of the development of the Koch and Smith D^*_{eq} taken from Appendix 1 of Koch and Smith[20].

The desire was to formulate a more general expression for the equivalent diffusion factor originally introduced by Lieblein in 1959 [21]. As with the minimum loss incidence angle correlation, his work was based on 2D, incompressible flow around ten-percent thick NACA 65-(A_{10})-series blades. Koch and Smith began by defining D^*_{eq} as the product of three velocity ratios:

$$D^*_{eq} = \frac{W_{max}}{W_{TE}} = \frac{W_p}{W_2} \cdot \frac{W_{max}}{W_p} \cdot \frac{W_2}{W_{TE}} \tag{26}$$

where

W_{max} = maximum suction surface velocity

W_{TE} = trailing edge velocity

W_p = mean passage velocity in blade passage throat region

Note that the symbol, W, is used to denote velocity in Equation (26) since it was applied in the relative frame of the rotating rotor in this research effort.

Relationships were derived for the first two terms on the right hand side of Equation (26). The third term can be calculated immediately from the inlet and exit velocity triangles of the rotor, which are usually known quantities. The ratio of passage throat velocity to inlet velocity was obtained from the following four equations:

$$\frac{W_p}{W_2} = \left[(\sin\beta_2 - 0.2445\sigma\Gamma^*)^2 + \left[\frac{\cos\beta_2}{A^*_p(\frac{\rho_p}{\rho_2})} \right]^2 \right]^{\frac{1}{2}} \tag{27}$$

where

$$\frac{\rho_p}{\rho_2} = 1 - \frac{M^2_{2n}}{1 - M^2_{2n}} \left(1 - A^*_p - 0.2445 \frac{\tan\beta_2}{\cos\beta_2} \sigma\Gamma^* \right) \tag{28}$$

$$A^*_p = \left[\frac{1 - 0.4458\sigma\frac{d}{L}}{\cos\overline{\beta}} \right] \left(1 - \frac{A_{a2} - A_{a3}}{3A_{a2}} \right) \tag{29}$$

$$\Gamma^* = \frac{R_2 W_{u2} - R_3 W_{u3}}{\overline{R}\sigma W_2} \tag{30}$$

and

Γ^* = blade circulation parameter

A_p^* = annulus area contraction ratio from cascade inlet to passage throat

A_a = annulus area

M_{2n} = axial Mach number at station 2

The use of Mach number in Equation (28) reveals the incorporation of compressibility effects by Koch and Smith. Equations (29) and (30) also show added sophistication, as compared to the Lieblein D_{eq}^*, by accounting for streamtube contraction and radial displacement, respectively. Finally, the ratio of maximum suction surface velocity to passage velocity was obtained from the following equation:

$$\frac{W_{max}}{W_p} = 1 + 0.7688\frac{d}{L} + 0.6024\Gamma^* \tag{31}$$

The equivalent diffusion factor for subsonic streamtubes is calculated within the TRANSROTOR subroutine entitled *verlustcompraxw* according to Equation (26).

The last on-design parameter that was needed as an input to calculating the on-design loss coefficient was the deviation angle. Çetin *et al.* found that the well-known deviation correlation known as *Carter's Rule* underestimated the deviation angles of their test data in a very consistent manner [2:6]. An in-depth discussion of Carter's Rule was found in Johnsen and Bullock[18], the same NASA report from which the minimum loss incidence angle correlation was taken. Reference 18 presented Carter's Rule as

$$\delta_{carter}^* = (K_\delta)_{sh}(K_\delta)_t(\delta_0)_{10} + \frac{m_{\sigma=1}}{\sigma^b}\varphi \tag{32}$$

where

$(K_\delta)_{sh}$ = correction for thickness distribution

$(K_\delta)_t$ = correction for maximum blade thickness

$(\delta_0)_{10}$ = zero-camber deviation angle for ten-percent thick 65-series blades

$m_{\sigma=1}$ = rate of change of deviation angle with camber angle for $\sigma = 1.0$

σ^b = term accounting for variable influence of solidity associated with β_2

Discrete values of $(K_\delta)_{sh}$, corresponding to various families of blade shapes, were given. The value of $(K_\delta)_t$ and $(\delta_0)_{10}$ were functions of the same parameters, β_2 and σ, as were the equivalent terms in the minimum loss incidence angle correlation. Both $m_{\sigma=1}$ and the solidity exponent, b, were simply functions of β_2. Two curves, corresponding to a circular-arc or NACA A_{10} camber line, were given in Johnsen and Bullock[18] for $m_{\sigma=1}$ versus β_2. The circular-arc camber line was selected as the more appropriate curve for use in the LM1 loss model.

Çetin *et al.* attributed the poor fit of this deviation angle correlation to the transonic and 3D effects associated with their test specimens. Because of the consistency of the difference between the predicted values from Equation (32) and the experimental values, they proposed a second order correction to Carter's Rule:

$$\delta^* = -1.099379 + 3.0186\delta^*_{carter} - 0.1988\delta^{*2}_{carter} \tag{33}$$

During development of the LM1 loss model, this correction was applied and the resulting TRANSROTOR-predicted exit flow angles were compared with the APNASA solution for the TESCOM blading. The uncorrected Carter's Rule (32) compared better than the corrected Carter's Rule (33). Therefore, the subroutine entitled *carter*, which calculates the value of δ^*, was coded according to Equation (32).

As mentioned in the discussion of the Koch and Smith design loss method, an alternative method for calculating the on-design loss coefficient based on D^*_{eq} was used. The selected relationship was published in a 1972 NASA report edited by Messenger and Kennedy [22]. A series of wake momentum thickness curves, representing proximity to the hub or casing, were plotted versus diffusion factor. By using these curves, an approximation of the effects of tip clearance, secondary, and end wall boundary layer losses was included in the calculation of on-design loss coefficient [15:118]. Minimum loss occurred at mid-span with loss increasing as the span location moved toward the walls. Because the relationship required D^*, the Koch and Smith D^*_{eq} had to be converted. This was accomplished using the Lieblein definitions of each parameter:

$$D^* = D^*_{eq}\frac{W_3}{W_2} - \frac{W_3}{W_2} \tag{34}$$

The end product of this calculation was the on-design total loss coefficient for subsonic streamtubes given by

$$\omega_w^* = \frac{2\sigma}{\cos\beta_3^*}\left(\frac{\theta}{L}\right)^* \tag{35}$$

where θ = wake momentum thickness. Determination of the appropriate wake momentum thickness curve to use in the wake momentum thickness calculation, as well as the calculation itself, is done in the *komegarechnung* subroutine of TRANSROTOR. The calculation of the on-design total loss coefficient, according to Equation (35), is accomplished within the subroutine entitled *verlustcompraxw*.

5.2.1.2 Off-Design. The previous section dealt only with the key parameters that defined the theoretical minimum loss condition for a subsonic streamtube that passes through a given rotor. In most cases, the rotor operates in an off-design state. Therefore, the results of the on-design calculations become a reference condition. Additional correlations were used to determine actual total loss of the rotor. Çetin *et al.* recommended the off-design deviation angle correlation published by Creveling [23] and proposed a new correlation to find the off-design total loss coefficient from the on-design total loss coefficient [2:5].

The off-design deviation angle of Creveling was expressed as

$$\delta = \delta^* + \left(\frac{\delta - \delta^*}{\epsilon^*}\right)\epsilon^* \tag{36}$$

where

$$\epsilon^* = (\beta_{m2} + i^*) - (\beta_{m3} + \delta^*) \tag{37}$$

and

ϵ^* = on-design flow turning angle

β_m = angle between mean camber line at blade tip and axial direction

The value of $(\delta - \delta^*)/\epsilon^*$ was obtained through a relationship with the quantity, $(i - i^*)/\epsilon^*$. Reference 23 contained three figures of curve fit data relating $(\delta - \delta^*)/\epsilon^*$ to $(i - i^*)/\epsilon^*$ for hub, mid-span, and tip regions. The difference of the three curves was

virtually indistinguishable. An equation representing the hub region curve was coded into the *carter* subroutine to calculate the off-design deviation angle.

During the research that led up to their off-design total loss coefficient correlation, Çetin *et al.* plotted experimental loss characteristics as $(\omega_w - \omega_w^*)$ versus $(i - i^*)$ for MCA and DCA blades. They noted that ω_w depended mainly on the inlet Mach number. They also noted that trends in the data could be separated according to blade type and positive or negative values of $(i - i^*)$. Using this breakdown, Çetin *et al.* built a table of equations to be used for determining the value of the coefficient, c_m, in their base equation for off-design total loss coefficient:

$$\omega = \omega^* + c_m(i - i^*)^2 \tag{38}$$

where

$$c_m = 0.02845M_{w2} - 0.01741 \text{ for } i - i^* < 0$$
$$c_m = 0.00363M_{w2} - 0.00065 \text{ for } i - i^* > 0$$

and c_m = correction for inlet Mach number. Since the geometry of an MCA-type blade is generally more similar to advanced compressor blades than the geometry of a DCA-type blade, the MCA equations for calculating c_m were programmed into the *verlustcompraxw* subroutine of TRANSROTOR.

5.2.2 Loss Correlations for Supersonic Flow. Only the deviation correlations, Equations (32) and (36), recommended by Çetin *et al.* were used for determining total loss within a supersonic streamtube. The reason the LM1 loss model was switched to a largely different set of correlations for supersonic loss analysis was the lack of loss distinction by the correlations of Çetin *et al.*[2]. In their approach, losses were considered as a whole. Profile, shock, and secondary losses were accounted for simultaneously by one total pressure loss coefficient. Çetin *et al.* argued that it was problematic to address loss sources individually. Such an approach requires that the individual loss sources be combined in some manner that may not completely account for their integrated effect. Despite this concern, it was

felt that the advantages of being able to examine the relative magnitudes of various loss sources in a preliminary design tool exceeded the problems associated with doing so. The LM1 loss model computes the total loss in a supersonic streamtube by summing a shock loss coefficient and profile loss coefficient.

5.2.2.1 Shock Loss. The shock loss coefficient of the LM1 loss model is calculated in subroutine *kanalstoss* according to

$$\omega_{shock} = \frac{\overline{P}_{w2} - \hat{P}_w}{P_{w2} - P_2} \tag{39}$$

where

$\overline{P}_{w2}$ = mass averaged total pressure based on total pressure downstream of bow shock and inlet total pressure

$\hat{P}_w$ = total pressure just downstream of passage shock

As seen in Equation (39), three total pressures from particular flow regions are used to calculate the shock loss coefficient. $\overline{P}_{w2}$ accounts for the minor total pressure loss that is incurred due to the bow shock propagating upstream. To do so, the total pressures just downstream of the bow shock at points B and S of Figure 2 are arithmetically averaged to represent the total pressure above the stagnation streamline. This quantity is then mass averaged with the freestream inlet total pressure, P_{w2}. The total pressure just downstream of the passage shock, $\hat{P}_w$, is found using standard compressible flow theory relationships for shock waves. It is assumed that the passage shock is normal to the flow, thus, the total pressure ratio across the passage shock is given by

$$\frac{\hat{P}_w}{\overline{P}_{w2}} = \left[1 + \frac{2\gamma}{\gamma+1}(\overline{M}_w^2 - 1)\right]^{-\frac{1}{\gamma-1}} \left[1 - \frac{2}{\gamma+1}\left(1 - \frac{1}{\overline{M}_w^2}\right)\right]^{-\frac{\gamma}{\gamma-1}} \tag{40}$$

$\overline{M}_w$ is the arithmetic average of the Mach number at point S and F of Figure 2.

5.2.2.2 Profile Loss. Added to the shock loss coefficient given by Equation (39) is a profile loss coefficient. The approach taken was quite different from what was done for the subsonic case due to the presence of the shock wave in the blade passage. It was

found that incorporating the flow conditions just downstream of the passage shock into the diffusion factor correlation produced better results than strictly using the inlet station flow conditions [24]. The diffusion factor correlation selected for supersonic streamtubes was the Monsarrat correlation [15:118]. Applying the correlation to this scenario, the diffusion factor was given by

$$D = 1 - \frac{W_3}{W_2} + \frac{\hat{r}\hat{W}_u - r_3 W_{u3}}{(r_2 + r_3)W_2\sigma} \tag{41}$$

The resulting diffusion factor determined the supersonic profile loss coefficient according to the same wake momentum thickness curves in the subsonic case. However, tuning of the supersonic portion of the LM1 loss model revealed that using the 20&70-percent span wake momentum curve for all span locations gave the best overall loss prediction [24]. The calculation of the supersonic profile loss coefficient is done according to

$$\omega_{profile} = \frac{2\sigma}{\cos\beta_3}\left(\frac{\theta}{L}\right) \tag{42}$$

within the subroutine entitled *verlustcompraxwsup.*

As mentioned previously, the total loss coefficient for a supersonic streamtube is the summation of Equations (39) and (42):

$$\omega_w = \omega_{shock} + \omega_{profile} \tag{43}$$

5.3 The LM2 Loss Model

König *et al.* drew comparisons with the Çetin *et al.* loss model, which was used as the foundation for the LM1 loss model. Measurement data from eight blades with substantially different shapes and design Mach numbers were researched for each of their two models. The result of this research was a set of correlations that were recommended for performance prediction of transonic compressors. Of the various correlations recommended, two could not be coded into TRANSROTOR due to lack of adequate information. These were the subsonic deviation and supersonic profile loss correlations. In each case, the corresponding

correlations from the LM1 loss model were substituted. These omissions are addressed again in the respective subsections.

5.3.1 Loss Correlations for Subsonic Flow.

5.3.1.1 On-Design. In the following development of the governing equations of the König *et al.* subsonic loss model [17], the asterisk used to denote the on-design condition was intentionally omitted for some parameters because the same equation was revisited for the off-design case. If the asterisk is present, it indicates that the respective equation is strictly used for on-design calculations.

König *et al.* used the same basic correlation by Lieblein [19] for predicting the minimum loss incidence angle as Çetin *et al.* used. They discussed their choices for the values of the two special factors, $(K_i)_{sh}$ and $(K_i)_t$. The factor $(K_i)_{sh}$ was set to unity since the thickness distributions of the blade shapes investigated were more similar to the thickness distributions of NACA-65 profiles than of DCA profiles [17:78]. The value of $(K_i)_t$, a factor that accounted for variation in maximum thickness, was also based on the comparative blade shapes. Since the Mach number-based incidence correction used by Çetin *et al.* was omitted from the LM1 loss model, both versions of TRANSROTOR calculate i^* the same way. Subroutine *minlossinc* is common between both loss models.

Prediction of both on-design and off-design losses in the subsonic regime were based on the relationship between momentum thickness in the blade wakes and diffusion of the flow along the blade suction surface. König *et al.* extended the Lieblein expression for D_{eq} to address compressible flow with a streamtube contraction around blades of arbitrary shape. The result of this effort was

$$D_{eq} = \frac{W_{max}}{W_3} = \frac{1}{\Omega}\frac{\rho_3}{\rho_2}\frac{\sin(\beta_3 + \frac{\pi}{2})}{\sin(\beta_2 + \frac{\pi}{2})}\frac{W_{max}}{W_2} \tag{44}$$

where Ω = streamtube contraction ratio or $(\rho_3 C_{3n})/(\rho_2 C_{2n})$. The $\pi/2$ radians added to each of the relative flow angles is a conversion since König *et al.* defined β_g as the angle between a normal to the axial direction and the blade chord.

The value of the velocity ratio in Equation (44) was determined by correlation. Lieblein deduced an incompressible, linear relationship based on the circulation parameter, Γ. For more modern blades that had a less cambered suction surface than the profiles considered by Lieblein, König *et al.* offered a parabolic relation. The appropriate equation to be used was determined by the value of Γ:

$$\left(\frac{W_{max}}{W_2}\right)_{inc} = 1.12 + 0.61\Gamma_{inc} \text{ for } \Gamma_{inc} > 0.2 \quad (45)$$

$$\left(\frac{W_{max}}{W_2}\right)_{inc} = 1.000 + 1.446\Gamma_{inc} - 1.180\Gamma_{inc}^2 \text{ for } \Gamma_{inc} \leq 0.2 \quad (46)$$

where

$$\Gamma_{inc} = \frac{2}{\sigma}\sin^2(\beta_2 + \frac{\pi}{2})\left[\Omega\frac{\rho_1}{\rho_2}\cot(\beta_3 + \frac{\pi}{2}) - \cot(\beta_2 + \frac{\pi}{2})\right] \quad (47)$$

and $_{inc}$ = incompressible. In this manner, D^*_{eq} is calculated within the subroutine entitled *verlustwsub.*

König *et al.* acknowledged the fact that Lieblein was successful in correlating wake momentum thickness with D^*_{eq}. However, they proposed two of their own correlations that were better suited for modern blade shapes. The two correlations were differentiated by the value of D^*_{eq}:

$$\left(\frac{\theta}{L}\right)^* = -0.0029 + 0.0071D^*_{eq} \text{ for } 1 \leq D^*_{eq} \leq 2 \quad (48)$$

$$\left(\frac{\theta}{L}\right)^* = 0.7111 - 0.7071D^*_{eq} + 0.1786D^{*2}_{eq} \text{ for } D^*_{eq} > 2 \quad (49)$$

These equations were also coded into the *verlustwsub* subroutine of TRANSROTOR. As will be shown, the acquired value of $(\theta/L)^*$ becomes an input into a correlation that relates the differences in on- and off-design wake momentum thicknesses and equivalent diffusion factors.

For determining deviation angles in the subsonic range, König *et al.* recommended the use of a singularity method published by U. Stark in 1987. Their apparent frustration in seeing little improvement upon deviation angle correlations over the past 40 years

motivated them to select this method which utilizes the capabilities of modern computers. König *et al.* discussed this method only by reference to Stark's paper rather than including the governing equations within their paper. The author of this thesis was unable to find an English version of the paper, which resulted in the exclusion of this deviation angle calculation method from the LM2 loss model. The LM1 loss model on- and off-design deviation correlations of Carter[18] and Creveling[23], respectively, were substituted.

5.3.1.2 Off-Design. The technique used in the LM2 loss model to determine the off-design total loss coefficient for subsonic streamtubes begins by computing the off-design equivalent diffusion factor, D_{eq}. This value is then used in the calculation of the off-design wake momentum thickness. A relation between wake momentum thickness and total pressure loss allows the off-design total pressure loss to be calculated. The correlations used to do this were given in König *et al.*[17] and are discussed below.

Equations (44) through (47) were revisited in the calculation of D_{eq}. In all cases, the inlet and exit flow angles corresponding to the minimum loss condition were replaced by the off-design or actual flow angles. Additionally, a shift was applied to Equations (45) and (46) to account for the incidence angle. Lieblein expressed this shift as

$$0.0117(\beta - \beta^*)^{1.43} \tag{50}$$

Although the two constants in Equation (50) were based on data from cascades with NACA-65 profiles, König *et al.* found them to be valid for the modern blade geometries examined in their research.

To calculate the off-design wake momentum thickness, König *et al.* selected a correlation published by Swan in 1961. It related the differences in on- and off-design wake momentum thicknesses and equivalent diffusion factors according to

$$\left(\frac{\theta}{L}\right) - \left(\frac{\theta}{L}\right)^* = K(D_{eq} - D_{eq}^*)^2 \tag{51}$$

where K = parabolic factor for differences in wake-momentum thickness.

Since Swan's work only dealt with blade rows of DCA profiles operating in the low subsonic range, Equation (51) had to be refined to account for arbitrary blade shapes and the effect of inlet Mach number. Using their cascade data, König *et al.* noted that the parabolic factor, K, reached a common minimum for all cascades below an inlet Mach number of approximately 0.5. For inlet Mach numbers greater than 0.5, the value of K began to rise exponentially once a particular Mach number was reached for a given blade geometry. This Mach number was referred to as the *blade-reference-Mach number.* König *et al.* proposed a function that incorporated these Mach number trends, as well as diffusion factor-based constants, to refine the parabolic factor:

$$K = c \cdot e^{d(M_2 - M_{ref})} \tag{52}$$

where

$$M_{ref} = -1.464\sqrt{\frac{w_{Seff}}{L}} + 1.043 \text{ for } \Delta D_{eq} < 0 \tag{53}$$

$$M_{ref} = -1.464\sqrt{\frac{w_{Seff}}{L}} + 1.198 \text{ for } \Delta D_{eq} > 0 \tag{54}$$

and

c = minimum value of K at low inlet Mach numbers

d = correction for rise of K

M_{ref} = blade-reference-Mach number

w_{Seff} = effective height of blade suction surface (Fig. 7)

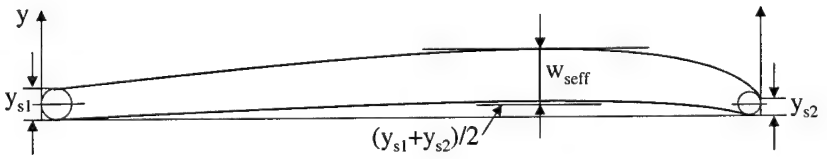

Figure 7 Effective Suction Side Height w_{Seff} of a Blade Shape

Figure 7 was reproduced from König *et al.*[17:75] to show the definition of w_{Seff}. The appropriate value for the constant c in Equation (52) was determined to be 0.032 and

0.016 for positive and negative values of ΔD_{eq}, respectively. The appropriate value for the exponent d in Equation (52) was determined to be 10.109 and 16.864 for positive and negative values of ΔD_{eq}, respectively. As can be seen by comparing Figures 1 and 7, the definition of f and w_{Seff} are slightly different. The mean height of the intersections of the suction surface with the LE and TE circles was used as the reference for w_{Seff}. The LE and TE circles were neglected in the blade profile definitions used in TRANSROTOR. Note that as the diameters of the circles approach zero, the definitions of f and w_{Seff} equalize. Since the diameters of the LE and TE circles of the TESCOM blading were quite small, the value of f was substituted for the value of w_{Seff} in Equations (53) and (54). Due to the extreme sensitivity of the value of K to the term $(M_2\text{-}M_{ref})$, K was limited to a maximum value of 0.84 in the LM2 loss model. In some cases, such a limit would be necessary to compensate for f being a poor approximation of w_{Seff}.

König *et al.* provided a Lieblein-derived relationship between wake momentum thickness and total pressure loss coefficient. This compressible, Q2D equation is used in the *verlustwsub* subroutine of the LM2 loss model to calculate the off-design total pressure loss in subsonic streamtubes:

$$\omega_w = \frac{P_{w2} - P_{w3}}{P_{w2} - P_2} = 2\left(\frac{\theta}{L}\right)\Omega^2\sigma\frac{\sin^2(\beta_2 + \frac{\pi}{2})}{\sin^3(\beta_3 + \frac{\pi}{2})}\frac{\rho_2}{\rho_3}\left(1 + \frac{\gamma - 1}{2}M_3^2\right)^{-\frac{1}{1-\gamma}} \tag{55}$$

5.3.2 Loss Correlations for Supersonic Flow. The LM2 loss model computes the total loss in a supersonic streamtube by summing a shock loss coefficient and a profile loss coefficient. König *et al.* surveyed a number of published shock loss models and came to the conclusion that the two-shock model of Gustafson (1975) best represented the actual flow situation noted for supersonic cascade inlet flow [6:81]. Since Gustafson's work [25] was with DCA-type blading, the original two-shock model was modified to be applicable to supersonic cascades with modern blade shapes. The flow features of this shock loss model that were of primary interest to the LM2 loss model included:

- a normal shock at the blade passage entrance with a λ shape due to interaction with the suction surface boundary layer
- flow reacceleration to supersonic velocities within the blade passage due to boundary layer thickening

- a normal shock close to the blade passage exit which decelerated the flow to subsonic velocities

Using Schlieren pictures and pressure distributions to visualize the flow, König *et al.* observed a two-shock system for all eight of the cascades they investigated.

As mentioned earlier, the supersonic profile loss correlation recommended by König *et al.* was the second correlation that could not be coded into TRANSROTOR. Multiple references were made to blade surface friction and wake-mixing losses and to the addition of these losses with the shock loss to determine the total loss [6:85]. However, only a brief section, entitled *Mixing of Blade Wakes*, was dedicated to discussing these other types of losses. A correlation for boundary-layer thickness at the passage exit was given but it was not related to a loss coefficient. Since the process by which König *et al.* determined viscous-type losses could not be confidently followed, the profile loss correlations from the LM1 loss model, Equations (41) and (42), were substituted.

5.3.2.1 Shock Loss. The total pressure ratio across a normal shock was presented in the LM1 shock loss discussion as Equation (40). A correction factor, P_{corr}, for the static pressure rise across a normal shock was introduced to account for the weakening of the shock by the shock-boundary-layer interaction:

$$\frac{\hat{P}_F}{\overline{P}_F} = 1 + \frac{2\gamma}{\gamma+1}(\overline{M}_{wF}^2 - 1) \cdot P_{corr} \tag{56}$$

where

$$P_{corr} = -0.5(\overline{M}_{wF} - 1) + 0.64 \tag{57}$$

and

$\hat{P}_F$ = static pressure just downstream of first passage shock

$\overline{P}_F$ = mass averaged static pressure just upstream of first passage shock

$\overline{M}_{wF}$ = average relative Mach number just upstream of first passage shock

The standard equations for a normal shock wave were used to find the relative Mach number just downstream of the first passage shock, $\hat{M}_{wF}$ [16:67].

The uniqueness of the modified two-shock model was the manner in which the Mach number just upstream of the second passage shock, M_{wJ}, was found. Since the LM2 loss model assumes the first shock is normal, the flow immediately behind the shock is subsonic. In order to have a second shock present, the flow must reaccelerate within the blade passage. König *et al.* described a technique to fictitiously accelerate the flow by means of a Laval-nozzle. The subroutine *passshock2* found in the LM2-version of TRANSROTOR was coded according to this technique. The entrance to a strictly divergent Laval-nozzle was given a flow cross section equal to the critical flow area, A*, based on $\hat{M}_{wF}$. To achieve acceleration through the divergent nozzle, Mach 1.0 flow must be assumed at the entrance. The exit area of the Laval-nozzle was set equal to the area of the blade passage entrance [6:85]. Following this logic, the Laval-nozzle area ratio can be expressed as

$$\frac{A_J}{A_F} \rightarrow \frac{A_F}{A^*} = f[\hat{M}_{wF}] \tag{58}$$

where

A_J = flow path cross section at location of second passage shock

A_F = flow path cross section at location of first passage shock

König *et al.* offered an equation that allowed M_{wJ} to be calculated iteratively as a function of area ratios, total pressure ratios, and total temperature ratios:

$$\frac{\left(1+\frac{\gamma-1}{2}M_{wJ}^2\right)^{\frac{\gamma+1}{2(\gamma-1)}}}{M_{wJ}} = \frac{\left(1+\frac{\gamma-1}{2}\hat{M}_{wF}^2\right)^{\frac{\gamma+1}{2(\gamma-1)}}}{\hat{M}_{wF}} \frac{A_J}{A_F}\frac{P_{wJ}}{\hat{P}_{wF}}\sqrt{\frac{\hat{T}_{wF}}{T_{wJ}}} \tag{59}$$

The appropriate value of the (A_J/A_F) term came from Equation (58). The radial shift of the streamlines through the compressor rotor was accounted for in the total temperature ratio term of Equation (59).

Once the value of M_{wJ} was known, Equations (40) and (56) were revisited to calculate the total and static pressures just downstream of the normal shock near the blade passage exit. Finally, the shock loss coefficient was written as

$$\omega_{shock} = \frac{\overline{P}_{w2} - \hat{P}_{wJ}}{\overline{P}_{w2} - P_2} \tag{60}$$

The subroutine entitled *kanalstoss* of the LM2-version of TRANSROTOR contains the coding of the entire shock loss process described above. The total loss coefficient for a supersonic streamtube is the summation of Equations (42) and (60).

5.3.2.2 Deviation Angle. König *et al.* discussed their selection of the best correlation for the exit flow angle, β_3. The results of their research showed that exit flow angles and mixing losses were best predicted when the direction of the exit flow was assumed to be parallel to the geometrical slope of the blade pressure surface (PS) at the trailing edge. The deviation angle was therefore equivalent to

$$\delta = \beta_{PS} - \beta_{m3} \tag{61}$$

where β_{PS} = angle between tangent to blade PS at TE and axial direction. The subroutine *carter2* was coded to calculate the deviation angle in supersonic streamtubes according to Equation (61).

5.4 The IGV Loss Model

A relatively simple correlation, known as *Soderberg's Correlation*, was included to model the loss from an optional IGV since IGV losses are generally small [24]. A further simplified version of this correlation, which was solely a function of the flow turning angle (ϵ) for a given ratio of d/L, was sufficient for the type of initial performance calculations done by TRANSROTOR [26:99]. The equation that can be found in the *verlustc* subroutine to calculate the IGV total loss coefficient is

$$\omega_c = 0.04 + 0.06\left(\frac{\epsilon}{100}\right)^2 \tag{62}$$

The TRANSROTOR subroutine *verlustc* contains a line of code that bypasses this correlation if ϵ equals 0. This allows the user to effectively eliminate the IGV by setting α_1 equal to α_2 for each streamtube. Since this research effort analyzed an isolated rotor, this technique was always used. Dixon provided some corrections to enhance this very simple method but the focus of this research effort did not warrant their inclusion.

VI. Results and Analyses

This chapter presents the results and analyses of the TRANSROTOR validation and parametric study objectives. The circumferentially averaged solutions generated by APNASA for the two TESCOM blade geometries were considered the benchmarks. Therefore, the validity of TRANSROTOR was evaluated relative to this 3D, viscous, Navier-Stokes-based CFD program. Overall rotor performance measures and spanwise distributions of flow properties were compared. BOWSHOCK, used for the blade geometry parametric study, was concurrently validated with TRANSROTOR since BOWSHOCK is, in essence, the supersonic portion of TRANSROTOR. BOWSHOCK and the LM1-version of TRANSROTOR share the same loss model. The parametric study of blade geometry accomplished using BOWSHOCK is discussed in relation to expected performance trends since no comparable study was available. The results of varying the four parameters that define MCA-profiles (Figure 1), as well as two rotor parameters, are presented.

6.1 TRANSROTOR Validation

The TRANSROTOR validation objective was accomplished by measuring the ability of the TRANSROTOR programs to predict the performance of a compressor rotor with specified blading and upstream flow conditions. The results in this section are presented in two ways - tabulated overall rotor performance measures and plotted spanwise distributions of flow properties. Mass averaged isentropic efficiency, total pressure ratio, and static pressure ratio describe the general performance of the compressor rotor while spanwise distributions of flow properties provide a more detailed look at blade performance. By comparing the TRANSROTOR generated solutions to the APNASA benchmarks, a determination of the validity of both TRANSROTOR versions was made.

6.1.1 Rotor Performance Measures. Table 3 presents the mass averaged isentropic efficiency, total pressure ratio, and static pressure ratio predicted by both versions of TRANSROTOR for the following case:

- APNASA flow properties at 1.05·L upstream of the blade LE used as station 1 input
- original TESCOM blade geometry

The APNASA values are included in the last row of the table.

Table 3 Rotor Performance - Station 1 Defined by APNASA Flow Properties 1.05·L Upstream of Blade LE, Original Blade

Program	η_{is} (%)	P_{c3}/P_{c2}	Error (%)	P_3/P_2	Error (%)
TRANS-LM1	90.1	1.845	1.5	1.487	6.5
TRANS-LM2	86.4	1.744	-4.1	1.408	0.8
APNASA	87.3	1.819	-	1.397	-

For ease of comparison with Table 3, Table 4 is immediately given. Table 4 presents the mass averaged isentropic efficiency, total pressure ratio, and static pressure ratio predicted by both versions of TRANSROTOR for the following case:

- APNASA flow properties at 0.15·L upstream of the blade LE indirectly inserted as station 2 input
- original TESCOM blade geometry

The APNASA values are included in the last row of the table.

Table 4 Rotor Performance - Station 2 Indirectly Defined by APNASA Flow Properties 0.15·L Upstream of Blade LE, Original Blade

Program	η_{is} (%)	P_{c3}/P_{c2}	Error (%)	P_3/P_2	Error (%)
TRANS-LM1	90.4	1.831	0.7	1.490	6.7
TRANS-LM2	87.4	1.737	-4.5	1.423	1.9
APNASA	87.3	1.819	-	1.397	-

Three evaluations were made of the data contained in these two tables. First, the accuracy of the TRANSROTOR program in predicting the performance of the second-stage transonic TESCOM rotor with original blading was determined. This was quantified as a difference or percent error from the benchmark APNASA values. Second, the differences between the LM1 and LM2 loss models were highlighted by comparing both TRANSROTOR predicted values for each performance measure. Third, the effect of running TRANSROTOR using known flow properties at station 1 versus station 2 was quantified. The following discussions address the results of these three evaluations. Only the original blade geometry is considered here.

As can be seen in Tables 3 and 4, all values predicted by either version of TRANSROTOR are within seven-percent of the corresponding APNASA values. The largest difference between a TRANSROTOR predicted value of isentropic efficiency and the APNASA benchmark is 3.1-percent. The largest percent errors of predicted values for total pressure ratio and static pressure ratio are -4.5-percent and 6.7-percent, respectively. These outlying values are quite indicative of the relative strengths and weaknesses of the two loss models. However, the intent of this first evaluation is only to show the general accuracy of TRANSROTOR as a transonic rotor analysis program, regardless of the loss model version. Considering the relative simplicity of the TRANSROTOR programs and the complexity of the flow field within transonic compressors, this level of agreement is within expectations. This is a promising indication that the TRANSROTOR program has potential to be used as a preliminary design tool.

Now that the general accuracy of TRANSROTOR has been stated, an evaluation of the two different loss models is appropriate. Since the differences between the LM1 and LM2 loss models hold true for both tables, it is unnecessary to consider the values in both tables. Therefore, Table 3 was arbitrarily chosen as the representative table to which numerical references are made. Distinct differences between the LM1 and LM2 loss models manifested themselves in the values of all three rotor performance measures.

The isentropic efficiency predicted by the LM2 loss model is 3.7-percent lower than the LM1 loss model. Because the premise of the LM2 loss model is a two-shock system within the blade passage and both are modeled as normal shocks, it would tend to predict a lower efficiency for a transonic rotor than a single passage shock loss model such as the LM1 loss model. Since isentropic efficiency is a function of the total pressure loss through the rotor [Equations (20) and (23)], the LM2 loss model is expected to predict this rotor performance measure more accurately. It accounts for total pressure losses across two passage shocks which agrees with the two passage shocks noted in the APNASA solution for this blade geometry. The LM2 loss model predicted a value within one efficiency percentage point of the APNASA value. This level of extreme accuracy is questionable due to the multitude of flow phenomena that TRANSROTOR either neglects or approximates. Additionally, the poor agreement in total pressure ratio between this loss model and APNASA

had to have been compensated for in the calculation of isentropic efficiency. Equation (20) indicates that the total temperature ratio, T_{c3}/T_{c2} , must have compensated. The efficiency overprediction by the LM1 loss model is, in part, attributed to the assumption of a single shock. The total pressure ratio discussion in the next paragraph further addresses the differences in these two loss models that contributed to the efficiency predictions.

The total pressure ratios shown in Table 3 exemplify the different manner in which the loss coefficients and deviation angles are calculated between the two loss models for supersonic streamtubes. The value of P_{c3}/P_{c2} predicted by the LM2 loss model is appreciably lower than the value predicted by the LM1 loss model and APNASA. The two-shock system and the geometrically fixed exit flow direction recommended by König *et al.* combined to drive the total pressure ratio lower than the LM1 loss model. As discussed in the previous paragraph, a total pressure loss is incurred for each of the two shocks. Even more significant is the König *et al.* correlation that fixes the direction of the exit flow to the geometrical slope of the blade PS at the trailing edge, Equation (61). Due to this correlation, the LM2 loss model predicted a higher deviation of the flow than the LM1 loss model. A higher deviation angle corresponds to less turning of the flow, and therefore, a lower pressure ratio across the rotor as seen in Equation (23). Although the loss models share the same deviation correlation for subsonic streamtubes, 70-percent of the blade span of this rotor has supersonic relative inlet flow. The subsonic correlations contributed little to the overall performance predictions. The -4.5-percent error in total pressure ratio sheds doubt on the assumption that the exiting flow remains parallel to the pressure side at the trailing edge. A more in-depth look at the results of this assumption is taken in the next section of this chapter.

Contrary to the poor performance of the LM2 loss model, the LM1 loss model predicted the total pressure ratio well - a 1.5-percent error. This attests to the weighting of relative total pressure loss and flow turning in the calculation of total pressure ratio. A more severe overprediction of P_{c3}/P_{c2} due to accounting for only a single passage shock was moderated by good agreement between the LM1 loss model and APNASA relative exit flow angles. An excellent match in mass averaged total temperature ratio contributed to this as well.

The LM2 loss model shows better results than the LM1 loss model for static pressure ratio. The LM2 loss model employs a static pressure correlation that has a strong conceptual basis. As was presented in Chapter V, König *et al.* applied a correction to the standard equation for the static pressure rise across a normal shock, Equation (57). Their justification for doing so was to account for the shock-boundary-layer interaction on the suction surface of the blade that weakens the shock and reduces the static pressure rise. This is a plausible flow feature within the TESCOM second rotor. However, the static pressure rise correction recommended by König *et al.* cannot be credited with the less than one-percent error in the LM2 loss model value of static pressure rise. Such tremendous accuracy must be questioned due to the simplicity of the analysis program. Isentropic relationships show that, for a given Mach number, static pressure drops with total pressure. A portion of this apparent accuracy in predicting static pressure ratio, therefore, must be attributed to the underprediction in total pressure ratio. While the extremely low percent error may be coincidental, the underlying concept is valid. In contrast, the 1.487 value of P_3/P_2 shown in Table 3 for the LM1 loss model, which is 6.5-percent higher than the APNASA value, is based on the basic equations for a normal shock.

The results shown in Table 3 are influenced by the manner in which TRANSROTOR calculates the flow properties at station 2 from the input flow properties at station 1. Since the optional IGV was removed by matching the inlet and exit flow angles, the flow was effectively passed through an isentropic converging duct between stations 1 and 2. Some amount of error is introduced by this simplistic treatment of the flow path. Viscous effects at the hub and tip would promote boundary layer growth. Results that were independent of this simplistic treatment of the flow path between stations 1 and 2 were sought by attempting to match APNASA flow properties just upstream of the detached shock. It was hypothesized that such a set of results would be the optimum results that could be expected from TRANSROTOR.

A comparison between the values in Table 3 and Table 4 shows that significant improvement in the predicted values is not realized by attempting to match APNASA flow properties at station 2. In fact, some predicted values are further from the APNASA benchmarks. A combination of factors caused such an unintuitive result. First, the sim-

plistic treatment of the flow path between stations 1 and 2 by TRANSROTOR was not as poor of an approximation as anticipated. This explains why the values in the two tables are very close. Second, the need to reduce 51 spanwise APNASA data points into a representative five as the flow property inputs into TRANSROTOR introduced some error. The sources of most of this error were the first and fifth streamtubes for which the lower and upper 20-percent of the APNASA data, respectively, had to be span-averaged. The quickly changing flow properties near the walls due to viscosity made these two inputs gross approximations of the APNASA data. The error introduced at station 2 by this span-averaging could exceed the error introduced by the simplistic treatment of the flow path from station 1 to station 2, thus degrading some predicted values. The next section of this chapter is dedicated to examining the spanwise distribution of flow properties. The result of span-averaging can be seen more clearly in the figures presented in that section.

The above three evaluations quantified the accuracy of the TRANSROTOR programs, the differences between the LM1 and LM2 loss models, and the effect of inputting flow properties at station 1 versus station 2. All of these evaluations were based on TRANSROTOR results for the original blade geometry. The same three evaluations, conducted using the TM1 blade geometry, yielded similar results. To avoid redundancy, a dedicated discussion of the TM1 blade geometry results was omitted. However, a fourth evaluation of TRANSROTOR is possible by comparing the predicted performance measures of the original blade to those of the TM1 blade. Such a comparison determines the ability of TRANSROTOR to identify trends in performance measures for different blading. Table 5 presents the mass averaged isentropic efficiency, total pressure ratio, and static pressure ratio predicted by both versions of TRANSROTOR for the following case:

- APNASA flow properties at 1.05·L upstream of the blade LE used as station 1 input
- TM1 TESCOM blade geometry

The APNASA values are included in the last row of the table.

For ease of comparison with Table 5, Table 6 is immediately given. Table 6 presents the mass averaged isentropic efficiency, total pressure ratio, and static pressure ratio predicted by both versions of TRANSROTOR for the following case:

Table 5 Rotor Performance - Station 1 Defined by APNASA Flow Properties 1.05·L Upstream of Blade LE, TM1 Blade

Program	η_{is} (%)	P_{c3}/P_{c2}	Error (%)	P_3/P_2	Error (%)
TRANS-LM1	90.3	1.850	-1.1	1.487	4.9
TRANS-LM2	86.5	1.725	-7.8	1.394	-1.6
APNASA	86.8	1.871	-	1.417	-

- APNASA flow properties at 0.15·L upstream of the blade LE indirectly inserted as station 2 input
- TM1 TESCOM blade geometry

The APNASA values are included in the last row of the table.

Table 6 Rotor Performance - Station 2 Indirectly Defined by APNASA Flow Properties 0.15·L Upstream of Blade LE, TM1 Blade

Program	η_{is} (%)	P_{c3}/P_{c2}	Error (%)	P_3/P_2	Error (%)
TRANS-LM1	91.6	1.847	-1.3	1.500	5.9
TRANS-LM2	88.9	1.742	-6.9	1.430	0.9
APNASA	86.8	1.871	-	1.417	-

A comparison of Table 3 with Table 5 and Table 4 with Table 6 reveals that neither version of TRANSROTOR matched the APNASA trend in the three rotor performance measures well. Tables 7 and 8 quantify the predicted trends of the three performance measures by the three programs. The values in these tables were calculated using the original blade tables as the baseline. A positive value indicates that the TM1 geometry caused the parameter value to increase. Trends in η_{is} are reported as differences whereas trends in P_{c3}/P_{c2} and P_3/P_2 are reported as percent differences.

Table 7 Rotor Performance Trends Due to Changes in Blade Geometry - Comparison of Tables 3 and 5

Program	$\Delta\eta_{is}$ (%)	P_{c3}/P_{c2} Pct Diff. (%)	P_3/P_2 Pct Diff. (%)
TRANS-LM1	0.25	0.25	0.01
TRANS-LM2	0.04	-1.10	-0.94
APNASA	-0.48	2.87	1.47

Table 8 Rotor Performance Trends Due to Changes in Blade Geometry - Comparison of Tables 4 and 6

Program	$\Delta\eta_{is}$ (%)	P_{c3}/P_{c2} Pct Diff. (%)	P_3/P_2 Pct Diff. (%)
TRANS-LM1	1.14	0.90	0.69
TRANS-LM2	1.50	0.27	0.47
APNASA	-0.48	2.87	1.47

In general, the LM1-version of TRANSROTOR is slightly better at matching the APNASA trends, especially the pressure ratios. Neither loss model, whether APNASA flow conditions were matched at station 1 or indirectly input at station 2, predicted a drop in efficiency from the original to the TM1 blade. The expectation of TRANSROTOR to accurately model the TESCOM blade-induced rotor performance trends may have been unrealistic. The APNASA benchmark trend values show that the actual performance changes between blade geometries are very small. The largest change in a performance measure is a 2.87-percent increase in total pressure ratio. This subtle change in performance is well within the demonstrated four-percent accuracy error of the LM2 loss model. The fact that the accuracy error of the program exceeds the percent difference in the performance measure it is trying to predict explains the lack of agreement in even the direction of the trends, increase or decrease. Additionally, small geometrical differences between two 3D, solid compressor blades could be largely missed by TRANSROTOR because of the blade profile input allowances. A maximum of seven 2D streamline cuts taken at intervals along the blade span must accurately represent the actual blade.

In summary, four evaluations were performed on the TRANSROTOR solution data to validate various aspects of these programs. These evaluations focused on the prediction of η_{is}, P_{c3}/P_{c2} , and P_3/P_2 , which are measures of overall rotor performance. The most significant results were:

- An examination of all results, including both loss models and both blade geometries, revealed that the largest error was a 7.8-percent underprediction in total pressure ratio. This data point can be seen in Table 5. This level of accuracy was within the expectations of a relatively simple compressor rotor analysis program based on a collection of correlations.

- The two-shock premise of the LM2 loss model and the assumption that the flow at the exit plane of the rotor was parallel to the pressure surface at the blade TE resulted in lower predicted values of isentropic efficiency and total pressure ratio.
- The single shock premise of LM1 loss model and the use of Carter's Rule to predict deviation angle resulted in higher predicted values of isentropic efficiency and total pressure ratio.
- The LM2 loss model correlation that reduced the static pressure rise achieved across a normal shock improved results.
- The TRANSROTOR solutions were only marginally affected by the station at which APNASA flow properties were input. Recall that the optional IGV between stations 1 and 2 was eliminated for this research.
- It is possible for the error band associated with the simplicity of TRANSROTOR to overwhelm small changes in blade and/or rotor geometry.

More detailed insight into the accuracy of each version of the TRANSROTOR program was achieved by comparing the spanwise distribution of individual flow properties to the APNASA benchmark distributions. The results of this analysis are presented next.

6.1.2 Spanwise Distribution of Flow Properties. As described in previous chapters, TRANSROTOR is an iterative program that calculates flow properties at the inlet (station 2) and exit (station 3) of successive streamtubes that divide the flow path. After convergence to a solution, the appropriate flow property values of all streamtubes are mass averaged to determine overall rotor performance, such as η_{is}, P_{c3}/P_{c2} , and P_3/P_2. An examination of the individual flow property values that contributed to these overall performance measures confirmed the strengths and weaknesses of the TRANSROTOR programs. In this section, the spanwise distribution of flow properties at stations 2 and 3 calculated by both versions of TRANSROTOR are plotted with the APNASA benchmark distributions. The results of the original blade analysis are presented first followed by the TM1 blade analysis. This was the second approach taken to determine the validity of both TRANSROTOR versions.

6.1.2.1 Station 2. In a physical sense, the flow conditions at station 2 are the flow conditions just upstream of the blade LE and, at supersonic span locations, just upstream of the shock. In a TRANSROTOR-computational sense, these flow conditions are the boundary conditions for every calculation and correlation related to the compressor

rotor. The manner in which TRANSROTOR determines the flow properties at station 2 ultimately influences the accuracy of its solutions. Since the only difference between the two versions of TRANSROTOR is the rotor loss model, all calculations performed up to station 2 are identical. Therefore, the comparisons of interest at this station are between the two TRANSROTOR data input techniques and the APNASA data. Figure 8 presents the spanwise distribution of flow properties at station 2 for the original blade geometry. The curve representing the case where APNASA flow properties at 1.05·L upstream of the blade LE were used as station 1 input is designated as *TRANSROTOR 1.05L* in the legend. The curve representing the case where APNASA flow properties at 0.15·L upstream of the blade LE were indirectly inserted as station 2 input is designated as *TRANSROTOR 0.15L* in the legend.

In Figure 8(a), the APNASA curve shows a static pressure gradient along the span whereas both TRANSROTOR curves indicate a constant pressure. This discrepancy was caused by the combination of two factors - the manner in which radial equilibrium is established within the TRANSROTOR subroutine *radgleich* and a nearly axial inlet flow. A station span-averaged static pressure is initially calculated to serve as a starting point from which Equation (1) is used to determine the static pressure in individual streamtubes. Since the incoming flow to this isolated rotor is nearly axial across the entire span, the C_u term in Equation (1) is approximately zero. Therefore, no gradient is calculated by TRANSROTOR. The effect of these two factors can also be seen in the axial velocity curves [Figure 8(b)] and the absolute Mach number curves [Figure 8(g)].

A comparison of the TRANSROTOR absolute total pressure curves in Figure 8(c) highlights the differences caused by inputting APNASA flow properties at station 1 versus station 2. At 1.05·L upstream of the blade LE in the APNASA solution data, the total pressure across the entire flow path was a constant 2.42 bar. Since the only loss mechanism TRANSROTOR models between station 1 and station 2 (IGV) was not used in this research, the distribution of total pressure remained constant. It is easy to see that the viscous effects at the walls are not taken into account using this input technique. In comparison, the second input technique was an attempt to capture changes in total pressure between stations 1 and 2. The APNASA curve in Figure 8(c) is the actual total

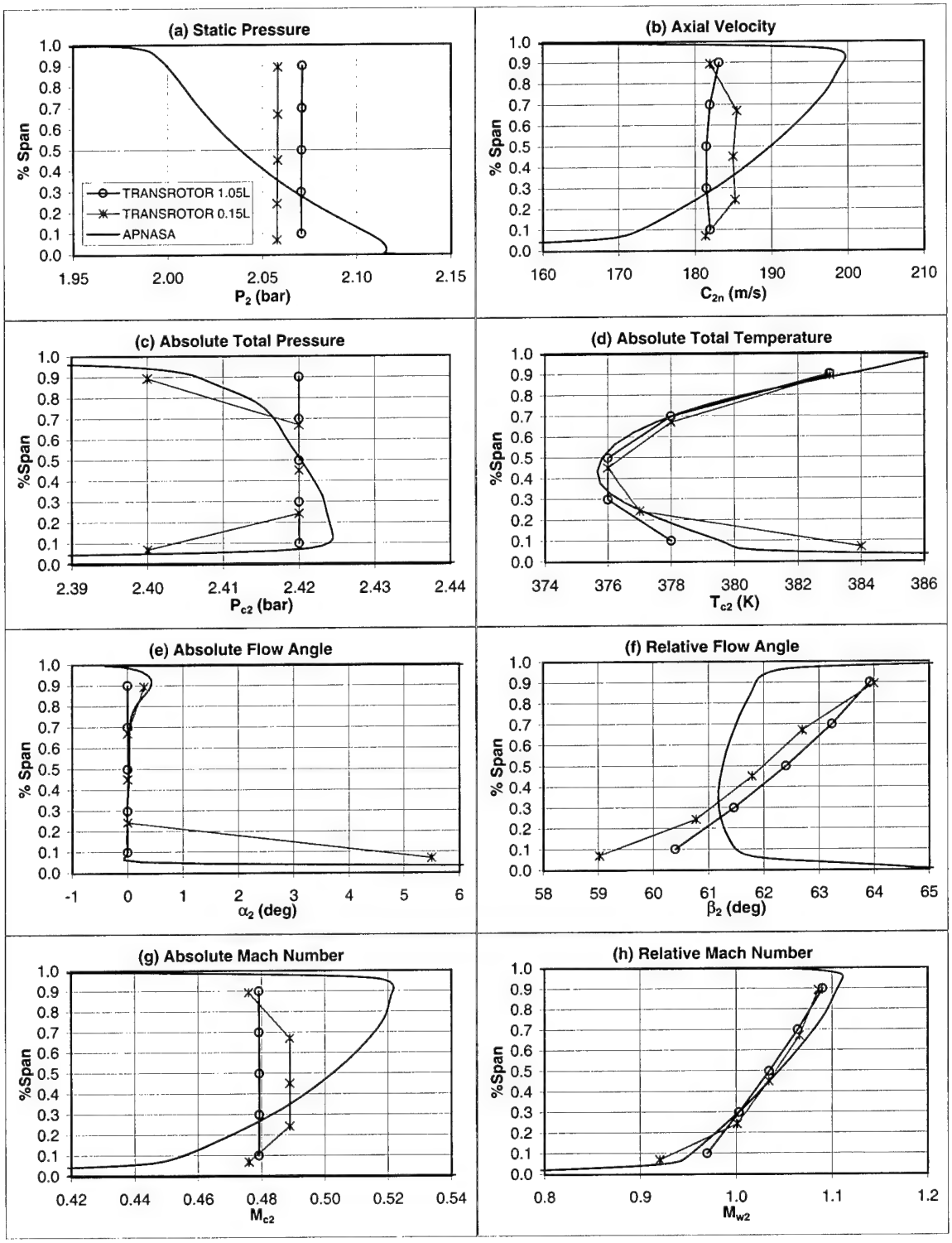

Figure 8 Station 2 Spanwise Distribution of Flow Properties - Original Blade

pressure ratio distribution at 0.15·L upstream of the blade LE. Therefore, the *TRANSROTOR 0.15L* curve represents the span-averaged, five-point approximation of the APNASA curve rounded to the nearest hundredth of a bar. As discussed in the previous section, this method is also prone to error. For example, the first and fifth data points are a very rough approximation of the total pressure in the lower and upper 20-percent of the flow path. The differences in the TRANSROTOR curves in Figures 8(d) and 8(e) were caused by the same data input technique issues. T_{c2} and α_2 are absolute quantities and, thus, unaffected by the manner in which TRANSROTOR develops the flow from station 1 to station 2.

Finally, Figures 8(f) and 8(h) present flow properties in the relative frame. As can be seen in Figure 8(f), the spanwise distributions of relative flow angle calculated by TRANSROTOR show a steady increase with span. This trend is also a result of the two factors that caused the static pressure discrepancy. If the axial velocity along the span is nearly constant, then an increase in blade speed, U, associated with moving closer to the blade tip results in a larger relative flow angle. A similar trend is not observed in the APNASA data because the axial velocity is increasing with span so the relative flow angle remains nearly constant. Good agreement between both TRANSROTOR curves and the APNASA curve for relative Mach number is shown in Figure 8(h). The relative flow velocities, W, are not greatly affected by the discrepancy in axial velocity. The minor affect that the axial velocity did have on relative Mach number can be seen in Figure 8(h) by the way in which the TRANSROTOR curves traverse the APNASA curve.

The results of the TM1 blade analysis were the same at station 2. This was expected since station 2 is at an axial location upstream of the rotor. The blades have not yet interacted with the flow. Figure 9 is presented for completeness. The minor differences noted between Figures 8 and 9 are due to slightly different mass flow rates, 11.63 lbm/s and 11.87 lbm/s respectively.

6.1.2.2 Station 3. While the axial location of station 3 within TRANSROTOR is adjustable by the program user, it best represents the exit plane of the rotor. TRANSROTOR does not contain a subroutine that adjusts the properties of the flow as a function of downstream distance from the blade TE. The spanwise distribution of flow

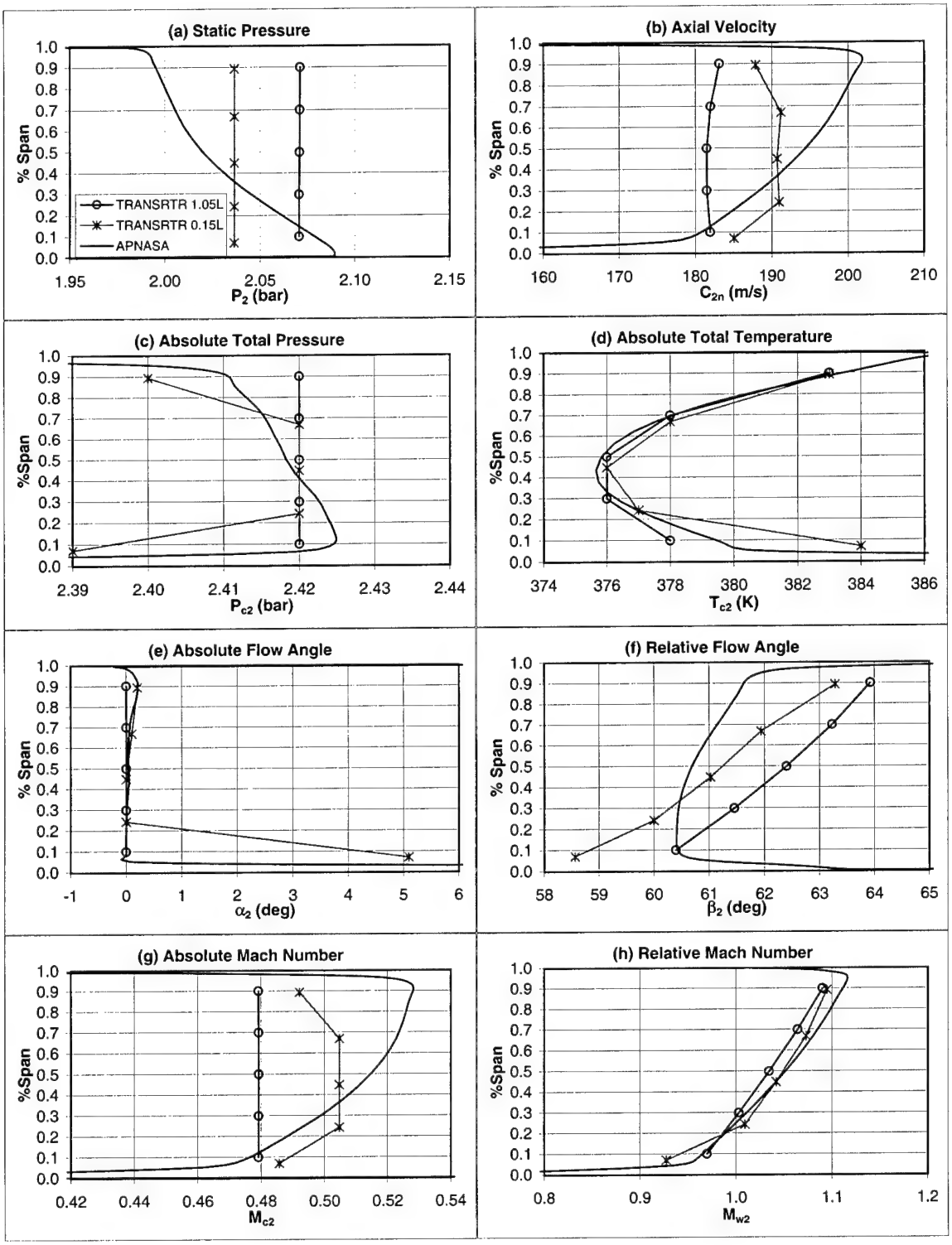

Figure 9 Station 2 Spanwise Distribution of Flow Properties - TM1 Blade

properties at station 3 gives the most detailed insight into the accuracy of each loss model version of TRANSROTOR, as well as the effect of the two input techniques on the exit flow properties. Figure 10 presents the spanwise distribution of flow properties at station 3 calculated by both versions of TRANSROTOR for the following case:

- APNASA flow properties at 1.05·L upstream of the blade LE used as station 1 input
- original TESCOM blade geometry

The APNASA benchmark distributions are also plotted. The curves representing the LM1- and LM2-versions of TRANSROTOR are designated as *TRANSROTOR-LM1* and *TRANSROTOR-LM2*, respectively, in the legend.

It is important to note that for the original blading, both versions of TRANSROTOR analyzed the first and second streamtubes as subsonic and the remaining three as supersonic. The separate treatment of streamtubes that have subsonic and supersonic relative inlet Mach numbers can result in abrupt property changes along the span. The transition between these flow regimes is most evident in the distribution of axial velocity [Figure 10(b)], absolute flow angle [Figure 10(e)], and relative Mach number [Figure 10(h)]. König *et al.* discuss this possibility for their model [6:86]. They also state that the manner in which losses are treated by the model of Çetin *et al.* avoids this issue. As is evident in the three aforementioned figures, the LM1 loss model has the potential for transition discontinuities due to its departure from the Çetin *et al.* loss model.

Of the flow properties presented, the absolute total pressure and relative flow angle at the exit are most directly affected by the differences in the loss models. These parameters are examined first. Figure 10(c) shows that both loss models predicted a spanwise trend in total pressure that approximates the APNASA trend, although neither predicted the local minimum at 30-percent span seen in the APNASA data. The viscous effects at the walls are quite clear in the APNASA curve. The first and fifth data points of the TRANSROTOR curves appear to be gross averages of these regions. While the spanwise trend in total pressure is similar between the two loss models, the magnitudes are quite different. The LM1 loss model agrees better with the APNASA benchmark by predicting a higher value of P_{c3} than the LM2 loss model at all locations. This is evidence that the subsonic and supersonic loss correlations of the LM2 loss model contributed to the overall

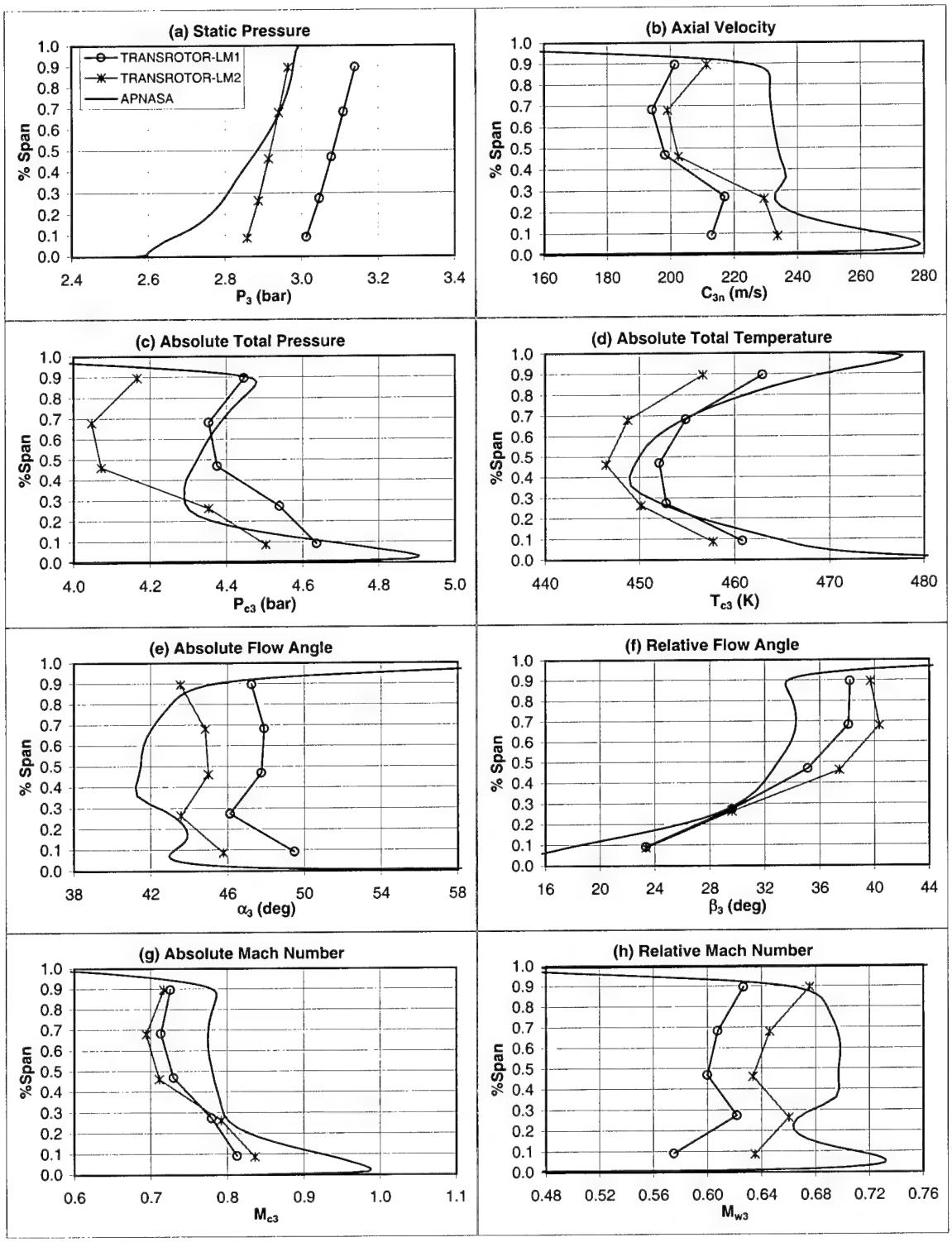

Figure 10 Station 3 Spanwise Distribution of Flow Properties - Station 1 Defined by APNASA Flow Properties 1.05·L Upstream of Blade LE, Original Blade

underprediction of total pressure ratio. Note that the lower two data points calculated by the two TRANSROTOR versions are closer in magnitude than the upper three data points. As discussed in Chapter V, the subsonic portion of the LM2 loss model was coded with the deviation angle correlation of the LM1 loss model. The direct affect of this shared correlation can be seen in the relative exit flow angle.

The TRANSROTOR distributions of relative flow angle shown in Figure 10(f) also exhibit trends that are in good agreement with the APNASA trend. However, both loss models show increasing overprediction with span for the supersonic streamtubes, with the LM2 loss model showing greater overprediction. The use of the Carter (32) and Creveling (36) deviation correlations in the LM1 loss model gave better results than the use of the König *et al.* geometrically fixed deviation correlation, Equation (61). As discussed in the *Rotor Performance Measures* section of this chapter, this five- to six-degree overprediction in relative exit flow angle was largely responsible for the overall total pressure ratio underprediction by the LM2 loss model. Both loss models calculate identical values for the two data points nearest the hub because they employ the same deviation correlation for subsonic streamtubes.

Figure 10(a) shows in greater detail why the LM2 loss model predicted a more accurate static pressure ratio than the LM1 loss model. It should be stated again that the level of agreement between the LM2-version of TRANSROTOR and APNASA is deceptively high. Had the total pressure prediction by TRANSROTOR been more accurate, the corresponding increase in static pressure would have shifted the TRANSROTOR-LM2 curve away from the APNASA curve. The boundary-layer-shock interaction correlation given by König *et al.* [Equation (56)] is still a modeling improvement to the standard normal shock relations used in the LM1 loss model. Both models show slightly less rates of increase in static pressure with span than APNASA. This can be attributed to the nearly constant static pressure computed by TRANSROTOR at station 2 [Figure 8(a)], as well as the radial equilibrium subroutine invoked at station 3.

Of the six flow properties plotted in Figure 10, TRANSROTOR appears to have the most difficulty modeling axial velocity (b), absolute flow angle (e), and relative Mach number (h). The trends predicted by both versions of TRANSROTOR are almost mirror images

of the corresponding APNASA trends. No single source was identified as the predominant cause of the point-to-point discrepancies between TRANSROTOR and APNASA. However, for computational purposes, the relative Mach number is the most fundamental flow property of the three. TRANSROTOR acquires the relative Mach number at each station based on the progression of flux density from station to station. The other two flow properties are then calculated at each station according to velocity triangle relationships. The similarities in the trends of these three parameters attest to their interdependence. Figure 10(h) shows that the LM2-version of TRANSROTOR predicted higher relative Mach numbers along the entire span than the LM1-version of TRANSROTOR. This result was caused by the affect of relative total pressure loss on the calculation of relative Mach number. The higher pressure losses predicted by the LM2 loss model corresponded to higher relative Mach numbers. The rapid change in all three flow properties that occurs just below 30-percent span is attributed to the transition between supersonic and subsonic flow. Note that the APNASA curves also show rapid changes at that approximate span location.

The spanwise distribution of absolute Mach number shown in Figure 10(g) compares better with the APNASA benchmark than the three previous flow properties. The spanwise trend approximates the APNASA trend even though absolute velocity, C, is also subject to velocity triangle relationships. This dubious improvement can be explained by offsetting errors in axial velocity and absolute flow angle. Both versions of TRANSROTOR underpredict the absolute Mach number. The amount of error seen in the third and fourth streamtubes corresponds with the majority of the error seen in the prediction of relative Mach number, as well as axial velocity and absolute flow angle. The large error of the first data points confirm that, regardless of the loss model, TRANSROTOR cannot capture the complexities of the flow very near the wall.

Finally, total temperature is modeled extremely well by both versions of TRANSROTOR. The calculated spanwise trends match the APNASA trend - the minimum temperature near 40-percent span with an almost symmetric rise in temperature as the span location approaches the hub and tip. Both versions of TRANSROTOR are within three-percent of the APNASA values for all streamtubes. Such good agreement is expected since the total temperature rise in a compressor is simply a function of the work, as shown

in the following form of Euler's equation.

$$T_{w3} = T_{w2} + \frac{U_3^2 - U_2^2}{2C_p} \tag{63}$$

Note that Equation (63) is in the relative frame. The two loss models cause slightly different radial displacements of streamtubes which is accounted for by Equation (63). The differences in magnitude between the LM1- and LM2-curves of T_{c3} in Figure 10(d) are primarily caused by the subsequent change in reference frame.

Now that the spanwise distribution of flow properties predicted by both versions of TRANSROTOR at station 3 have been thoroughly examined for the original blade geometry, the results and analyses of the three remaining cases focus on how the prediction of flow properties differ from this baseline case. The three remaining cases are: the TM1 blade geometry with APNASA flow properties at 1.05·L upstream of the blade LE used as station 1 input, the original blade geometry with APNASA flow properties at 0.15·L upstream of the blade LE indirectly inserted as station 2 input, and the TM1 blade geometry with APNASA flow properties at 0.15·L upstream of the blade LE indirectly inserted as station 2 input. In all three cases, this data presentation technique offers a more detailed look at how TRANSROTOR responded to these subtle changes.

Other than the difference in blade geometry, there was one critical difference in the way TRANSROTOR analyzed the TM1 blade as compared to the original blade that caused much of the changes in station 3 flow properties. Recall that for the original blade, the logic of the program determined the first and second streamtubes to be subsonic. For the TM1 blade, only the first streamtube was considered subsonic. The fact that approximately 20-percent more of the blade span was analyzed as supersonic flow contributed significantly to the differences between these two cases. Little can be said as to which flow property changes were caused by the change in blade geometry and which were caused by the change in streamtube treatment. Figure 11 presents the spanwise distribution of flow properties at station 3 calculated by both versions of TRANSROTOR for the following case:

- APNASA flow properties at 1.05·L upstream of the blade LE used as station 1 input
- TM1 TESCOM blade geometry

The APNASA benchmark distributions are also plotted.

The most noticeable difference between Figures 10 and 11 is the absence of abrupt flow property changes just below 30-percent span in Figure 11. This is one change that can be linked to the treatment of the second streamtube as supersonic for the TM1 blade case. Note that the APNASA curves also lack rapid changes at that approximate span location. In addition to eliminating the discontinuity at 30-percent span, the change in blade geometry also caused both versions of TRANSROTOR to predict more linear spanwise distributions of axial velocity [Figure 11(b)], absolute flow angle [Figure 11(e)], and relative Mach number [Figure 11(h)]. This resulted in better agreement between TRANSROTOR and APNASA in axial velocity for the TM1 blade case. In this sense, TRANSROTOR responded well to the change in blade geometry. However, the same cannot be said for absolute flow angle and relative Mach number. As can be seen in Figure 11(e) and (h), the slope of these linear distributions results in over- or underpredictions at the outer span locations. For relative Mach number, the errors of the first and last data points reach 20-percent for both loss models. Because the TRANSROTOR predicted distributions traverse the APNASA distributions, averaged quantities would still show good agreement. This is why the spanwise distributions of flow properties are important for complete understanding of the accuracy of the loss models.

Table 7 showed that the LM2 loss model predicted a drop in total pressure ratio from the original blade to the TM1 blade. This was the opposite trend predicted by the LM1 loss model and APNASA. The underlying reason for these trends is clarified by comparing the spanwise distributions of flow properties at station 3, specifically relative exit flow angle and absolute total pressure. A comparison of Figure 10(f) and Figure 11(f) shows that a small overall decrease in APNASA β_3 resulted in even smaller overall decreases by both versions TRANSROTOR. This alone would cause both loss models to predict a small rise in total pressure ratio. Since the LM2 loss model predicted a drop in total pressure ratio, a larger increase in predicted pressure losses must have more than offset the decrease in β_3. A comparison of Figure 10(c) and Figure 11(c) confirms this hypothesis. The second

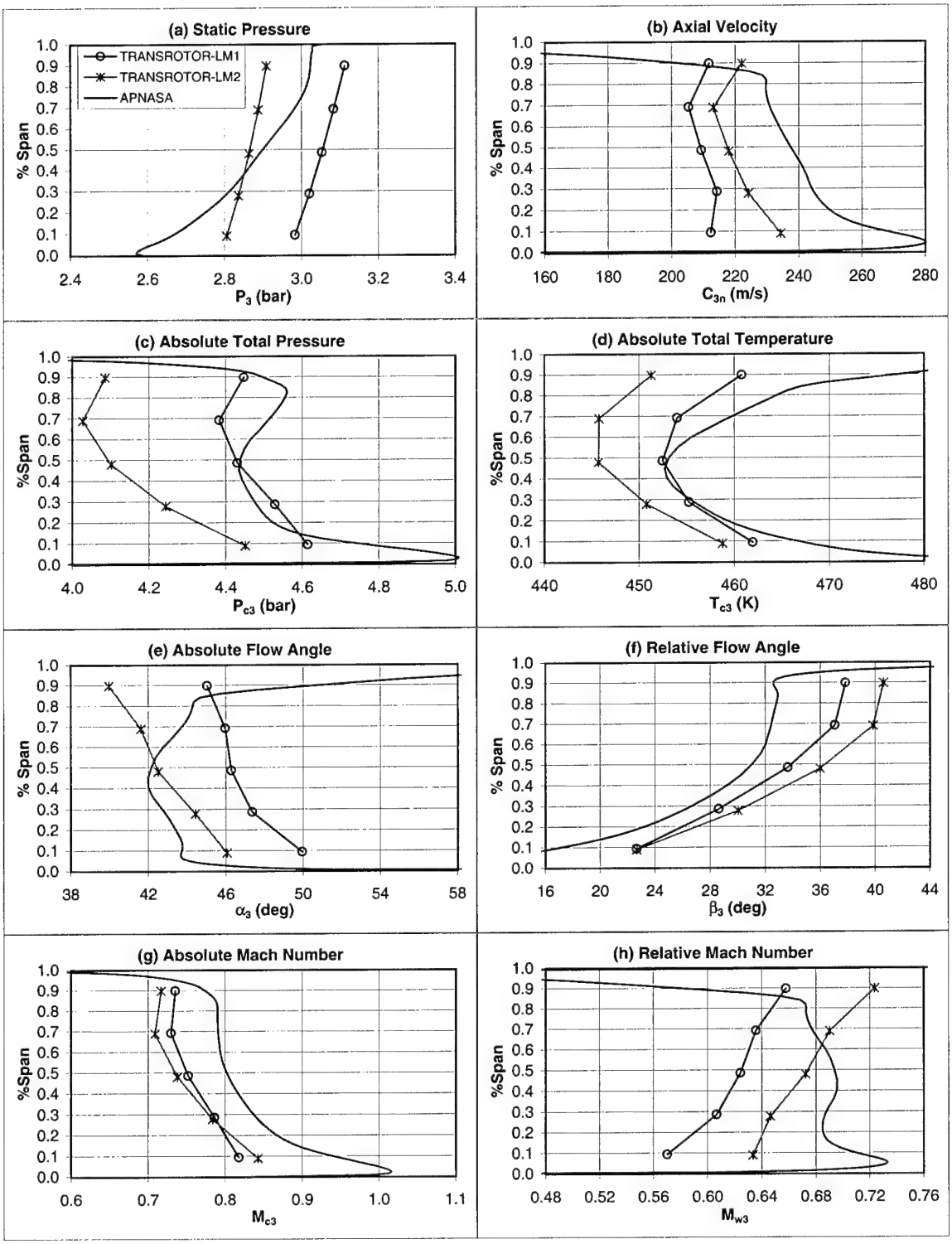

Figure 11 Station 3 Spanwise Distribution of Flow Properties - Station 1 Defined by APNASA Flow Properties 1.05·L Upstream of Blade LE, TM1 Blade

streamtube has the largest difference between LM2-predicted total pressure data points. This is the streamtube that was analyzed as a subsonic streamtube for the original blade and as a supersonic streamtube for the TM1 blade. Since the LM2 loss model uses a two-shock system and an exit flow angle parallel to the pressure surface at the trailing edge for supersonic streamtubes, a much higher pressure loss was calculated for the second streamtube than was calculated in the original blade case. This did not occur with the LM1 loss model because the weak single passage shock did not add a significant amount of pressure loss.

A comparison of Figure 10(a) and Figure 11(a) shows that the static pressure curves of both versions of TRANSROTOR shifted slightly lower for the TM1 blade. This is opposite the trend of the APNASA curves. Most of the increase in static pressure for the TM1 blade, as compared to the original blade, can be seen in the upper 60-percent of the blade span. The lower static pressure calculated by TRANSROTOR at station 2 for the TM1 blade contributed to the station 3 shift. The additional influence of the increase and decrease in total pressure for the LM1 and LM2 loss models, respectively, was enough to cause each model to predict opposite trend directions for the mass averaged static pressure ratio.

Finally, a slightly reduced absolute total temperature over the entire span is indicated by APNASA for the TM1 blade geometry [Figure 11(d)]. Both loss models show a matching reduction in the first two streamtubes but a slight increase for the remaining three. The absolute Mach number [Figure 11(g)] changes very little between the two blade geometries. There is good agreement between all three curves for this parameter.

The last cases to be discussed are those cases in which APNASA flow properties at 0.15·L upstream of the blade LE were indirectly inserted as station 2 input. In the *Rotor Performance Measurement* section of this chapter, it was stated that the mass averaged TRANSROTOR solutions were only marginally affected by the station at which APNASA flow properties were input. A comparison of the two input techniques done by examining the spanwise distribution of flow properties at station 3 reveals one distinct difference that was subdued by the mass averaging of the data points. Since this one distinct difference is common to both blade geometries, the two associated figures are presented together and

are not uniquely discussed. Figure 12 presents the spanwise distribution of flow properties at station 3 calculated by both versions of TRANSROTOR for the following case:

- APNASA flow properties at 0.15·L upstream of the blade LE indirectly inserted as station 1 input
- original TESCOM blade geometry

Figure 13 presents the spanwise distribution of flow properties at station 3 calculated by both versions of TRANSROTOR for the following case:

- APNASA flow properties at 0.15·L upstream of the blade LE indirectly inserted as station 1 input
- TM1 TESCOM blade geometry

The one distinct difference that can be seen between these two figures and Figures 10 and 11 is in the first streamtube. Some of the TRANSROTOR predicted values, common to both loss models, are severely skewed in the direction of the APNASA curve near the hub. This result is most apparent in the plots of C_{3n}, T_{c3}, α_3, and M_{w3}. As discussed previously, this input technique was used to capture alterations that occurred as the flow proceeded to the rotor inlet plane. Boundary layers along the walls were the dominant source of flow alteration. Span-averaging of the APNASA data produced single values that represented the flow properties of these chaotic regions in the TRANSROTOR input file. The results of this span-averaging can be seen in Figures 8 and 9. The skewed values of the first streamtube at station 3 are the result of input values that grossly approximated the flow in the viscosity-dominated wall regions. A similar, but much less pronounced, effect is also seen in the fifth streamtube. Clearly, it was these data points that marginally affected the mass averaged TRANSROTOR solutions. For the cases where the span-averaged input value was a good approximation, the accuracy of the predicted rotor performance improved. For the cases where the span-averaged input value was a poor approximation, the accuracy of the predicted rotor performance degraded.

In summary, the spanwise distribution of flow properties at station 2 and station 3 were examined to fully understand what contributed to the results of the rotor performance measures. The the effect of the two input techniques on the inlet flow conditions (station 2) was analyzed first. The second half of this section contained an analysis of the spanwise

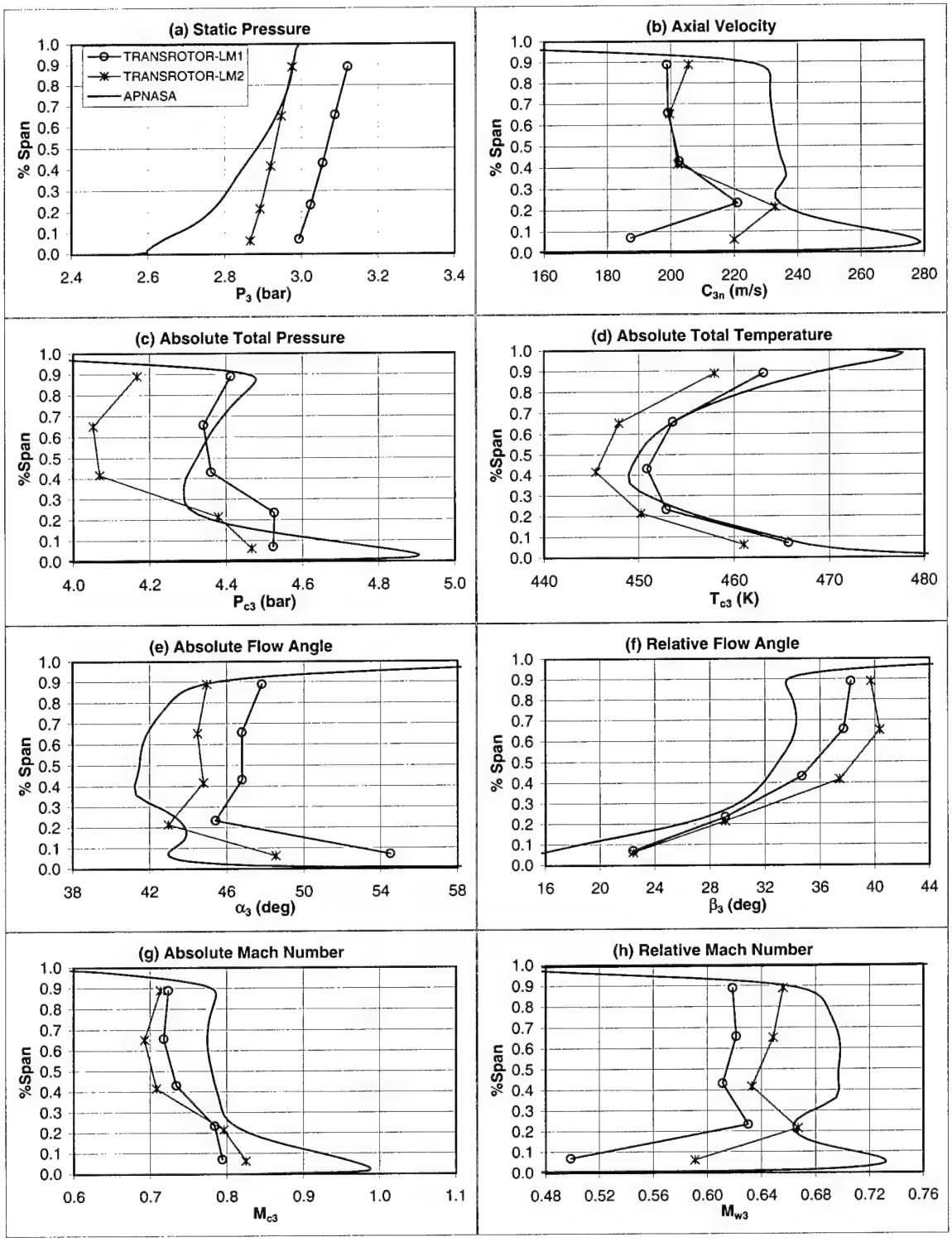

Figure 12 Station 3 Spanwise Distribution of Flow Properties - Station 2 Indirectly Defined by APNASA Flow Properties 0.15·L Upstream of Blade LE, Original Blade

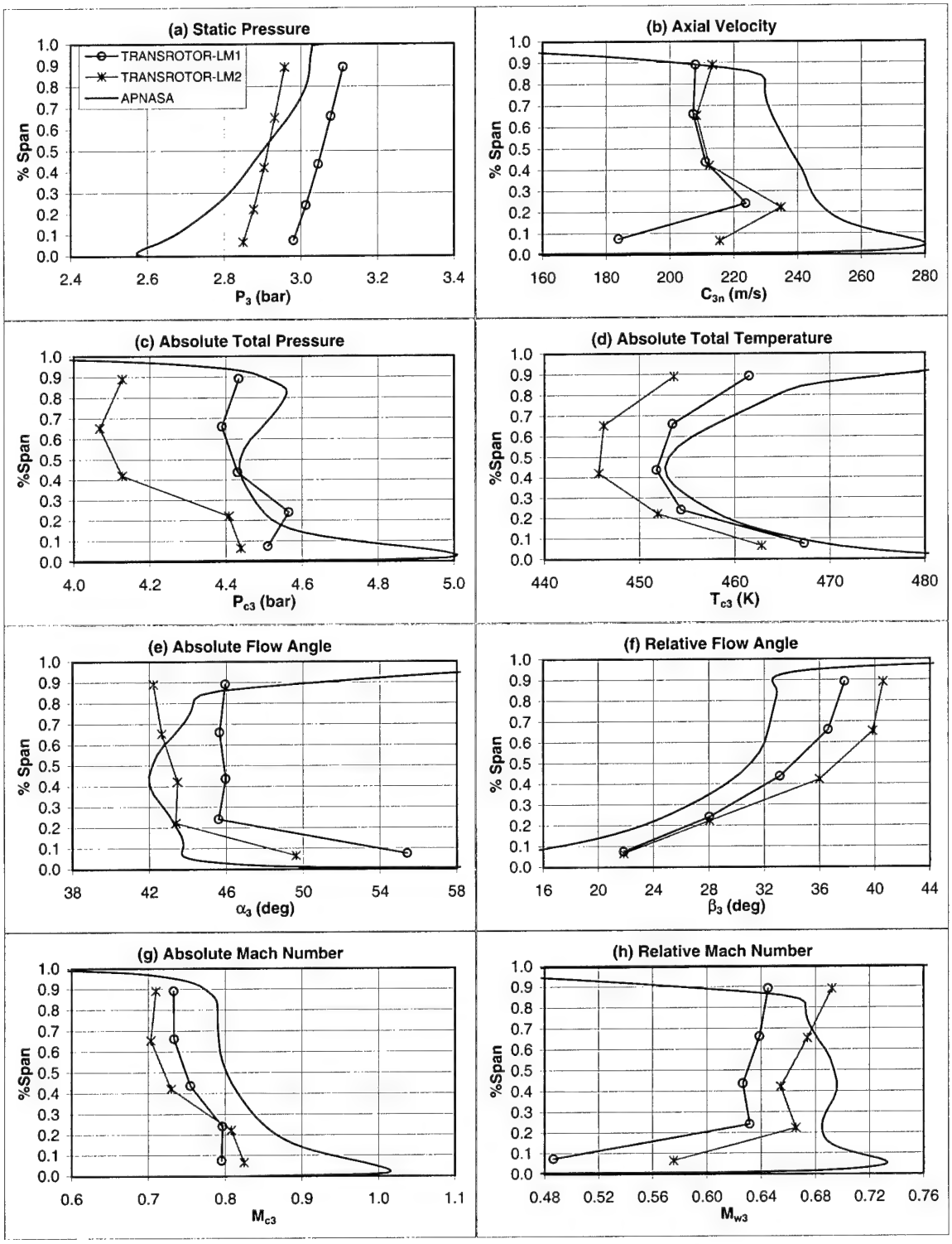

Figure 13 Station 3 Spanwise Distribution of Flow Properties - Station 2 Indirectly Defined by APNASA Flow Properties 0.15·L Upstream of Blade LE, TM1 Blade

distribution of flow properties at station 3. The differences caused by the two loss models, the two blade geometries, and the two input techniques were identified and explained. The corresponding impact on the rotor performance measures was also described. The most significant results were:

- The combination of axial inlet flow and the method by which TRANSROTOR establishes radial equilibrium resulted in poor agreement of some flow properties with the APNASA benchmark distributions.
- Both loss models had the most difficulty predicting the spanwise distribution of axial velocity, absolute flow angle, and relative Mach number.
- Both loss models had the most success predicting the spanwise distribution of absolute total temperature.
- The superiority of the LM1 loss model in predicting relative exit flow angle, and therefore, absolute total pressure was confirmed.
- The conceptual superiority of the LM2 loss model in predicting static pressure at station 3 was confirmed. However, the demonstrated accuracy was challenged due to the LM2 loss model error in total pressure.
- The two data input techniques primarily affected the streamtubes nearest the walls due to the rapidly changing flow properties in these regions.
- Both input techniques introduced error into the TRANSROTOR solution. Neither technique was found to be superior.
- The classification of the streamtube nearest the transition point from subsonic to supersonic inlet flow has the potential to greatly influence the overall solution, especially when a large percentage of the span is encompassed by that streamtube.

6.2 Parametric Study

The capability demonstration objective was accomplished by conducting a parametric study of compressor blade geometry using BOWSHOCK. The results of this study are presented graphically. Two sets of graphs were generated for each parameter that was varied. Figure 14 presents the response of the two rotor performance measures, P_{c3}/P_{c2} and η_{is}, to variations in blade geometry. These graphs are the primary results from this parametric study. To explain the trends seen in Figure 14, Figure 15 was generated. Relative exit flow angle, shock loss coefficient, and profile loss coefficient are plotted in this figure. As will be discussed, the change in relative exit flow angle is the dominant factor in determining the change in total pressure ratio since it signifies flow turning. The sum

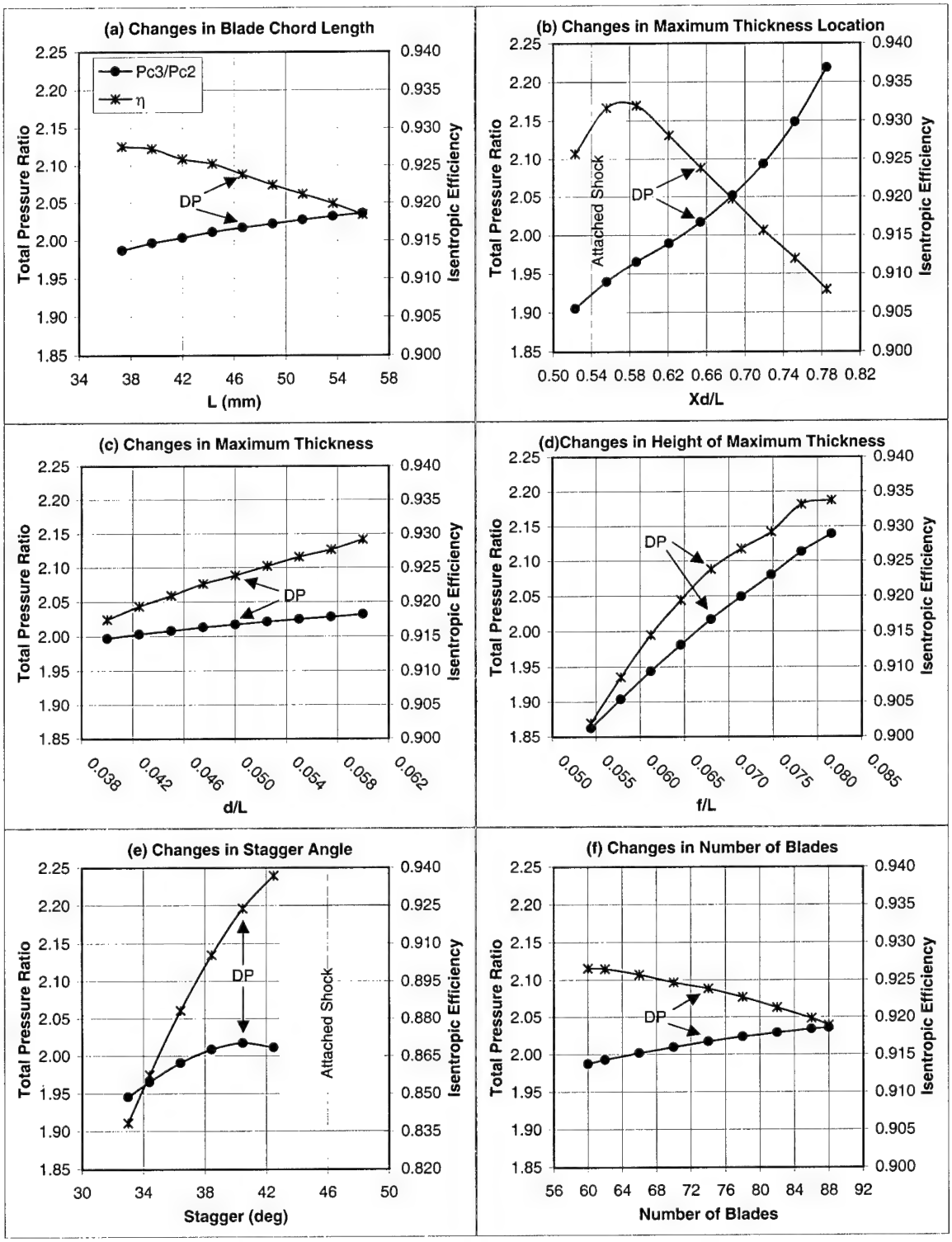

Figure 14 Response of Total Pressure Ratio and Isentropic Efficiency to Changes in Blade Geometry

of the shock and profile losses largely determines isentropic efficiency. The limits of the dependent axes are set to the same values so that a direct comparison of the curves between graphs is meaningful. Likewise, the limits of the independent axes are all approximately +/-20-percent of the design point value. The two exceptions to this are Figure 14(e) and the companion Figure 15(e) for which the secondary y-axis had to be significantly expanded to encompass all data. The design point, from which the five-percent increments were calculated, is identified in each graph by *DP*.

A number of limitations and assumptions inherent in the BOWSHOCK program must be understood to qualify the results seen in Figures 14 and 15. First, since BOWSHOCK only analyzes a single streamtube, the results obtained are influenced only by the given inlet conditions at one span location. Second, the contraction ratio and the radial development of the single streamtube that BOWSHOCK models is fixed by the user. Therefore, any change in the streamtube that would actually occur as a result of a change in blade geometry is not modeled. TRANSROTOR was used to investigate the significance of this limitation. It was found that the characteristics of the streamtubes were insensitive to moderate changes in blade geometry. Third, the LM1 loss model incorporated into BOWSHOCK does not identify conditions that would normally result in severe flow separation or stall. The performance trends found in this study are based on the assumption that the flow remains predominantly attached to the blade surface. Fourth, the flow scenario that BOWSHOCK analyzes assumes that the shock wave is standing off some distance from the leading edge. Significant deviation of some parameters from the design point resulted in the violation of this assumption. These points will be identified in the following parameter discussions.

Figure 14(a) presents the results of changes in blade chord length, L. Recall that the other three parameters that define the blade geometry are non-dimensionalized by L. Therefore, the entire blade is scaled when L is changed. Increasing L resulted in increasing P_{c3}/P_{c2} and decreasing η_{is}. Both of these trends are a direct result of the change in solidity. Equation (32) shows an inverse relationship between solidity and deviation angle. Decreased deviation angle corresponds to more flow turning, and therefore, a higher total pressure rise. The negative slope of the β_3 curve of Figure 15(a) confirms the moderate amount of flow turning that was gained. The drop in η_{is} was driven by the changes in

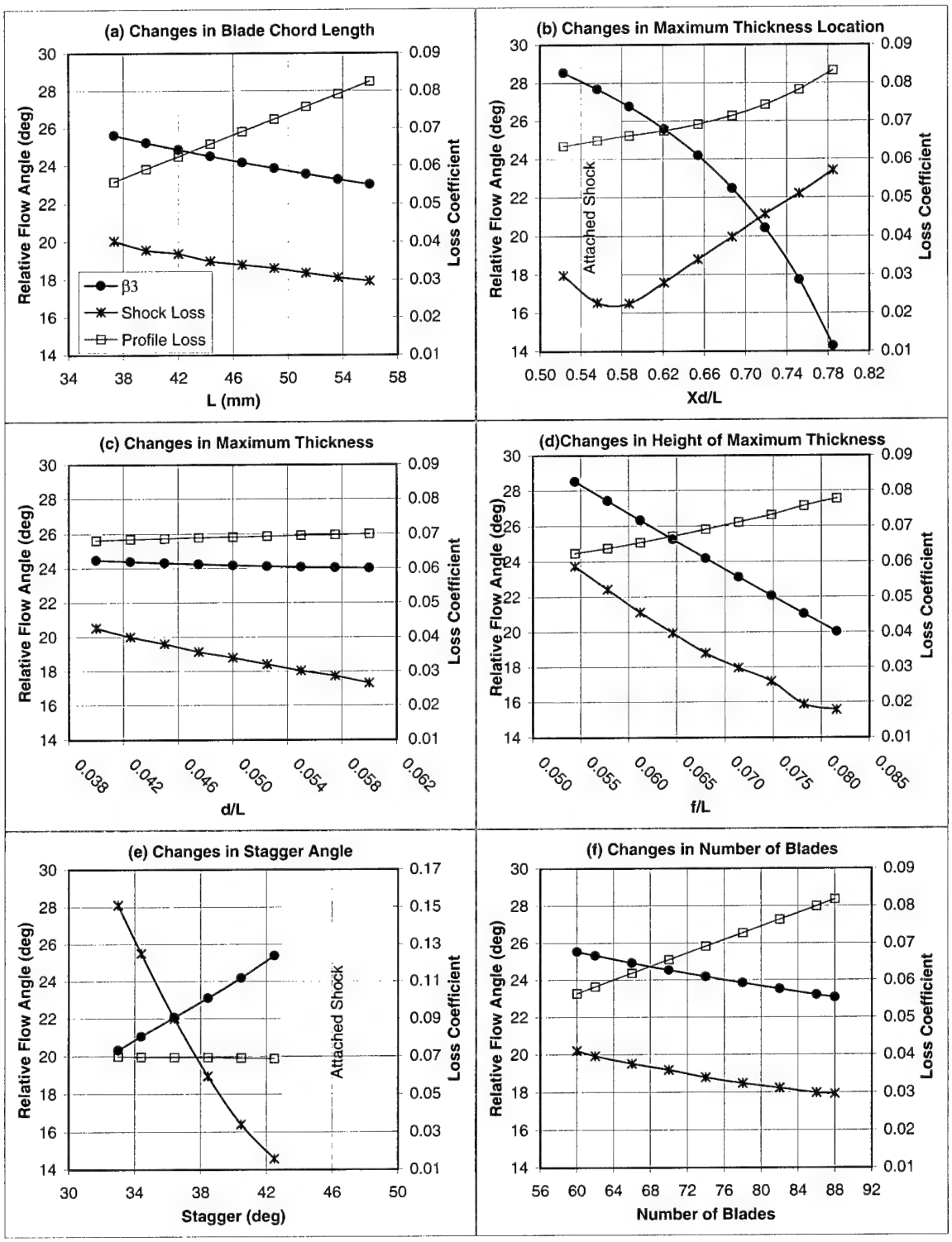

Figure 15 Response of Relative Exit Flow Angle and Loss Coefficients to Changes in Blade Geometry

the loss coefficients. Equation (42) shows that profile losses increase with an increase in solidity. Figure 15(a) shows a 19-percent increase in the profile loss coefficient for the 20-percent increase in L from the design point. Opposing this increase in loss is a 13-percent decrease in shock loss. This occurs due to the impingement point of the passage shock on the blade suction surface moving forward. Of the six parameters varied for this study, changes in blade chord length produced relatively minor changes in the two performance measures.

Figure 14(b) presents the results of changes in the maximum thickness location as a percentage of the chord, X_d/L. An increase in this parameter shifts the distribution of the blade camber toward the blade TE. Changes in this parameter had large consequences on both performance measures. A significant increase in P_{c3}/P_{c2} and a sharp decrease in η_{is} was caused by increasing X_d/L. The tradeoff between flow turning and flow deviation is evident in these trends. As the maximum thickness is moved closer to the trailing edge, the angle of the mean camber line at the trailing edge drops exponentially in reference to the axial direction which results in more flow turning. This trend can be seen in the relative exit flow angle curve of Figure15(b). Because the blade camber becomes concentrated in a smaller portion of the blade, the flow is increasingly unable to negotiate the high gradients near the trailing edge. Profile losses mount as the flow deviates from the direction of the mean camber line. Additionally, the flow incidence angle and the distance to the impingement point of the passage shock with respect to the blade LE both increase with X_d/L. Thus, the inlet flow is accelerated through a stronger Prandtl-Meyer expansion for a longer distance which increases the Mach number at the passage shock. Figure 15(b) shows the resulting increase in the shock loss coefficient. The reduction in shock loss coefficient that occurs between the -20- and -15-percent points is due the violation of an assumed detached shock. This corresponds to the brief increase in η_{is} in Figure 14(b). In reality, the very high values of X_d/L are also suspect since, at some large value of X_d/L, severe flow separation or even general blade stall would occur.

Increasing and decreasing the design point d/L by 20-percent had the least effect on P_{c3}/P_{c2} and η_{is} of the six parameters investigated. However, this was the first parameter that did not show a tradeoff between the two performance measures. As seen in Figure

14(c), an increase in d/L results in increases in both P_{c3}/P_{c2} and η_{is}. As the thickness of the blade increases, the suction surface becomes slightly more curved. The flow, which follows the blade surface, must turn an additional amount. This accounts for the minor drop in β_3 of Figure 15(c) and, subsequently, the minor rise in P_{c3}/P_{c2}. The associated higher flow diffusion results in a higher value of momentum thickness (θ/L) in Equation (42), which explains the slight increase in the profile loss coefficient. The most pronounced effect seen in Figure 15(c) is the drop in the shock loss coefficient. As d/L increases, the Mach number upstream of the passage shock is reduced by movement of the shock impingement point toward the blade LE. The incremental decreases in shock loss exceed the incremental increases in profile loss resulting in a net decrease in total loss.

The performance and flow property trends that resulted from changes in f/L were in the same direction as the d/L curves, but more pronounced. Figure 14(d) presents the magnitude of these trends. The height of the center of the maximum thickness circle from the chord line is a representation of the overall blade camber. Therefore, an increase in f/L corresponds to an increase in blade camber. As discussed previously, higher blade camber creates more flow turning and diffusion. These increases raise the absolute total pressure at the cost of additional profile loss. Figure 15(d) shows that a 20-percent increase in f/L from the design point results in a 17-percent decrease in β_3 and a 13-percent increase in $\omega_{profile}$. The primary cause of the reduction in the shock loss coefficient was found to be a reduction in the flow incidence angle with increasing camber. This was expected since there was a positive incidence angle at the design point. Figure 15(d) shows a 47-percent decrease in ω_{shock} for the same 20-percent increase in f/L from the design point. Clearly, this is the principal difference in loss that results in the net increase in η_{is}.

Figure 14(e) presents the results of changes in stagger angle. Stagger angle is one of the two parameters investigated that does not change the geometry of the blade. It is also the parameter to which η_{is} was most sensitive. In fact, changes in stagger angle caused such a large change in efficiency that the secondary y-axis could not have the same limits as the other five graphs. It should also be noted that the maximum increment for which BOWSHOCK could converge to a solution was the five-percent increase from the design point. For the ten-percent increase and beyond, the assumption of a detached

shock became too poor. Figure 14(e) shows the tremendous increase in η_{is} caused by the increase in stagger angle. Figure 15(e) shows an equally tremendous decrease in the shock loss coefficient. The combination of a significantly reduced incidence angle and movement of the passage shock impingement point forward drove the value of $\overline{M}_w$ from 1.52 for 33-degrees of stagger to 1.21 for 42-degrees of stagger. Since no changes were made to the geometry of the blade, the profile loss coefficient remained essentially constant. As was stated in the *Transonic Compressor Blading* section of Chapter I, stagger angle is very influential in determining the outlet flow direction. The rising curve of β_3 in Figure 15(e) agrees with this assertion. Perhaps the most interesting occurrence of all six graphs in Figure 14 is the maximum that the P_{c3}/P_{c2} curve achieves at the stagger angle design point. Despite the increase in relative exit flow angle as stagger increases from 33-degrees, the total pressure ratio increases. It is the tremendous drop in total losses up to the design point that more than compensate for the reduction in flow turning. However, once the stagger angle increases beyond the design point, shock losses do not drop as rapidly and the continued reduction in flow turning causes P_{c3}/P_{c2} to finally drop.

Finally, Figure 14(f) presents the results of changes in the number of blades around the rotor. It is not a coincidence that Figures 14(f) and 15(f) are virtually identical to Figures 14(a) and 15(a). The discussion of the blade chord results focused on how solidity was the primary cause of the trends seen in the performance measures and flow properties. Recall that solidity is the ratio of blade chord to spacing.

$$\sigma = \frac{L}{s} = \frac{L \cdot N}{2\pi r} \tag{64}$$

where

s = blade spacing

N = number of blades

Equation (64) shows that a given percent change in either L or N affects the solidity in the exact same way. Therefore, the trends seen in Figures 14(f) and 15(f) are explained by the same reasoning given for changes in blade chord.

In summary, a parametric study the four parameters that define MCA-profiles, as well as two rotor parameters, was accomplished using BOWSHOCK. The purpose of this study was to demonstrate the capabilities of BOWSHOCK and the potential use of it in the preliminary design of compressor blades. Total pressure ratio and isentropic efficiency were used as the dependent variables in this study. For this test case, the following trends were observed for +20-percent variations in parameter values from the design point:

- Increased blade chord length resulted in increased total pressure ratio and decreased isentropic efficiency. These trends were explained by the direct affect of chord on solidity.
- Moving the blade maximum thickness toward the trailing edge resulted in increased total pressure ratio and decreased isentropic efficiency. Total pressure ratio was most sensitive to this parameter. Increasing the concentration of the blade camber at the trailing edge resulted in higher flow turning at the cost of additional profile and shock losses.
- Increased blade maximum thickness resulted in increased total pressure ratio and increased isentropic efficiency. Minor increases in suction surface curvature and movement of the passage shock impingement point forward caused these trends. Total pressure ratio was least sensitive to this parameter.
- Increased blade camber resulted in increased total pressure ratio and increased isentropic efficiency. The additional profile loss associated with higher flow turning was more than compensated for by a reduction in shock losses due to decreased incidence angle.
- Increased stagger angle resulted in a maximum in total pressure ratio and increased isentropic efficiency. Isentropic efficiency was most sensitive to this parameter. The substantial rise in isentropic efficiency was due to a substantial reduction in shock losses caused by decreased incidence angle and movement of the passage shock impingement point forward. Total pressure ratio reached a maximum at the design point when the effect of decreased flow turning exceed the effect of decreased shock losses.
- Increasing the number of blades resulted in increased total pressure ratio and decreased isentropic efficiency. Isentropic efficiency was least sensitive to this parameter. This parameter had the same effect on solidity as chord length.

These results are represented pictorially in Figure 16 as modified versions of an approximation of the design point blade. In one case, the design point blade geometry is altered, in an exaggerated fashion, to achieve maximum total pressure ratio. In the other case, the design point blade geometry is altered to achieve maximum isentropic efficiency. As mentioned previously, there are limitations and assumptions of the BOWSHOCK pro-

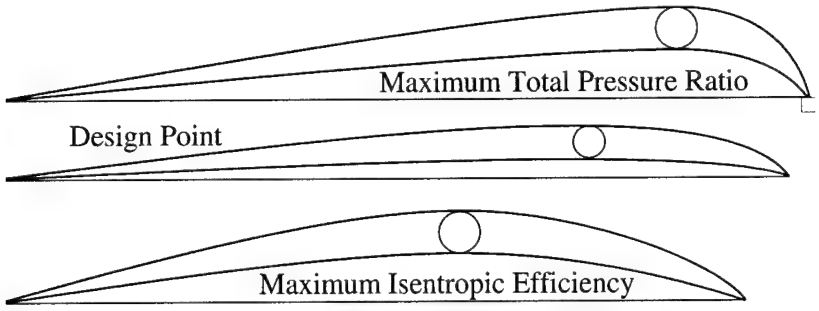

Figure 16 Modified Blades Based on Blade Geometry Parametric Study

gram that must be considered when interpreting the results. However, the blade profiles shown in Figure 16 are examples of the way in which BOWSHOCK could be used for preliminary blade design.

6.3 Computational Speed

An important feature of these desktop computer programs is the time is takes to produce a solution. For preliminary design purposes, a lesser degree of accuracy is acceptable for a higher computational speed. If an exhaustive parametric study of blade geometry is to be conducted for a transonic rotor, computational time becomes a major factor.

The *Executor®2* emulator, which allows *Macintosh®* programs to be run on a personal computer (PC), was run on a desktop PC platform with a 450 MHz *Pentium III®* processor in order to use these programs. The run times quoted are based on this hardware and software configuration. It is unknown how the emulator affected the processing speed of the central processing unit (CPU). It was noted that some interim calculation displays were not posted to the screen when TRANSROTOR and BOWSHOCK were run on the emulator.

Three factors greatly affected the time it took TRANSROTOR to produce a solution: the total number of streamtubes, the number of subsonic and supersonic streamtubes, and the number of iterations required to converge to a solution. A total of five streamtubes was used in every case for this research. Subsonic streamtubes required very little computational time (less than 0.5 seconds) as compared to supersonic streamtubes (approximately

four seconds). One iteration was defined as the completed modification of all five streamtubes. Table 9 presents a summary of the computational times required to produce the eight solutions used in this thesis. The format of the table entries is the number of iterations separated by a hyphen from the total time in minutes. For each blade design there are two columns for the two input techniques used. The label for these columns corresponds to the distance of the boundary conditions upstream from the blade LE. As can be seen in

Table 9 TRANSROTOR Computational Times for Solutions

	Original Blade		TM1 Blade	
Program	1.05·L	0.15·L	1.05·L	0.15·L
TRANS-LM1	9-2.83	7-2.33	8-3.38	16-5.05
TRANS-LM2	8-2.62	9-2.93	8-3.40	6-2.30

Table 9, the longest time required to reach a solution was just over five minutes. Considering the fact that CFD codes can take several days to converge to a solution while using multiple processors, this was very fast. The 16 iterations required to converge caused this particular run to take longer than the average time of 3.11 minutes. Undoubtedly, these times were increased by the numerous interim calculation displays that allow the user to follow the sequence of calculations in detail. If faster computational speed is desired, most of these displays could be removed. The demonstrated speed of TRANSROTOR is a very desirable attribute for the preliminary design phase of transonic rotors.

Computational times for BOWSHOCK are not presented because the calculation sequence is broken by pauses so that the user can see interim steps. The four seconds quoted above as the computational time for supersonic streamtubes is a low-end approximation of the average time for BOWSHOCK to arrive at a solution uninterrupted.

VII. Conclusions and Recommendations

Based on this research effort, it was concluded that TRANSROTOR has the potential to be used for preliminary design of transonic compressor rotors. Predicted transonic rotor performance was within ten-percent of the CFD-based benchmark performance. This was a level of accuracy commensurate with the expected capability of a correlation-based program. Results that indicated accuracy higher than this were scrutinized and sometimes found to be the result of off-setting errors. Such was the case with the LM2 loss model-predicted static pressure ratio and the spanwise distributions of absolute Mach number. Future use of this program will lead to refined estimates of accuracy. A sacrifice in accuracy is acceptable for the high computational speed and low cost that is inherent in this desktop computer program. TRANSROTOR is not advocated as a substitute for the more sophisticated CFD programs. Rather, it is envisioned that the approximate solution from TRANSROTOR could be used as the starting point for a more sophisticated program.

No conclusion could be made as to the superiority of one rotor loss model over the other. While the LM2 loss model was an attempt to improve upon the LM1 loss model, some results compared worse to the APNASA benchmarks. Each loss model used correlations that produced superior results than the other. The deviation angle correlations used by the LM1 loss model better predicted the flow deviation at the blade TE. This resulted in a more accurate prediction of total pressure ratio. Since a second shock was noted in the blade passage of the TESCOM blading, the two-shock system of the LM2 loss model was conceptually more accurate. The reduction in the static pressure rise across a normal shock by the LM2 loss model resulted in better agreement with the APNASA static pressure rise.

Even if one loss model had shown consistently better results, a conclusion proclaiming its superiority would be somewhat presumptuous. The results in this thesis were produced by two blade geometries, one of which was a descendant of the other. While these blade designs were satisfactory for the scope of this thesis, increased confidence in and differentiation of the loss models can be gained by analyzing additional blade designs. The foundation has been laid so that future users and/or modifiers of TRANSROTOR can adeptly run additional test cases. Comparison with experimental data from a large variety

of transonic compressor rotors would be ideal. Once a large enough database of test cases is compiled, further tuning of the loss models would be justified. In addition, a hybrid loss model, which combines the best correlations from the LM1 and LM2 loss models, could be properly examined. The coding an such a loss model into TRANSROTOR would require less effort than the subsequent justification and validation of the LM1/LM2 hybrid loss model.

TRANSROTOR was originally designed to analyze a single compressor stage consisting of an IGV upstream of the rotor. The potential exists to run TRANSROTOR sequentially so that the output flow conditions of one stage calculation become the input flow conditions for the next stage calculation. In this way, the approximate performance of an entire multi-stage compressor could be analyzed. The effort required to add this capability depends on the level of accuracy desired. Although the results of this research showed that the simplistic treatment of the flow path between blade rows would not add a significant amount of error to the solution, refinement of the program would be necessary to adequately model this added complexity. Accurate modeling of stator performance must be assured to avoid compounding errors. A realistic compressor map could not be generated unless logic to identify compressor stall was added. The ability to toggle between sets of correlations specifically intended for transonic or subsonic compressor rotors would be a useful feature since latter stages would tend to be subsonic. Modeling of rotor performance could be improved by increasing the number of streamtubes that divide the flow path. Additional streamtubes would increase the fidelity of the solution but reduce computational speed. These competing traits would have to be balanced. Finally, attempting to model the interaction between stator vanes and rotor blades would certainly be a daunting task. The reward of such an endeavor would be the validated use of TRANSROTOR in analyzing a multi-stage compressor - a significant addition to its overall utility.

The parametric study of blade geometry demonstrated the potential use of BOWSHOCK in the preliminary design of supersonic compressor blading. The predicted variation in blade performance due to changes in six blade parameters was verified and quantified. The results showed that isentropic efficiency was most sensitive to stagger angle and least sensitive to blade spacing. Total pressure ratio was most sensitive to blade maximum

thickness location and least sensitive to blade maximum thickness. The sophistication of BOWSHOCK was high enough to appropriately account for small changes in blade geometry. The lack of minimums and maximums seen in the trends of the performance measures was attributed, in part, to the absence of flow separation or stall prediction correlations.

The primary reason BOWSHOCK was used for the blade geometry parametric study was the MCA-profile option that allowed the blade geometry to be manually changed easily and systematically. The ultimate utility of BOWSHOCK for blade design purposes is not as a stand-alone program. Results from an analysis of a single isolated profile have little intrinsic value and simple stacking of a number of these profiles would lead to erroneous blade shapes. Recall that BOWSHOCK is, in essence, the supersonic analysis routine invoked within TRANSROTOR. An optimization routine could be used to systematically change the profile geometries within TRANSROTOR. Not only would an optimization routine alleviate the difficulty of changing the required xy-coordinate defined profiles, it would also take advantage of the high degree of freedom afforded by point-defined blade surfaces. Because each change in geometry would be followed by a complete blade performance calculation, the influence of the changes on the entire solution would be accounted for. The research reported in this thesis proved that such a concept could be made a reality.

Appendix A. INCIDUNIQUE Computer Program Summary

This appendix contains discussions of the INCIDUNIQUE desktop computer program that was purchased with BOWSHOCK and TRANSROTOR but was not used in this research.

INCIDUNIQUE is a sister program to BOWSHOCK. It is a blade-to-blade calculation of a single streamtube. The calculation is made Q3D by a user-defined streamtube contraction. Since an attached bow shock is assumed, the relative inlet Mach number must be supersonic.

This program calculates the inlet flow angle required to achieve the unique incidence condition for a given set of supersonic inlet conditions and determines the flow properties at the rotor entrance and exit. The unique incidence condition is a phenomenon caused by supersonic flow entering a blade row for which the bow shock is attached to the blade LE. The incident flow angle at which this scenario occurs is unique because it is the only flow condition that can be periodic around the cascade. The range of inlet flow velocities applicable to this scenario is bounded by the bow shock becoming detached at low speeds and the axial flow becoming supersonic at high speeds. Figure 17 depicts the type of scenario within a blade row that INCIDUNIQUE is designed to analyze and includes associated nomenclature. INCIDUNIQUE offers the same blade geometry choices

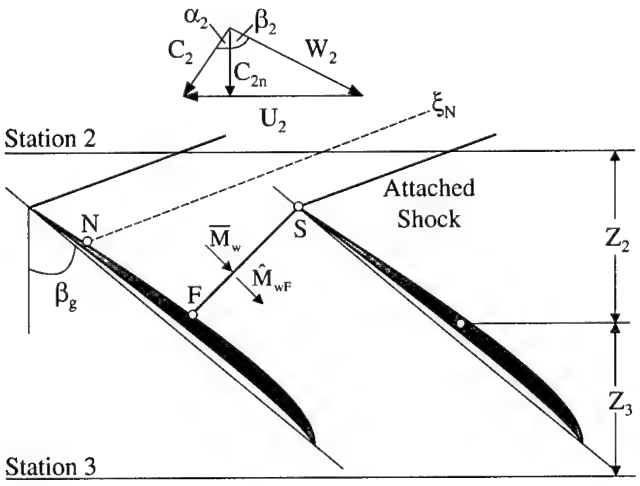

Figure 17 INCIDUNIQUE Flow Scenario - Blade-to-blade Perspective

as BOWSHOCK. Blade and rotor geometry definitions are identical (Figures 1 and 3). The only difference in user input between the two programs is that INCIDUNIQUE does not require a value for the absolute inlet velocity, C_2, since it is a dependent variable. As with BOWSHOCK, the program echoes the input values back to the user so that the entries can be changed before program execution.

The general calculation sequence of INCIDUNIQUE is described below. The relative inlet flow angle, β_2, is approximated so that the inlet velocity triangle is defined. The inlet flow velocity is checked to ensure it falls between the low and high speed boundaries for an attached bow shock. The neutral point on the profile suction surface is found. The left-running characteristic, ξ_N, begins at infinity in the inlet flow field and terminates at the neutral point. Thus, the neutral point is the point where the tangent to the surface equals the inlet flow angle. After the local streamtube thickness, radius, and total pressure are calculated and corresponding corrections are made to μ and λ, the Mach number at the neutral point is found as a function of the Prandtl-Meyer expansion angle (Θ_*). The neutral point is used as the starting point to find additional points along the blade suction surface. Subsequently, the Mach number and flow angle at the blade LE, point S in Figure 17, is found. Note that β_S corresponds to the unique incidence angle for the leading edge Mach number, M_S. The leading edge incidence angle is compared to the critical incidence angle to verify that the bow shock remains attached. Enough information is now known to calculate the shock angle and its properties. Finally, the relative inlet flow angle is corrected and compared to the previous value of β_2. This is repeated until convergence to the final value of β_2 [11:12]. Following the establishment of the relative inlet flow angle, the profile and shock losses through the rotor are calculated. The majority of the outputs of this program are the same as those given by BOWSHOCK.

Appendix B. Subroutine Listing

This appendix lists the subroutines called by all three programs (INCIDUNIQUE, BOWSHOCK, and TRANSROTOR) in alphabetical order. A short description of the main purpose of each subroutine is given.

Notes:

1. The capital letters enclosed in parentheses immediately following the subroutine name indicate the programs that were coded with that subroutine (I = INCIDUNIQUE, B = BOWSHOCK, T = Both versions of TRANSROTOR, T1 = LM1-version of TRANSROTOR only, T2 = LM2-version of TRANSROTOR only).
2. Subroutine names are repeated if the same subroutine name is coded differently between programs.

abstroemung (I,B,T) - Converts total loss coefficient into a total pressure loss and calculates some flow conditions at station 3.

amin (B,T) - Calculates and displays the location of the minimum area within the blade passage.

anfangswerte1 (I,B) - Prompts user to enter the name of the input text file containing the initial data for an MCA- or S-profile blade. The option to *go* or *stop* is given. If the user selects *go*, the input file is read.

anfangswerte2 (I,B) - Prompts user to enter the name of the input text file containing the initial data for a blade defined by pairs of xy-coordinates. The option to *go* or *stop* is given. If the user selects *go*, the input file is read.

anstroemzustand (I) - Confirms inlet axial Mach number is subsonic and uses the MOC to find the corrected inlet flow angle.

ausdruck (B,T) - Displays summary of flow properties at the stagnation streamline, passage shock, station 2, and station 3.

ausgabe1 (T) - Displays comprehensive list of calculated flow properties for each streamtube at station 1.

ausgabe2 (T) - Displays comprehensive list of calculated flow properties for each streamtube at station 2.

ausgabe3 (T) - Displays comprehensive list of calculated flow properties for each streamtube at station 3.

bilddarstellung (I,B) - Displays blade-to-blade figure on input screen that shows the primary flow features that are assumed and the associated nomenclature. Figures 17 and 2 are reproductions of the figures displayed by this subroutine.

canalzeichnen (T) - Displays meridional view of the actual development of all streamtubes from station 1 to station 3 after convergence to a solution. Streamtubes are differentiated by colored shading.

carter (I) - Calculates relative exit flow angle using Carter's Rule, Eq. (32).

carter (B,T1) - Calculates the on-design relative exit flow angle using Carter's Rule, Eq. (32). The off-design relative flow angle is calculated using Creveling's correlation, Eq. (36).

carter1 (T2) - Calculates the on-design relative exit flow angle using Carter's Rule, Eq. (32). The off-design relative flow angle is calculated using Creveling's correlation, Eq. (36).

carter2 (T2) - Calculates relative exit flow angle using a correlation by König *et al.*, Eq. (61).

charaschnitt (B,T) - Uses the MOC to define the characteristic, ξ_{DC}, and determines the coordinates where it impinges on the SS.

datenlesen - (I,B,T) Reads xy-coordinate pairs from input text file and calculates blade geometrical parameters.

deltalamda (I,B,T) - Performs Q3D characteristic corrections to the value of λ to account for changes in streamtube thickness [Eq. (12)], radius [Eq. (14)], and total pressure [Eq. (16)].

deltamu (I,B,T) - Performs Q3D characteristic corrections to the value of μ to account for changes in streamtube thickness [Eq. (13)], radius [Eq. (15)], and total pressure [Eq. (17)].

diagramliste (T) - Displays buttons allowing the user to select a flow property to be plotted.

diagramme (T) - Creates and formats the plot on which the radial distribution of a selected flow property will be shown.

diagramzeichnen (T) - Plots the radial distribution of a selected flow property. The distribution at all three stations is shown on the same plot.

druckgradientuberschall (T) - Calculates and displays the static pressures at the boundaries of each streamtube, Eq. (1). This subroutine serves the same purpose as *radgleichgew* does for INCIDUNIQUE and BOWSHOCK.

eingabegroessen (T) - Displays main input screen. Initial values for all parameters are shown.

eingabegroessen1 (I,B) - Displays main input screen for MCA- and S-profile blades. Initial values for all parameters are shown.

eingabegroessen2 (I,B) - Displays main input screen for blades defined by xy-coordinate pairs. Initial values for all parameters are shown.

einlesen (T) - Assigns main input screen values to program variables.

einlesen1 (I,B) - Assigns main input screen values to program variables for MCA- and S-profile blades.

einlesen2 (I,B) - Assigns main input screen values to program variables for blades defined by xy-coordinate pairs.

gamastoss (B,T) - Calculates the shock angle.

gechwindigkeitswerte (B,T) - Displays velocity triangle information at station 2, just upstream of the passage shock, just downstream of the passage shock, and at station 3.

gitter (I,B,T) - Displays blade-to-blade view of the actual flow features and plots the evolution of the streamtube from inlet to exit.

incidunic (I) - Uses the MOC to calculate the unique incidence condition.

kanalstoss (B,T1) - Calculates flow properties upstream and downstream of the detached shock wave. The shock loss coefficient is computed according to Eq. (39).

kanalstoss (T2) - Calculates flow properties upstream and downstream of the detached shock wave. The shock loss coefficient is computed according to Eq. (60).

komegarechnung (T) - Calculates the wake momentum thickness required for Eq. (35) depending on the proximity of the streamtube to the hub and casing.

konstante (I,B,T) - Assigns constant names to frequently used expressions involving the ratio of specific heats, γ.

kritabl (I) - Calculates critical LE incidence angle to determine if the bow shock is attached or detached.

machaustetax (I,B,T) - Calculates Mach number from Θ_*. A numerical approximation of Eq. (7) is used.

machstoss (I) - Calculates the Mach number after a shock wave

massenbilanz (B,T) - Determines point B on the bow shock by balancing the mass flow through the sonic lines AB and BD.

minimal (T) - Sets the minimum value of the plot x-axis.

minimalwinkel (T) - Sets the minimum value of the plot x-axis when flow angles are plotted. This subroutine has slightly different criteria than *minimal*.

minlossinc (B,T) - Calculates the minimum loss incidence angle according to Eq. (24).

mss-rechnen (B,T) - Uses the MOC to calculate the Mach number at point S on the stagnation streamline just before the shock.

mprechnung (I) - Uses the MOC to calculate the Mach number and flow angle at points P and S of Figure 17.

neutralpunkt (I,B,T) - Uses the MOC to find the location of the neutral point, N, on the blade SS.

output (T) - Opens a user-named file into which a multitude of flow property values are output. The data is labeled within the output file. The output file is comma delimited.

passshock2 (T2) - Fictitiously accelerates blade passage flow by means of a Laval-nozzle in order to have a second shock near the blade TE. Equations (58) and (59) are coded in this subroutine.

plotdiagr1 (T) - Creates and formats the first six plots on which the radial distribution of flow properties will be shown. This subroutine prepares the plots to be printed.

plotdiagr2 (T) - Creates and formats the last six plots on which the radial distribution of flow properties will be shown. This subroutine prepares the plots to be printed.

profil+winkel (I,B) - Displays the blade profile and plots the value of tangent angles from LE to TE.

profilkoordinaten (I,B) - Calculates the radius of the four circular arcs that define the MCA-profile blade surfaces and calculates geometrical parameters.

profilmachzahl (I) - Calculates and displays velocity triangles and the Mach number distribution along the SS from the LE to the passage shock impingement point.

profilmachzahl (B,T) - Calculates the Mach number distribution along the SS from the LE to the passage shock impingement point F.

profilo (I,B) - Determines the appropriate subroutine to be used for calculating SS coordinates based on the input text file.

profilocos (I,B) - Calculates functions describing the SS of an S-profile blade forward of and behind the point of maximum thickness.

profilocosdata (I,B) - Calculates xy-coordinate pairs and tangent angles along the SS of an S-profile blade.

profilodata (I,B,T) - Calculates y-coordinate and tangent angle of the SS for a given x-coordinate.

profilomca (I,B) - Calculates functions describing the SS of an MCA-profile blade forward of and behind the point of maximum thickness.

profilomcadata (I,B) - Calculates xy-coordinate pairs and tangent angles along the SS of an MCA-profile blade.

profilpunkt (I,B,T) - Finds the point on the SS where the tangent angle is equal to the freestream flow angle (neutral point).

profilschallpunkt (B,T) - Finds the coordinates of point A on the SS using the MOC.

profilu (I,B) - Determines the appropriate subroutine to be used for calculating PS coordinates based on the input text file.

profilua (I,B) - Calculates functions describing the PS of an MCA- or S-profile blade forward of and behind the point of maximum thickness.

profiluadata (I,B) - Calculates xy-coordinate pairs along the PS of an MCA- or S-profile blade.

profiludata (I,B,T) - Calculates y-coordinate and tangent angle of the PS for a given x-coordinate.

profvit (B,T) - Plots the Mach number distribution along the SS from the LE to the passage shock impingement point F.

radgleich (T) - Iteratively establishes radial equilibrium at a given station. The static pressures at the borders of adjacent streamtubes must match. The static pressure at the borders of a streamtube are found using Eq. (1).

radgleichgew (I,B) - Calculates and displays the static pressures at the boundaries of the streamtube, Eq. (1).

radius (I,B,T) - Calculates the radial location of the streamtube given a position along the blade chord. A sine wave-type evolution of the streamtube is assumed. A linear evolution can be selected within the source code.

rechenergebnisse (I) - Displays results of flow property calculations after each iteration.

schicht (I,B,T) - Calculates the streamtube thickness given a position along the blade chord. A sine wave-type evolution of the streamtube is assumed. A linear evolution can be selected within the source code.

schnitg (B,T) - Calculates the intersection of two straight lines.

section1 (T) - Calculates flow properties at station 1.

section2 (T) - Calculates flow properties at station 2.

section3subsonic (T) - Calculates flow properties at station 3 for subsonic flow. This subroutine is the branch of TRANSROTOR that calculates the flow properties of streamtubes with a subsonic M_{w2}.

staustromlinie (B,T) - Calculates coordinates of points along the stagnation streamline using the MOC.

stosschallpunkt (B,T) - Calculates coordinates of points C and D shown in Figure 2 and calculates the Mach number just upstream of the shock at point B using the MOC.

stossfusspunkt (B,T) - Calculates the shock standoff distance and calculates the coordinates of point F where the passage shock impinges on the SS using the MOC.

stossw (I) - Calculates the shock angle.

streckep1p2 (B,T) - Mass flow-based calculation that determines the distance between two points. This subroutine is used as part of the calculations that find the location of various points in the flow field.

stromdichte (I,B,T) - Calculates Mach number based on the flux density.

stromdichtes (T) - Calculates Mach number based on the flux density. This subroutine is called during supersonic calculations only.

supersonic (T) - This subroutine is the branch of TRANSROTOR that calculates the flow properties of streamtubes with a supersonic M_{w2}. The primary purpose of this subroutine is to call the supersonic flow-related subroutines.

total (I,B,T) - Calculates total temperature and total pressure based on radial location.

totaldruecke (B,T) - Calculates average total pressures at various points in the flow field using the *total* subroutine

twpwrechnung (I) - Calculates inlet flow properties and confirms that the inlet Mach number is supersonic but the axial component is still subsonic.

verlustc (T) - Calculates the IGV profile loss coefficient according to Eq. (62).

verlustcompraxw (T1) - Calculates the on- and off-design rotor loss coefficients for subsonic flow according to Equations (35) and (38), respectively.

verlustcompraxwsup (T1) - Calculates the rotor profile loss coefficient for supersonic flow according to Equations (41) and (42).

verlustw (I,B) - Calculates the rotor profile loss coefficient according to Equations (41) and (42).

verlustwsub (T2) - Calculates the off-design rotor loss coefficient for subsonic flow according to Eq. (55).

verlustwsup (T2) - Calculates the rotor profile loss coefficient for supersonic flow according to Equations (41) and (42).

weiter1 (B,T) - Prompts user to make a decision by displaying the *continue* and *stop* buttons.

weiter2 (I,B,T) - Prompts user to make a decision by displaying the *next input* and *stop* buttons.

weiter3 (I,B,T) - Prompts user to make a decision by displaying the *continue*, *next input*, and *stop* buttons.

weiter4 (I) - Prompts user to make a decision by displaying the *next n-rotation* and *end* buttons.

weiter4 (B) - Prompts user to make a decision by displaying the *next C2*, *PRINT*, *last C2*, and *stop* buttons.

weiter5 (B) - Prompts user to make a decision by displaying the *next C2*, *last C2*, and *stop* buttons.

weiter6 (B) - Prompts user to make a decision by displaying the *next alfa*, *next n-rotation*, and *end* buttons.

zeichnen (B,T) - Displays blade-to-blade view of the actual position of the detached shock and other flow features. The shock standoff distance from the LE (e/L) and the shift in the stagnation streamline near the LE (j/L) are displayed.

zustroemung (B,T) - Calculates flow properties at station 2.

Appendix C. Computer Program Flow Diagrams

This appendix contains the subroutine flow diagrams of all three programs (INCIDUNIQUE, BOWSHOCK, and TRANSROTOR) discussed in this thesis. Below is a key to the blocks, lines, and other information found in the flow diagrams. Major program

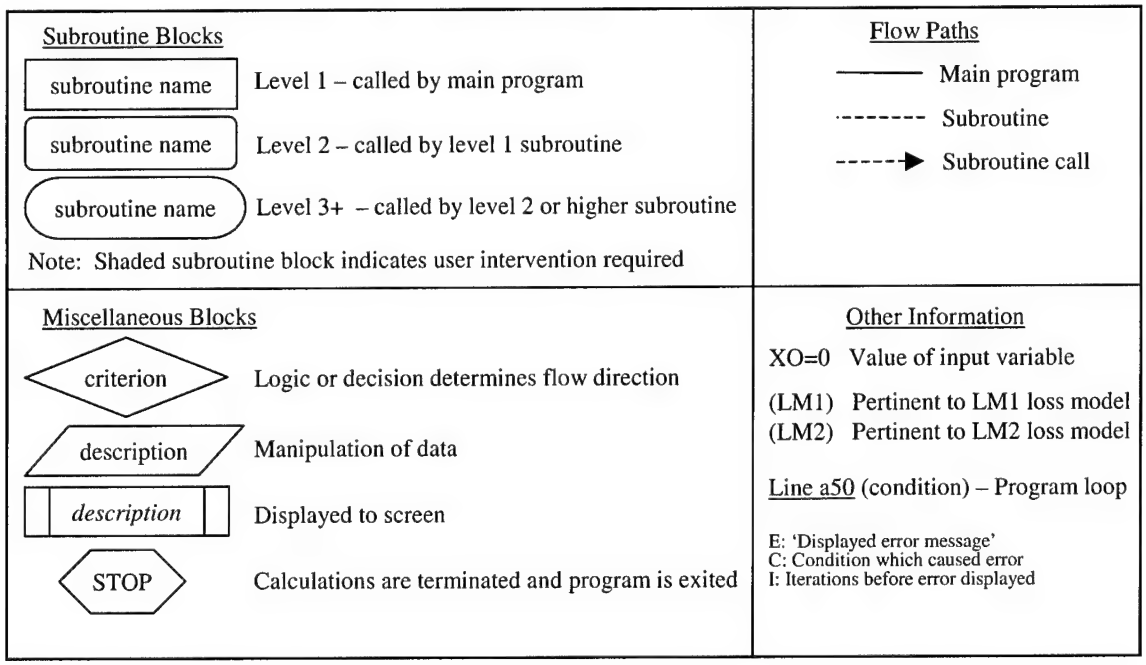

loops, which are external to individual subroutines, are identified by the line numbers at which the loops begin. One flow diagram is provided for both versions of TRANSROTOR. The differences between the LM1 and LM2 loss models are signified by the labels within parentheses.

C.1 INCIDUNIQUE

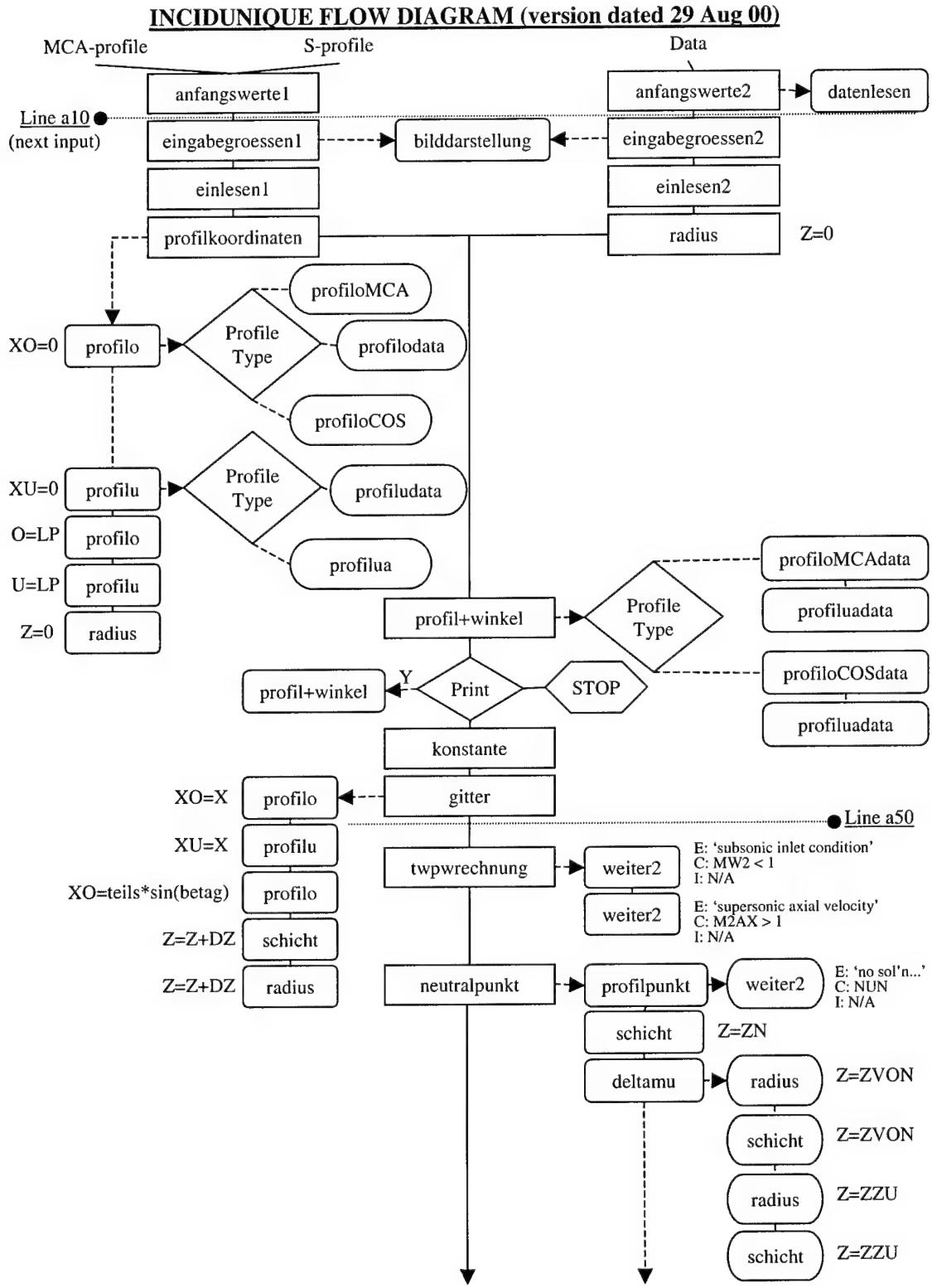

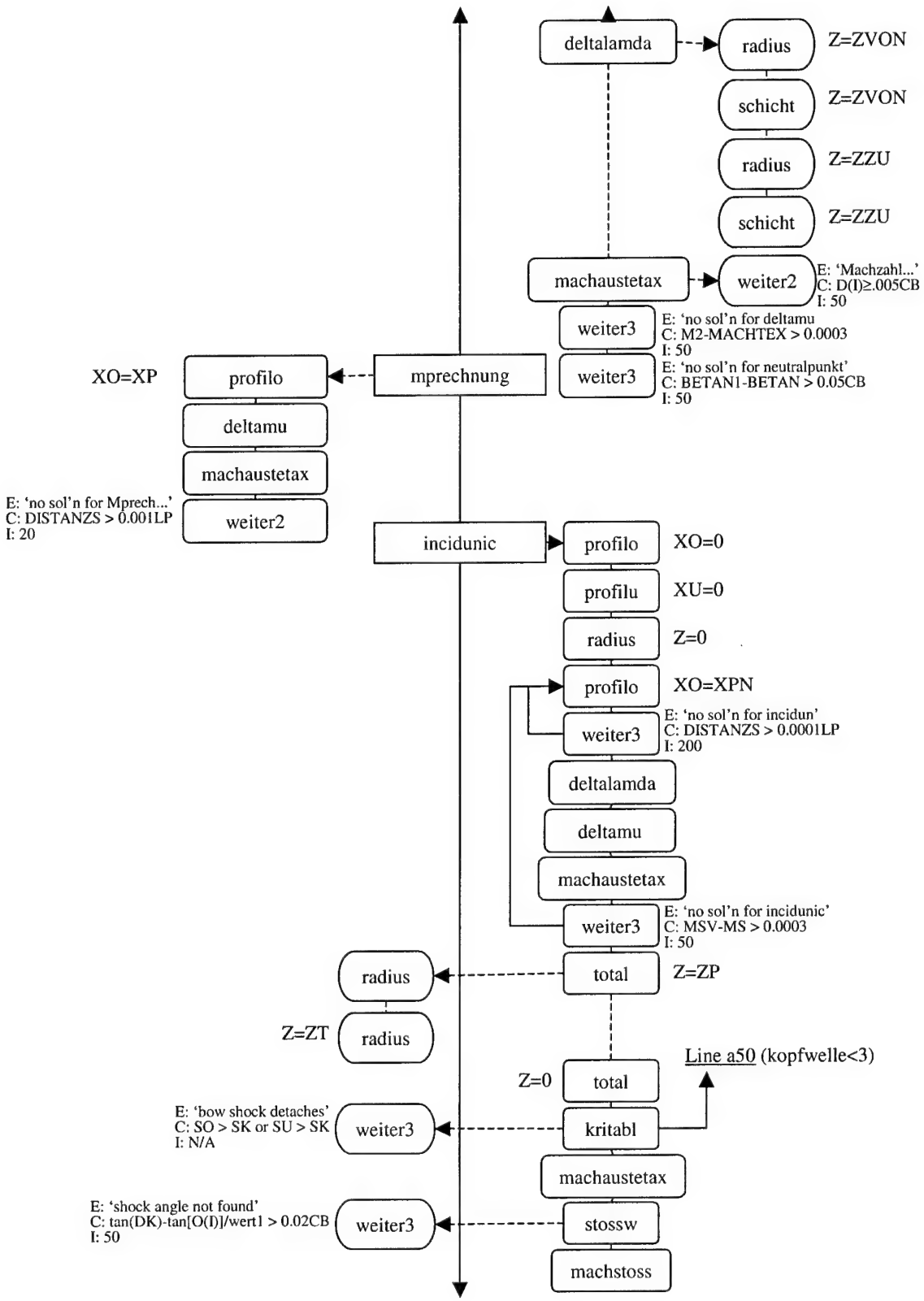
deltalamda
radius
Z=ZVON
schicht
Z=ZVON
radius
Z=ZZU
schicht
Z=ZZU
machaustetax
weiter2
E: 'Machzahl...'
C: D(I)≥.005CB
I: 50
weiter3
E: 'no sol'n for deltamu
C: M2-MACHTEX > 0.0003
I: 50
weiter3
E: 'no sol'n for neutralpunkt'
C: BETAN1-BETAN > 0.05CB
I: 50
mprechnung
XO=XP
profilo
deltamu
machaustetax
weiter2
E: 'no sol'n for Mprech...'
C: DISTANZS > 0.001LP
I: 20
incidunic
profilo
XO=0
profilu
XU=0
radius
Z=0
profilo
XO=XPN
weiter3
E: 'no sol'n for incidun'
C: DISTANZS > 0.0001LP
I: 200
deltalamda
deltamu
machaustetax
weiter3
E: 'no sol'n for incidunic'
C: MSV-MS > 0.0003
I: 50
total
Z=ZP
radius
Z=ZT
radius
Line a50 (kopfwelle<3)
Z=0
total
E: 'bow shock detaches'
C: SO > SK or SU > SK
I: N/A
weiter3
kritabl
machaustetax
E: 'shock angle not found'
C: tan(DK)-tan[O(I)]/wert1 > 0.02CB
I: 50
weiter3
stossw
machstoss

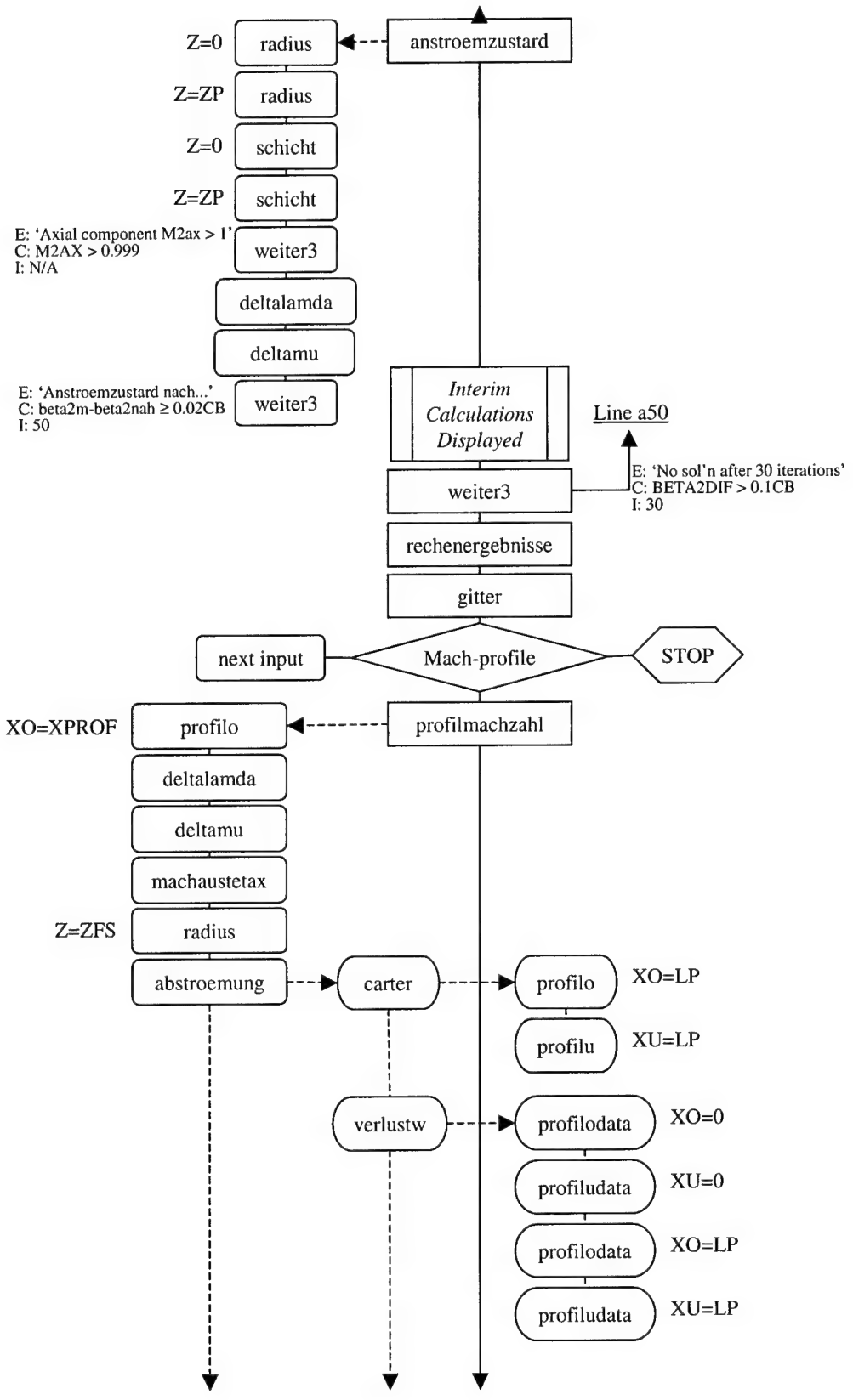
anstroemzustard
Z=0
radius
Z=ZP
radius
Z=0
schicht
Z=ZP
schicht
E: 'Axial component M2ax > 1'
C: M2AX > 0.999
I: N/A
weiter3
deltalamda
deltamu
E: 'Anstroemzustard nach...'
C: beta2m-beta2nah ≥ 0.02CB
I: 50
weiter3
Interim Calculations Displayed
Line a50
E: 'No sol'n after 30 iterations'
C: BETA2DIF > 0.1CB
I: 30
weiter3
rechenergebnisse
gitter
next input
Mach-profile
STOP
XO=XPROF
profilo
profilmachzahl
deltalamda
deltamu
machaustetax
Z=ZFS
radius
abstroemung
carter
profilo
XO=LP
profilu
XU=LP
verlustw
profilodata
XO=0
profiludata
XU=0
profilodata
XO=LP
profiludata
XU=LP

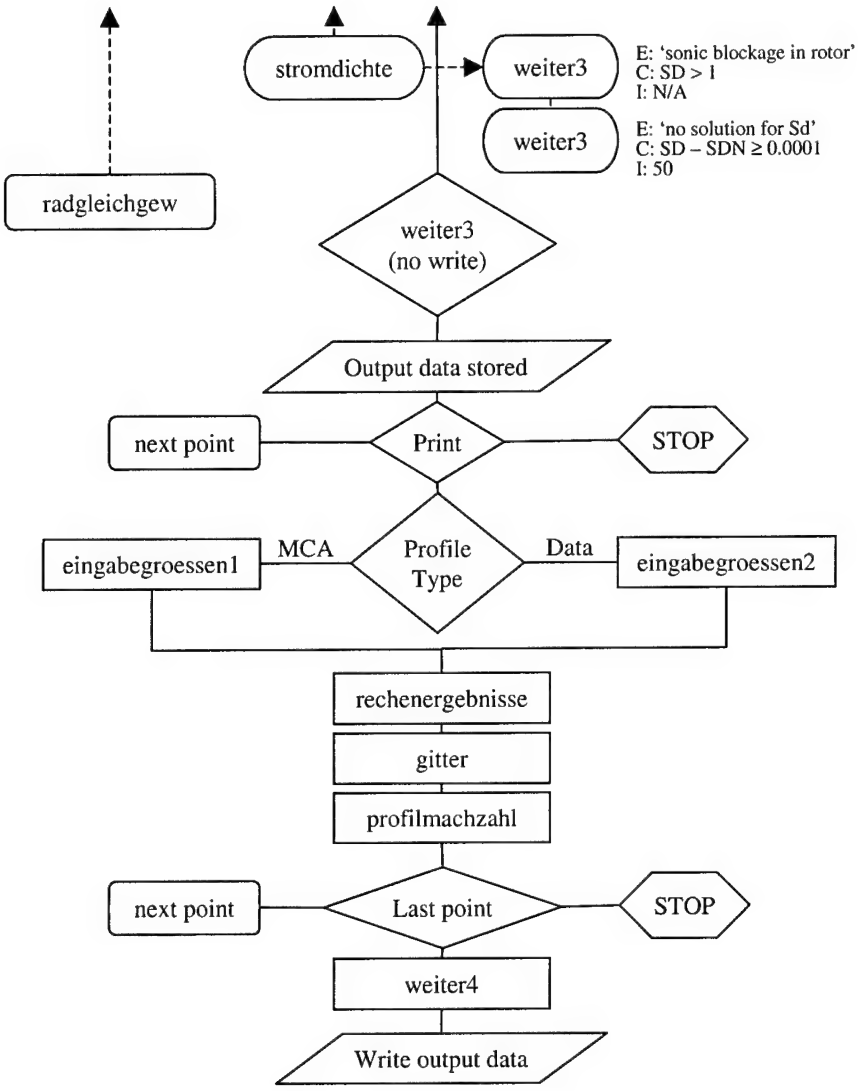
stromdichte
weiter3
E: 'sonic blockage in rotor'
C: SD > 1
I: N/A
weiter3
E: 'no solution for Sd'
C: SD – SDN ≥ 0.0001
I: 50
radgleichgew
weiter3
(no write)
Output data stored
next point
Print
STOP
eingabegroessen1
MCA
Profile
Type
Data
eingabegroessen2
rechenergebnisse
gitter
profilmachzahl
next point
Last point
STOP
weiter4
Write output data

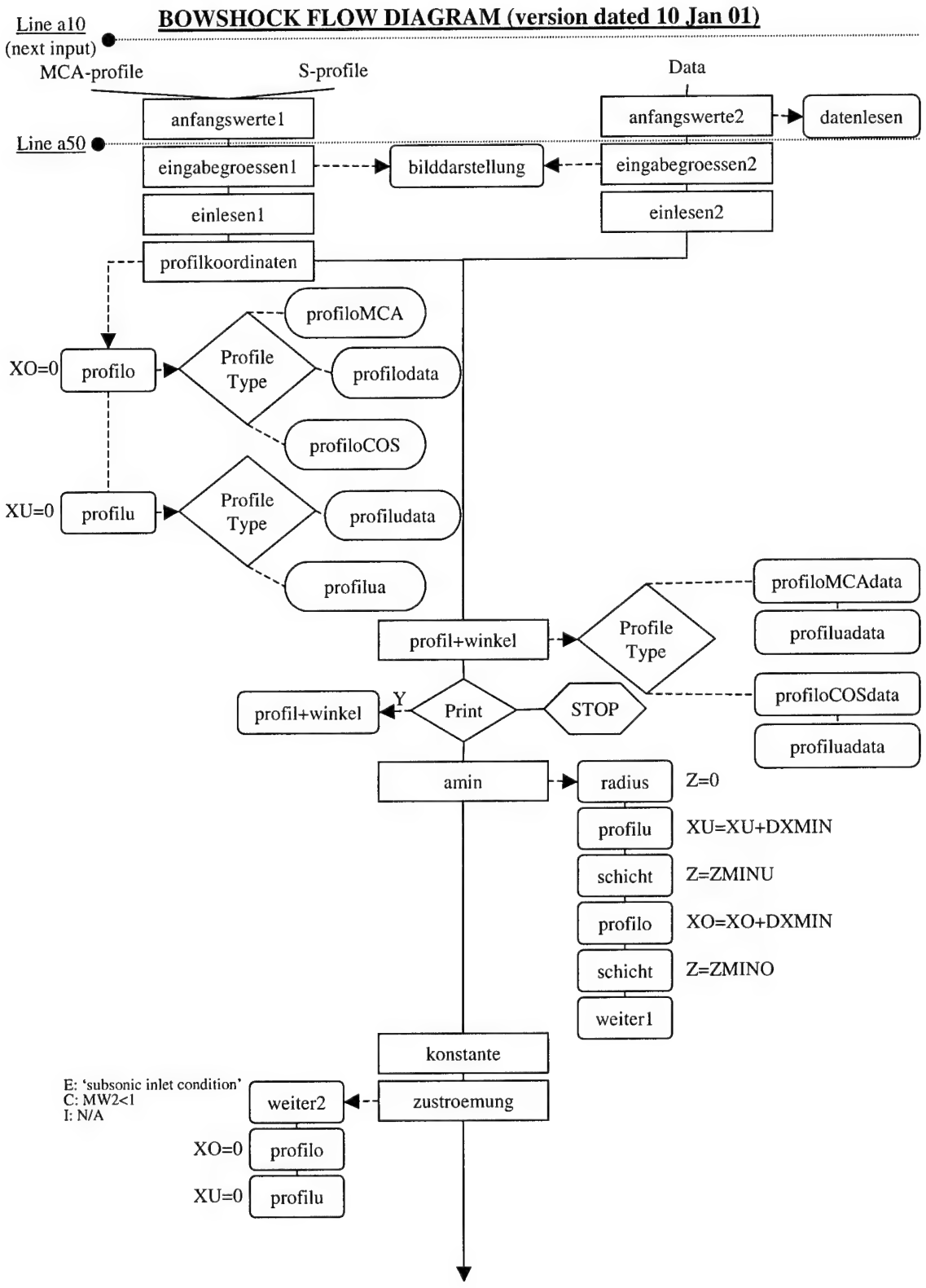
BOWSHOCK FLOW DIAGRAM (version dated 10 Jan 01)
Line a10
(next input)
MCA-profile
S-profile
Data
anfangswerte1
anfangswerte2
datenlesen
Line a50
eingabegroessen1
bilddarstellung
eingabegroessen2
einlesen1
einlesen2
profilkoordinaten
profiloMCA
XO=0
profilo
Profile Type
profilodata
profiloCOS
XU=0
profilu
Profile Type
profiludata
profilua
profiloMCAdata
profil+winkel
Profile Type
profiluadata
profiloCOSdata
profil+winkel
Y
Print
STOP
profiluadata
amin
radius
Z=0
profilu
XU=XU+DXMIN
schicht
Z=ZMINU
profilo
XO=XO+DXMIN
schicht
Z=ZMINO
weiter1
konstante
E: 'subsonic inlet condition'
C: MW2<1
I: N/A
weiter2
zustroemung
XO=0
profilo
XU=0
profilu

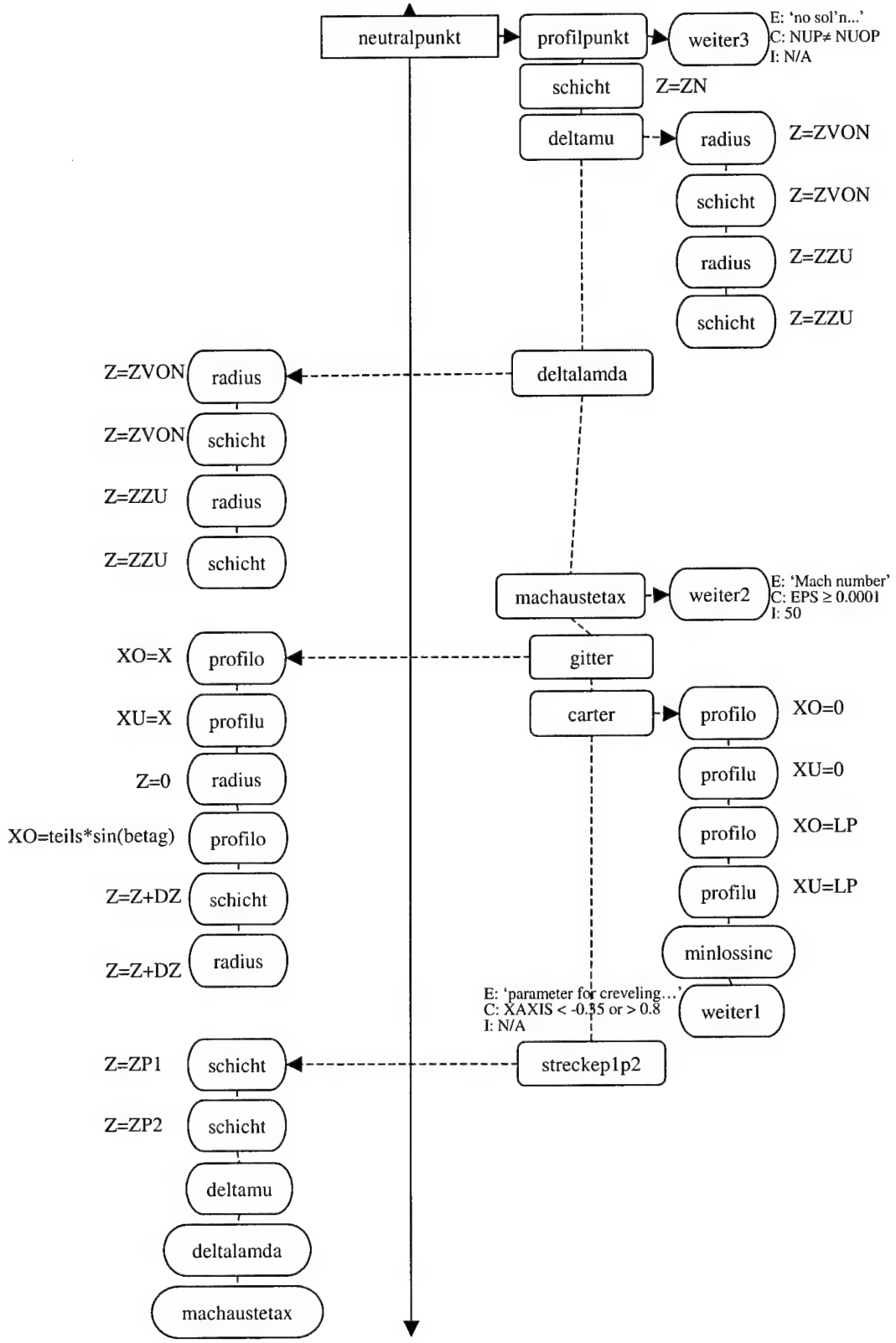
neutralpunkt
profilpunkt
weiter3
E: 'no sol'n...'
C: NUP≠ NUOP
I: N/A
schicht
Z=ZN
deltamu
radius
Z=ZVON
schicht
Z=ZVON
radius
Z=ZZU
schicht
Z=ZZU
deltalamda
Z=ZVON
radius
Z=ZVON
schicht
Z=ZZU
radius
Z=ZZU
schicht
machaustetax
weiter2
E: 'Mach number'
C: EPS ≥ 0.0001
I: 50
gitter
XO=X
profilo
XU=X
profilu
Z=0
radius
XO=teils*sin(betag)
profilo
Z=Z+DZ
schicht
Z=Z+DZ
radius
carter
profilo
XO=0
profilu
XU=0
profilo
XO=LP
profilu
XU=LP
minlossinc
weiter1
E: 'parameter for creveling...'
C: XAXIS < -0.35 or > 0.8
I: N/A
streckep1p2
Z=ZP1
schicht
Z=ZP2
schicht
deltamu
deltalamda
machaustetax

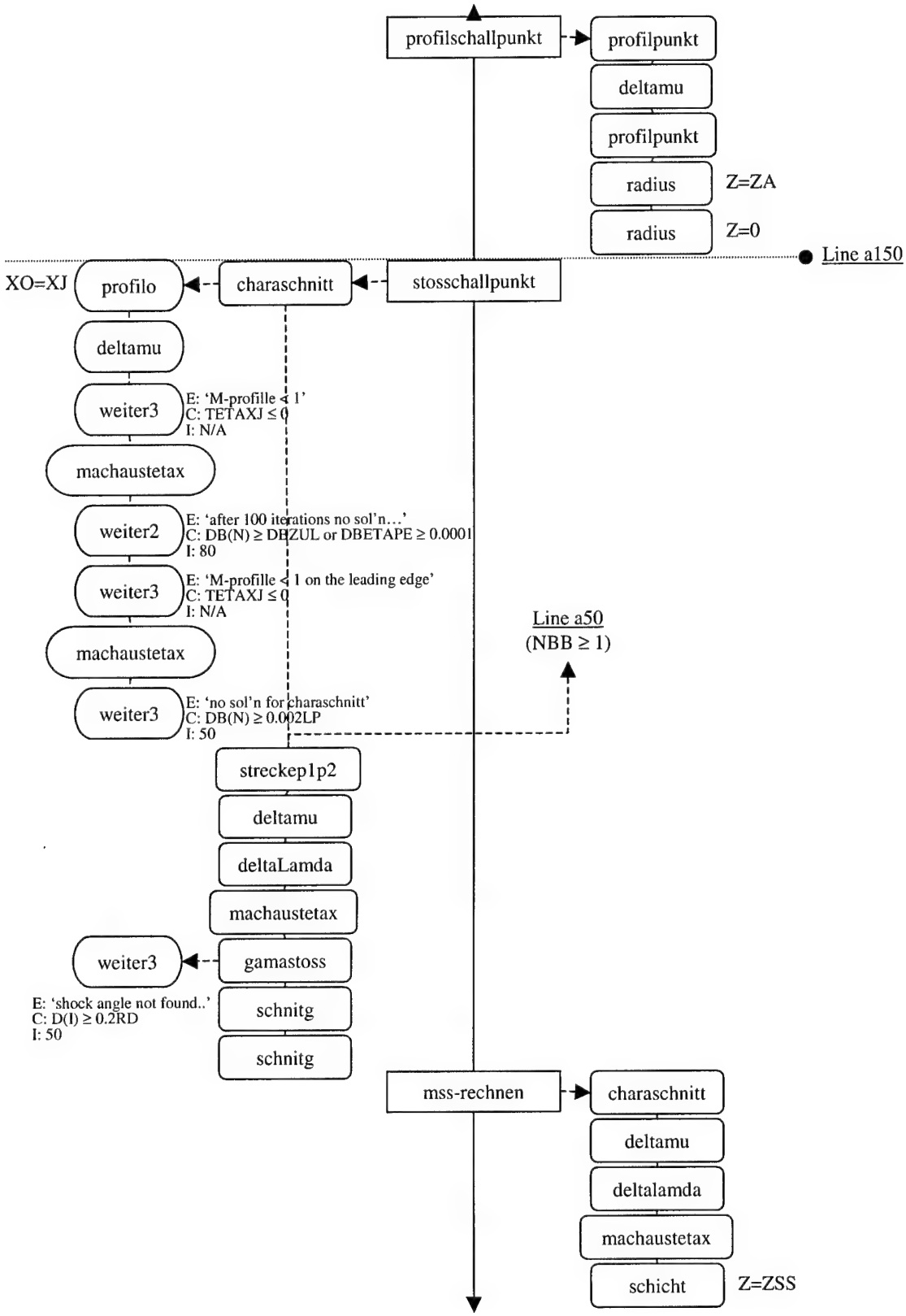
profilschallpunkt
profilpunkt
deltamu
profilpunkt
radius
Z=ZA
radius
Z=0
Line a150
XO=XJ
profilo
charaschnitt
stosschallpunkt
deltamu
weiter3
E: 'M-profille < 1'
C: TETAXJ ≤ 0
I: N/A
machaustetax
weiter2
E: 'after 100 iterations no sol'n…'
C: DB(N) ≥ DBZUL or DBETAPE ≥ 0.0001
I: 80
weiter3
E: 'M-profille < 1 on the leading edge'
C: TETAXJ ≤ 0
I: N/A
machaustetax
Line a50
(NBB ≥ 1)
weiter3
E: 'no sol'n for charaschnitt'
C: DB(N) ≥ 0.002LP
I: 50
streckep1p2
deltamu
deltaLamda
machaustetax
weiter3
gamastoss
E: 'shock angle not found..'
C: D(I) ≥ 0.2RD
I: 50
schnitg
schnitg
mss-rechnen
charaschnitt
deltamu
deltalamda
machaustetax
schicht
Z=ZSS

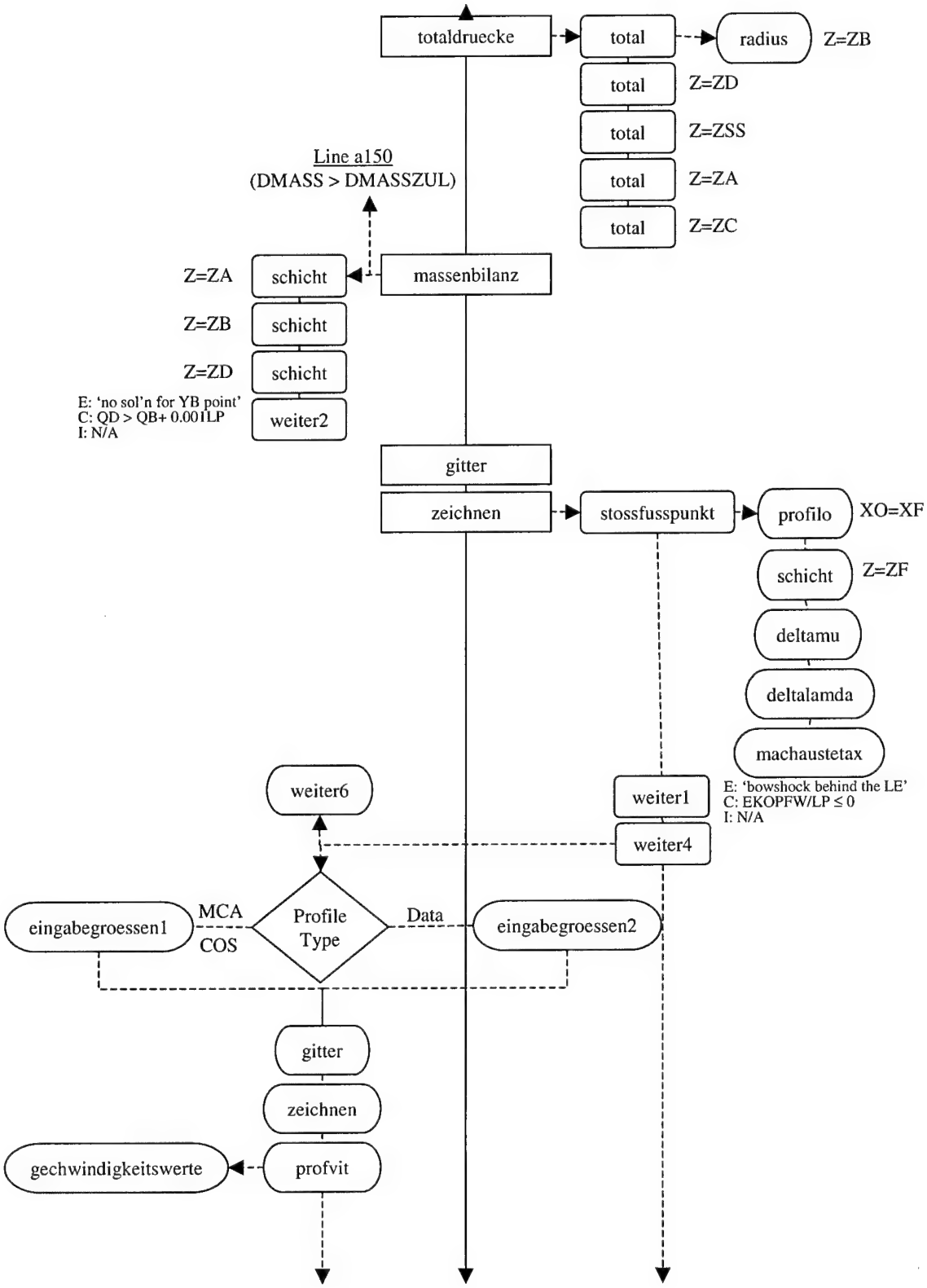
totaldruecke
total
radius
Z=ZB
total
Z=ZD
total
Z=ZSS
total
Z=ZA
total
Z=ZC
Line a150
(DMASS > DMASSZUL)
massenbilanz
Z=ZA
schicht
Z=ZB
schicht
Z=ZD
schicht
weiter2
E: 'no sol'n for YB point'
C: QD > QB+ 0.001LP
I: N/A
gitter
zeichnen
stossfusspunkt
profilo
XO=XF
schicht
Z=ZF
deltamu
deltalamda
machaustetax
E: 'bowshock behind the LE'
C: EKOPFW/LP ≤ 0
I: N/A
weiter6
weiter1
weiter4
eingabegroessen1
MCA
COS
Profile
Type
Data
eingabegroessen2
gitter
zeichnen
gechwindigkeitswerte
profvit

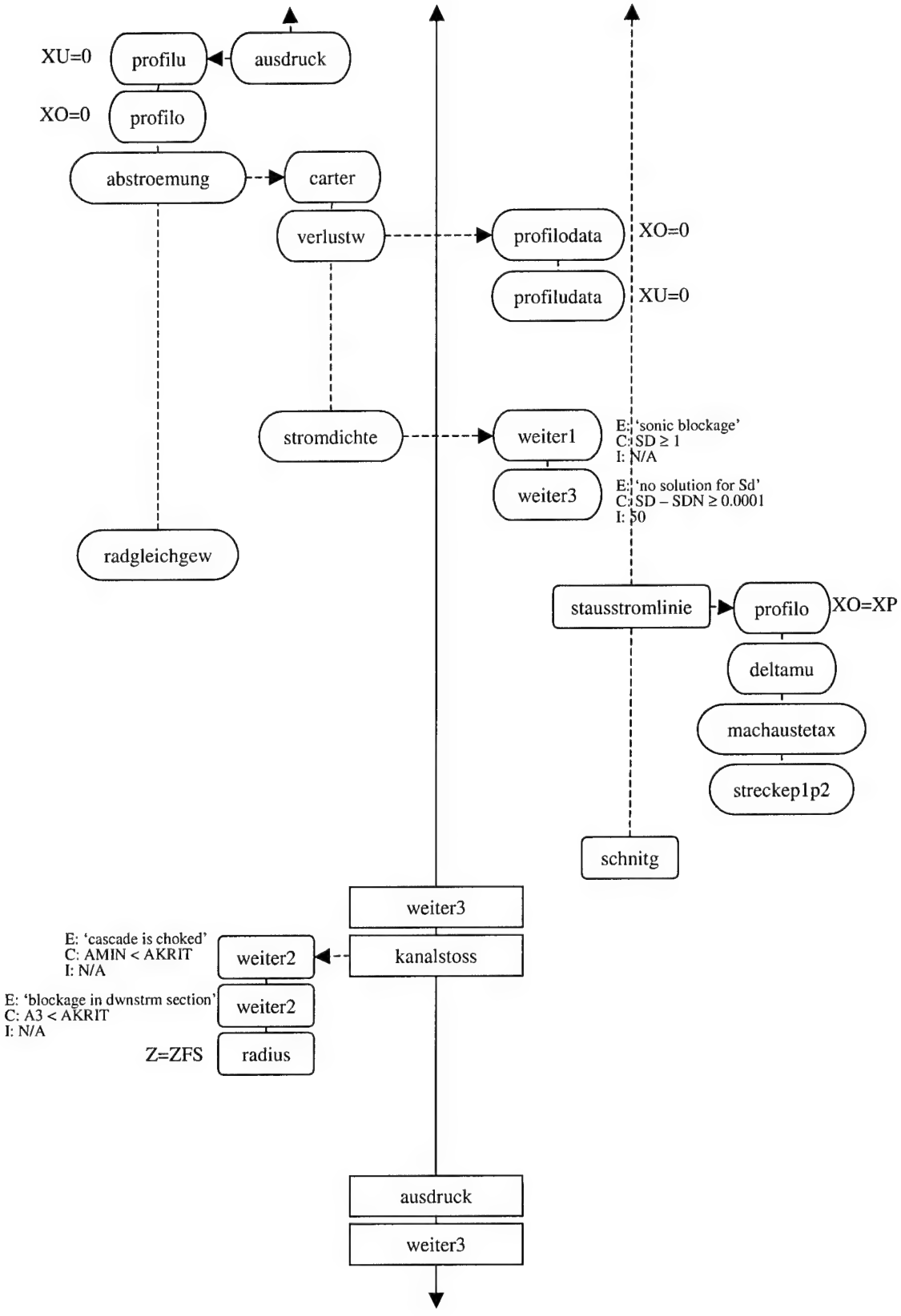
XU=0
profilu
ausdruck
XO=0
profilo
abstroemung
carter
verlustw
profilodata
XO=0
profiludata
XU=0
stromdichte
weiter1
E: 'sonic blockage'
C: SD ≥ 1
I: N/A
weiter3
E: 'no solution for Sd'
C: SD – SDN ≥ 0.0001
I: 50
radgleichgew
stausstromlinie
profilo
XO=XP
deltamu
machaustetax
streckep1p2
schnitg
weiter3
E: 'cascade is choked'
C: AMIN < AKRIT
I: N/A
weiter2
kanalstoss
E: 'blockage in dwnstrm section'
C: A3 < AKRIT
I: N/A
weiter2
Z=ZFS
radius
ausdruck
weiter3

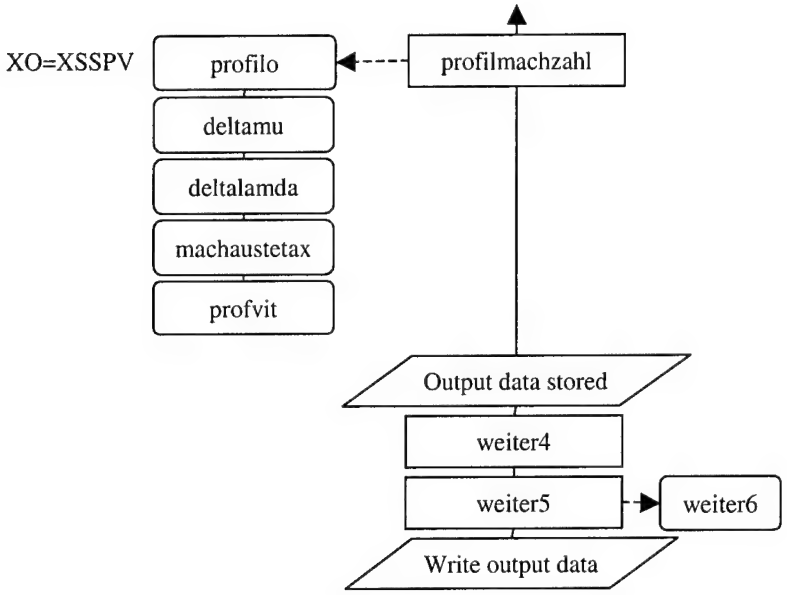
XO=XSSPV
profilo
profilmachzahl
deltamu
deltalamda
machaustetax
profvit
Output data stored
weiter4
weiter5
weiter6
Write output data

TRANSROTOR FLOW DIAGRAM (version dated 3 Dec 00)

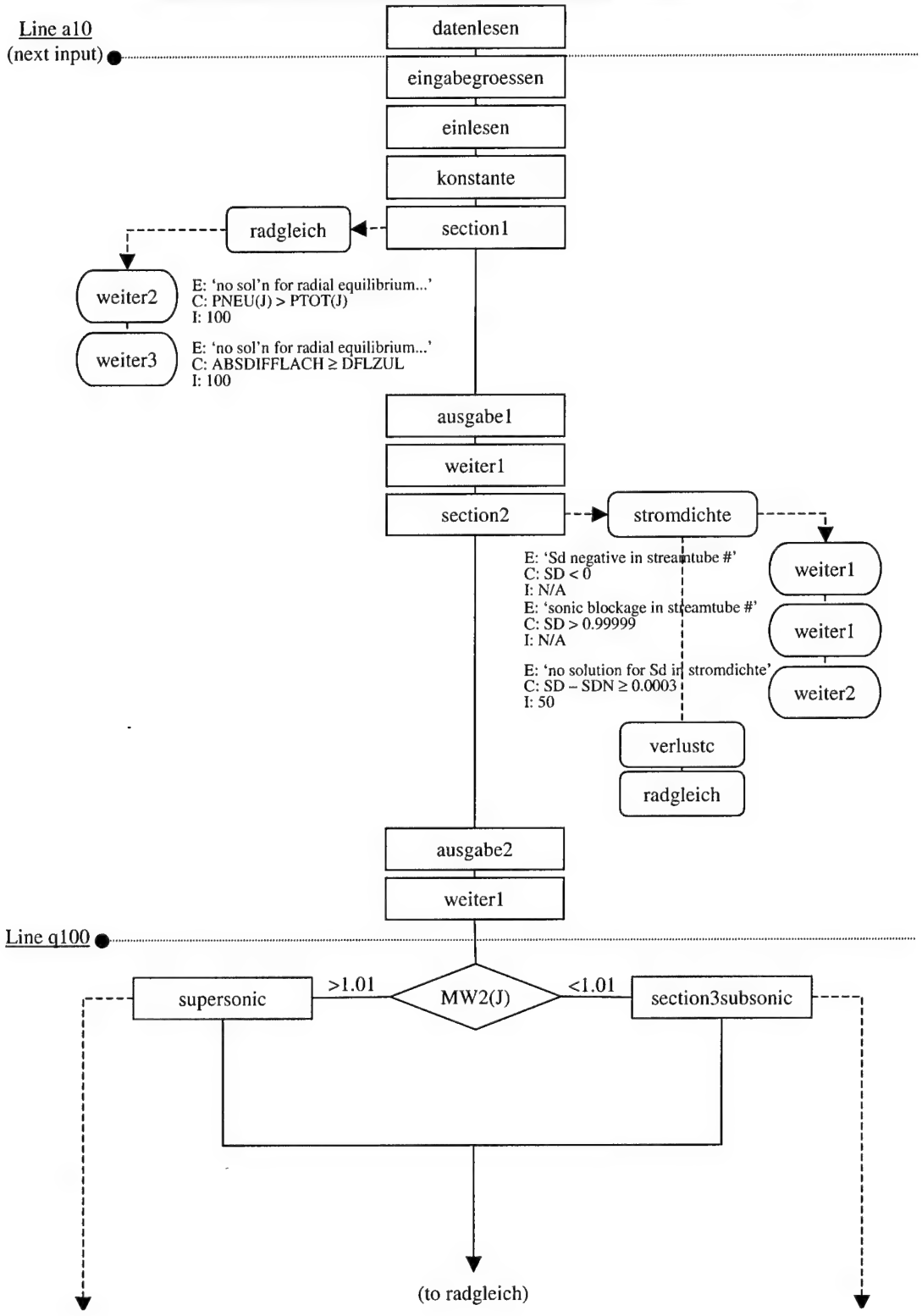

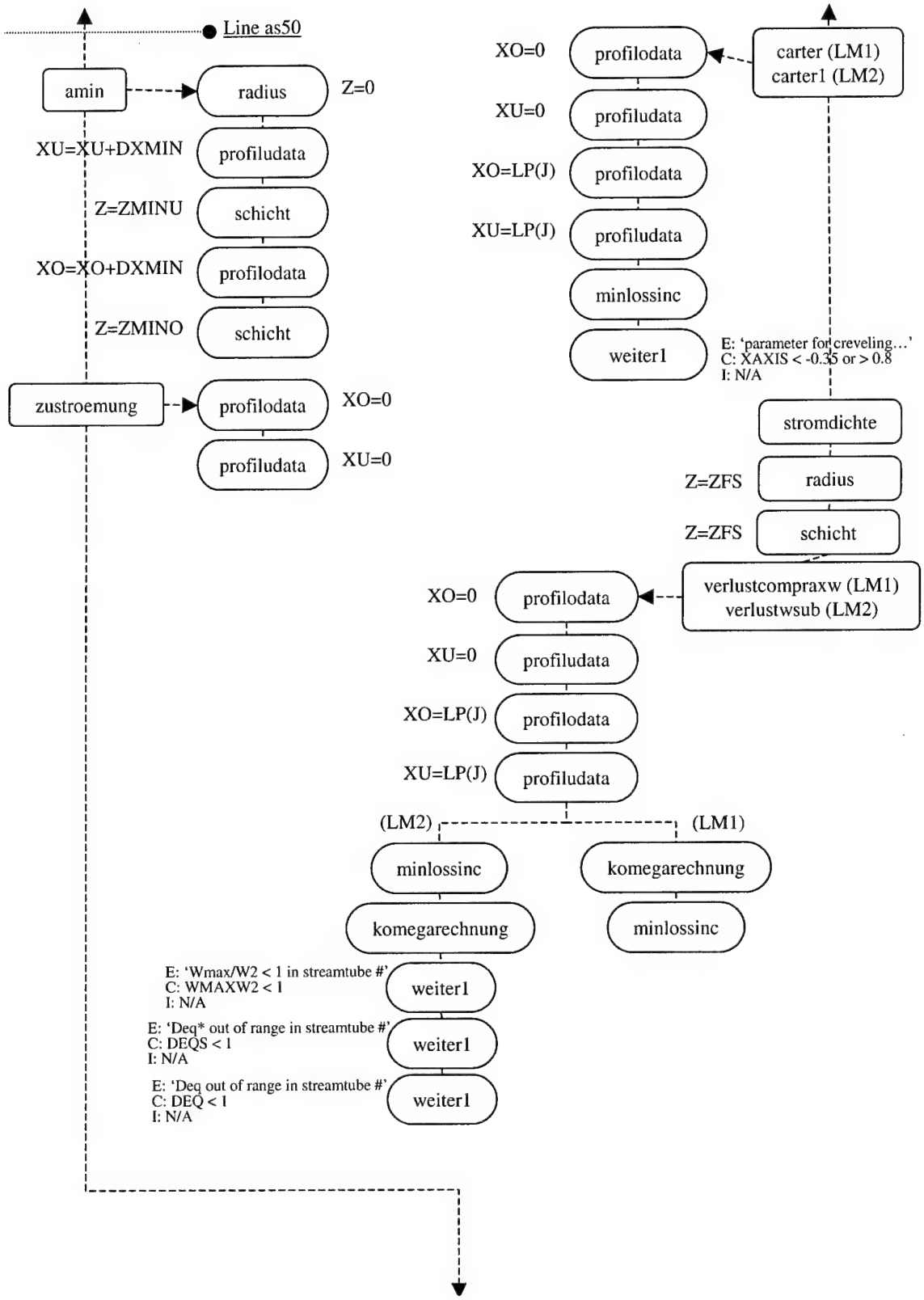
Line as50
amin
radius
Z=0
XU=XU+DXMIN
profiludata
Z=ZMINU
schicht
XO=XO+DXMIN
profilodata
Z=ZMINO
schicht
zustroemung
profilodata
XO=0
profiludata
XU=0
XO=0
profilodata
XU=0
profiludata
XO=LP(J)
profilodata
XU=LP(J)
profiludata
minlossinc
weiter1
carter (LM1)
carter1 (LM2)
E: 'parameter for creveling...'
C: XAXIS < -0.35 or > 0.8
I: N/A
stromdichte
Z=ZFS
radius
Z=ZFS
schicht
verlustcompraxw (LM1)
verlustwsub (LM2)
XO=0
profilodata
XU=0
profiludata
XO=LP(J)
profilodata
XU=LP(J)
profiludata
(LM2)
(LM1)
minlossinc
komegarechnung
komegarechnung
minlossinc
E: 'Wmax/W2 < 1 in streamtube #'
C: WMAXW2 < 1
I: N/A
weiter1
E: 'Deq* out of range in streamtube #'
C: DEQS < 1
I: N/A
weiter1
E: 'Deq out of range in streamtube #'
C: DEQ < 1
I: N/A
weiter1

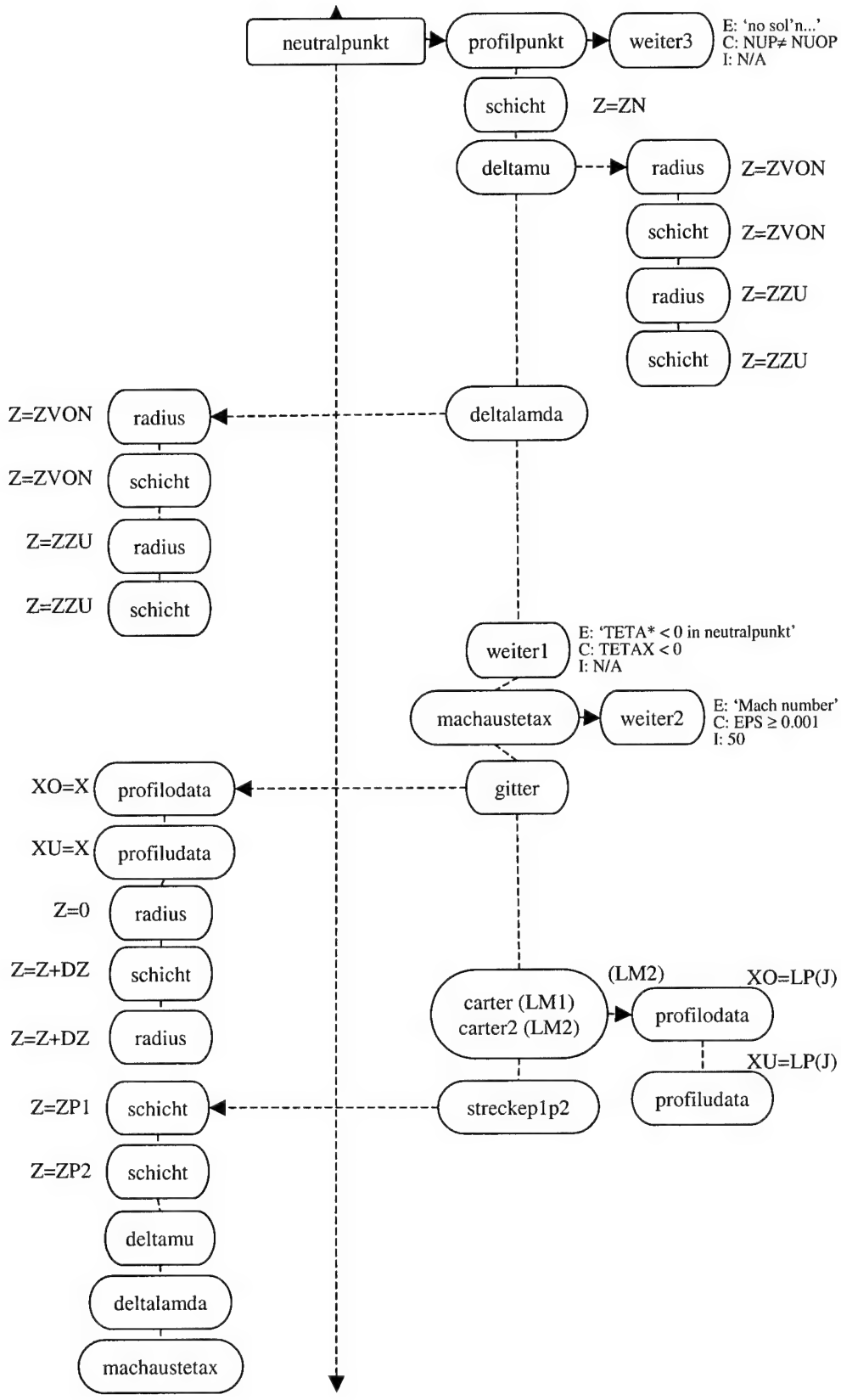
neutralpunkt
profilpunkt
weiter3
E: 'no sol'n...'
C: NUP≠ NUOP
I: N/A
schicht
Z=ZN
deltamu
radius
Z=ZVON
schicht
Z=ZVON
radius
Z=ZZU
schicht
Z=ZZU
deltalamda
Z=ZVON
radius
Z=ZVON
schicht
Z=ZZU
radius
Z=ZZU
schicht
weiter1
E: 'TETA* < 0 in neutralpunkt'
C: TETAX < 0
I: N/A
machaustetax
weiter2
E: 'Mach number'
C: EPS ≥ 0.001
I: 50
gitter
XO=X
profilodata
XU=X
profiludata
Z=0
radius
Z=Z+DZ
schicht
Z=Z+DZ
radius
carter (LM1)
carter2 (LM2)
(LM2)
XO=LP(J)
profilodata
XU=LP(J)
profiludata
Z=ZP1
schicht
streckep1p2
Z=ZP2
schicht
deltamu
deltalamda
machaustetax

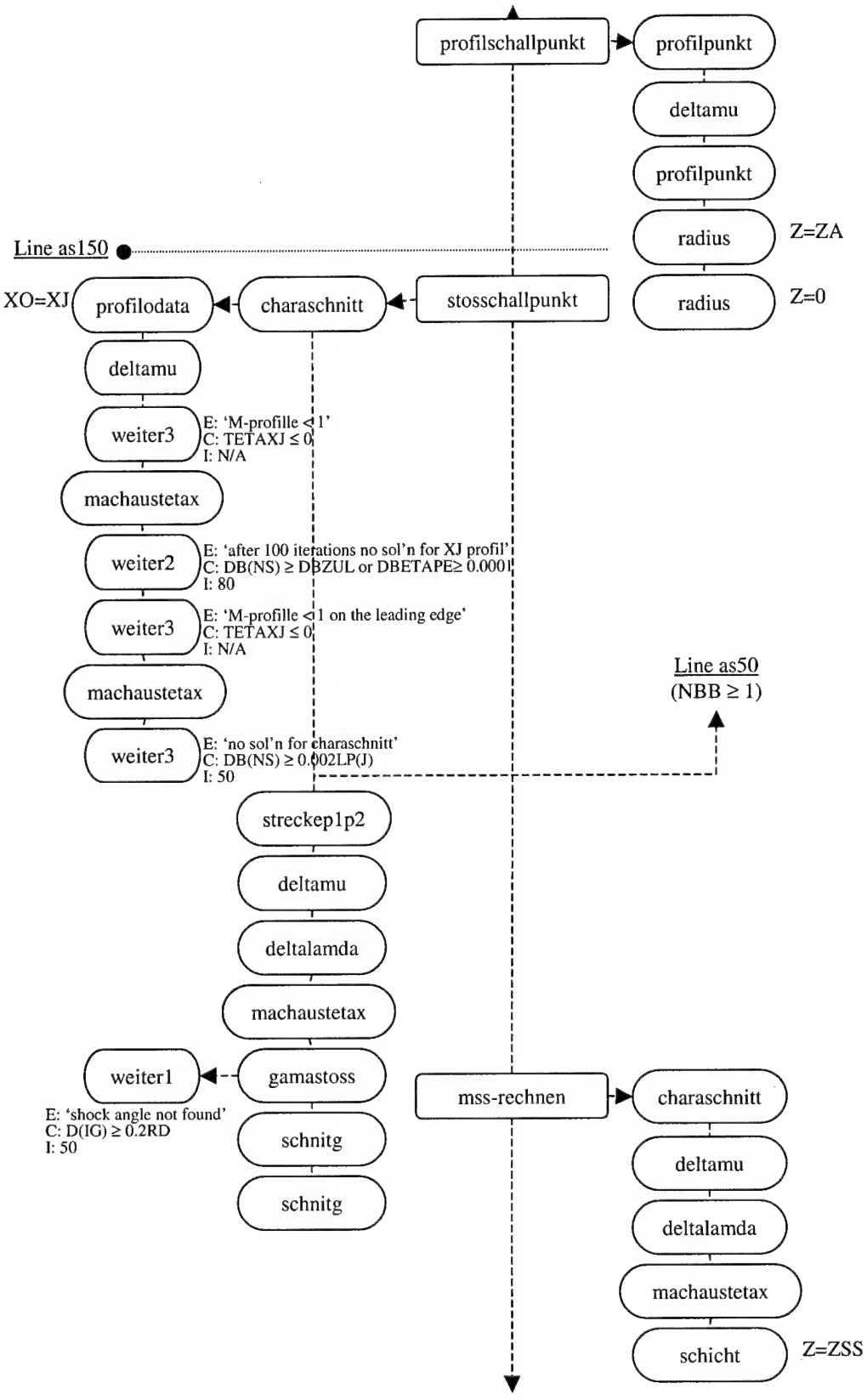
profilschallpunkt
profilpunkt
deltamu
profilpunkt
radius
Z=ZA
Line as150
XO=XJ
profilodata
charaschnitt
stosschallpunkt
radius
Z=0
deltamu
weiter3
E: 'M-profille < 1'
C: TETAXJ ≤ 0
I: N/A
machaustetax
weiter2
E: 'after 100 iterations no sol'n for XJ profil'
C: DB(NS) ≥ DBZUL or DBETAPE≥ 0.0001
I: 80
weiter3
E: 'M-profille < 1 on the leading edge'
C: TETAXJ ≤ 0
I: N/A
machaustetax
Line as50
(NBB ≥ 1)
weiter3
E: 'no sol'n for charaschnitt'
C: DB(NS) ≥ 0.002LP(J)
I: 50
streckep1p2
deltamu
deltalamda
machaustetax
weiter1
gamastoss
E: 'shock angle not found'
C: D(IG) ≥ 0.2RD
I: 50
schnitg
schnitg
mss-rechnen
charaschnitt
deltamu
deltalamda
machaustetax
schicht
Z=ZSS

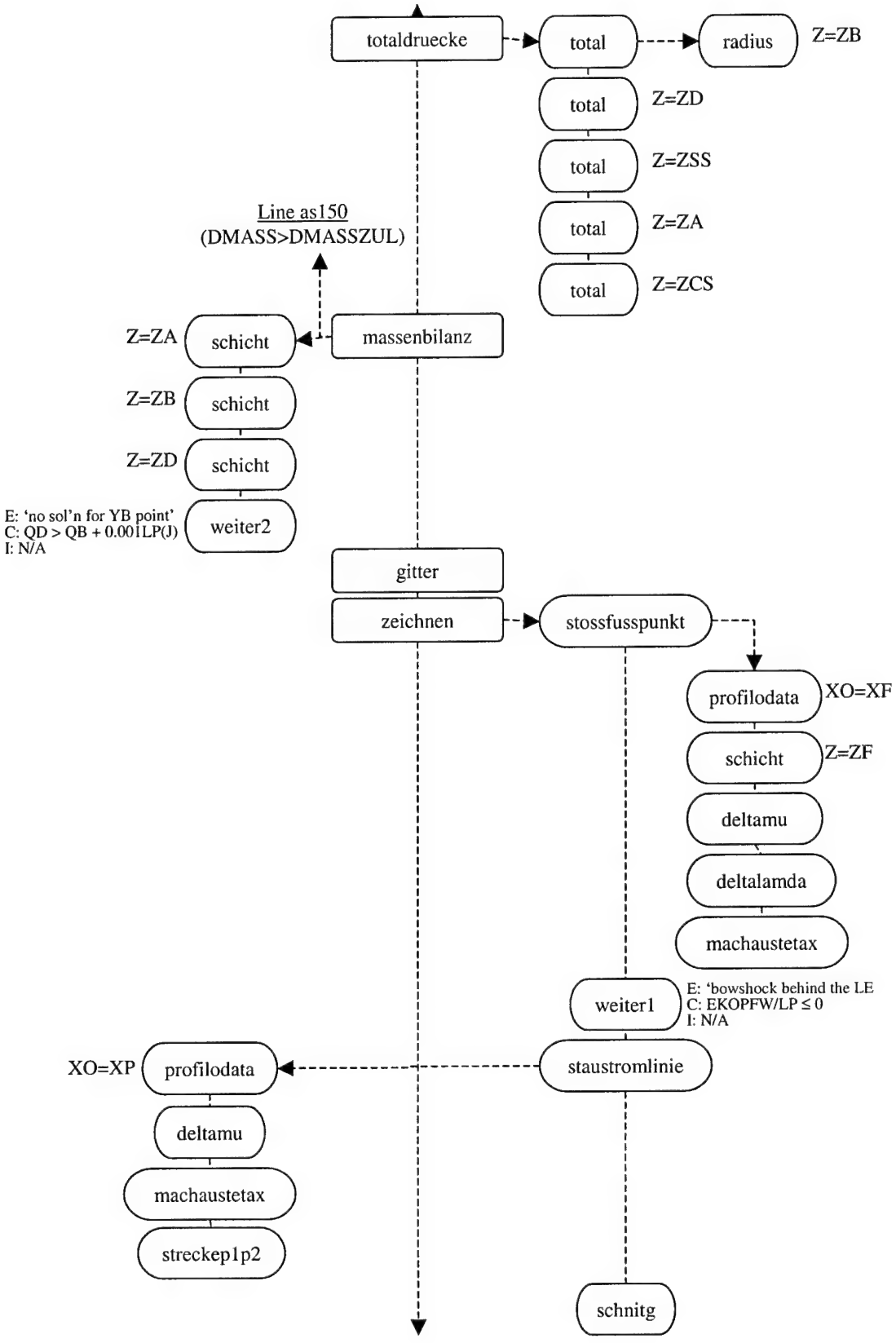
totaldruecke
total
radius
Z=ZB
total
Z=ZD
total
Z=ZSS
total
Z=ZA
total
Z=ZCS
Line as150
(DMASS>DMASSZUL)
massenbilanz
Z=ZA
schicht
Z=ZB
schicht
Z=ZD
schicht
E: 'no sol'n for YB point'
C: QD > QB + 0.001LP(J)
I: N/A
weiter2
gitter
zeichnen
stossfusspunkt
profilodata
XO=XF
schicht
Z=ZF
deltamu
deltalamda
machaustetax
weiter1
E: 'bowshock behind the LE
C: EKOPFW/LP ≤ 0
I: N/A
XO=XP
profilodata
staustromlinie
deltamu
machaustetax
streckep1p2
schnitg

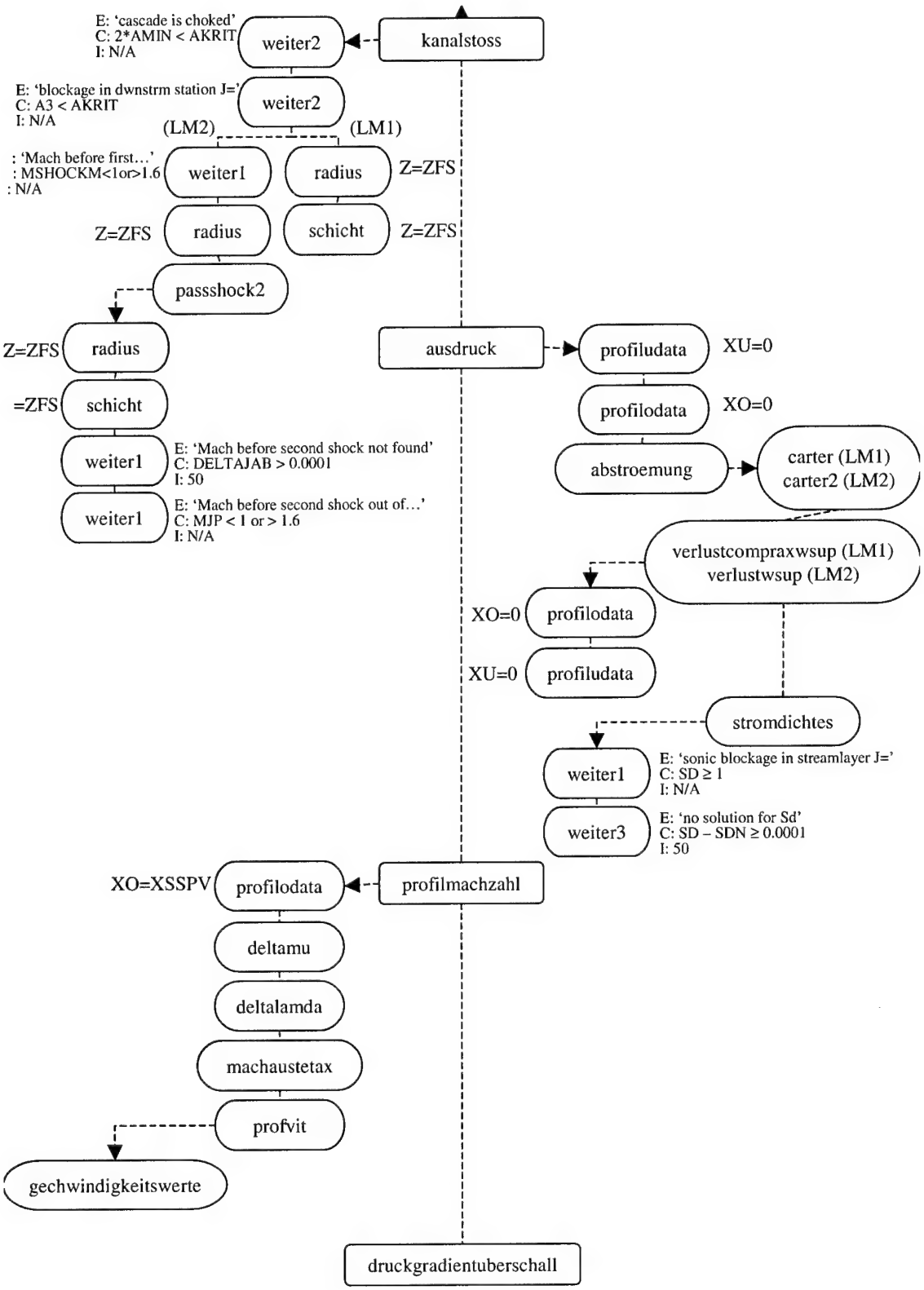
E: 'cascade is choked'
C: 2*AMIN < AKRIT
I: N/A
weiter2
kanalstoss
E: 'blockage in dwnstrm station J='
C: A3 < AKRIT
I: N/A
weiter2
(LM2)
(LM1)
: 'Mach before first...'
: MSHOCKM<1or>1.6
: N/A
weiter1
radius
Z=ZFS
Z=ZFS
radius
schicht
Z=ZFS
passshock2
Z=ZFS
radius
=ZFS
schicht
weiter1
E: 'Mach before second shock not found'
C: DELTAJAB > 0.0001
I: 50
weiter1
E: 'Mach before second shock out of...'
C: MJP < 1 or > 1.6
I: N/A
ausdruck
profiludata
XU=0
profilodata
XO=0
abstroemung
carter (LM1)
carter2 (LM2)
verlustcompraxwsup (LM1)
verlustwsup (LM2)
XO=0
profilodata
XU=0
profiludata
stromdichtes
weiter1
E: 'sonic blockage in streamlayer J='
C: SD ≥ 1
I: N/A
weiter3
E: 'no solution for Sd'
C: SD – SDN ≥ 0.0001
I: 50
XO=XSSPV
profilodata
profilmachzahl
deltamu
deltalamda
machaustetax
profvit
gechwindigkeitswerte
druckgradientuberschall

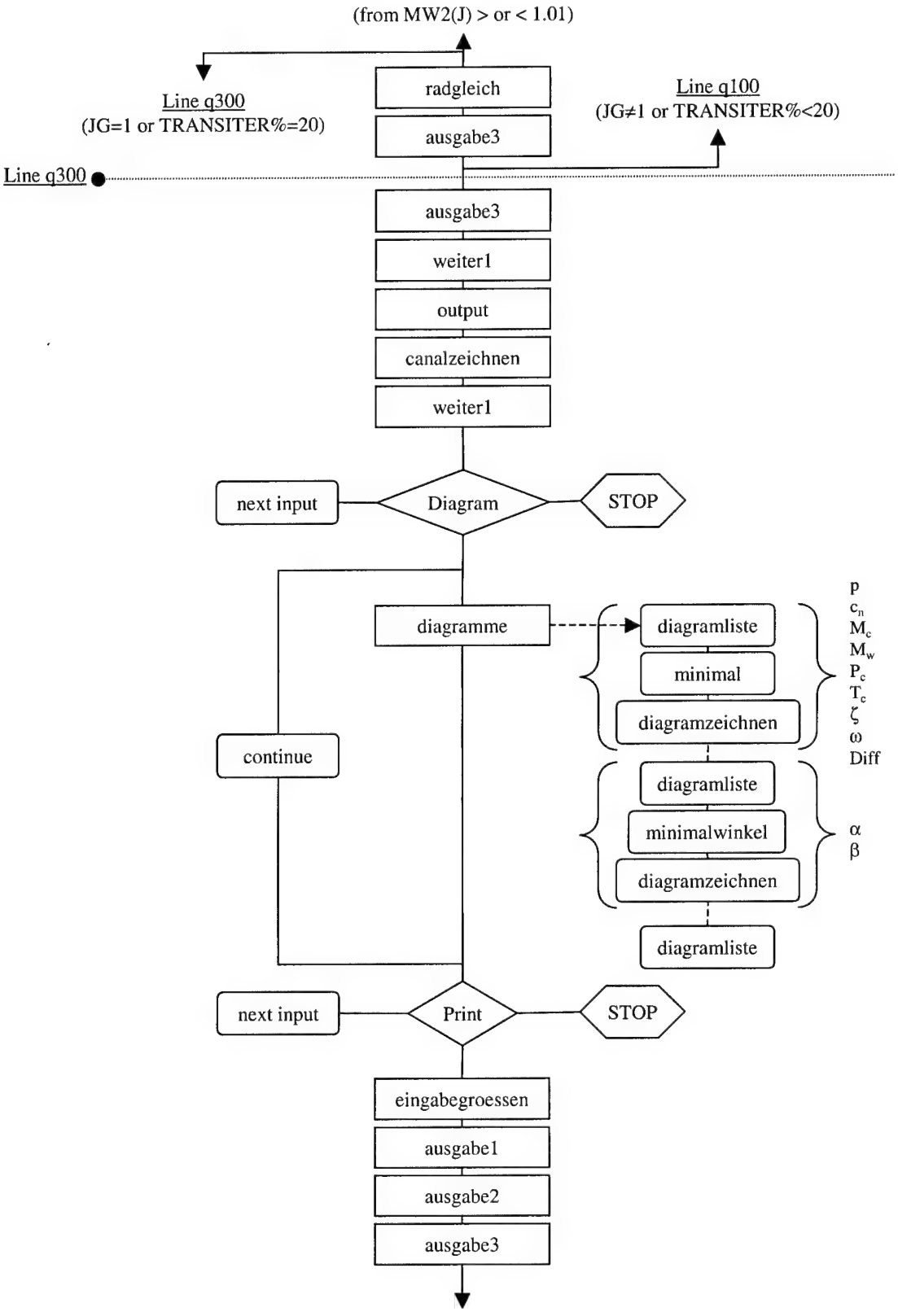
(from MW2(J) > or < 1.01)
Line q300
(JG=1 or TRANSITER%=20)
radgleich
ausgabe3
Line q100
(JG≠1 or TRANSITER%<20)
Line q300
ausgabe3
weiter1
output
canalzeichnen
weiter1
next input
Diagram
STOP
diagramme
diagramliste
minimal
diagramzeichnen
p
c_n
M_c
M_w
P_c
T_c
ζ
ω
Diff
continue
diagramliste
minimalwinkel
diagramzeichnen
α
β
diagramliste
next input
Print
STOP
eingabegroessen
ausgabe1
ausgabe2
ausgabe3

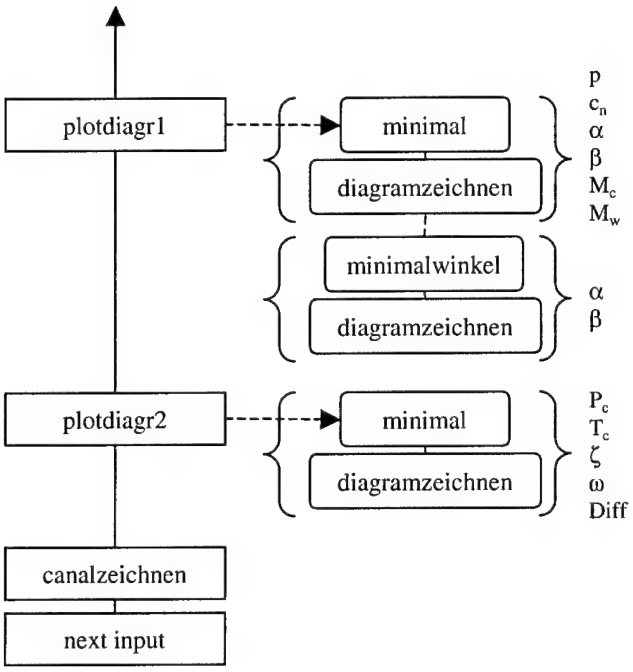
plotdiagr1
minimal
diagramzeichnen
p
c_n
α
β
M_c
M_w
minimalwinkel
diagramzeichnen
α
β
plotdiagr2
minimal
diagramzeichnen
P_c
T_c
ζ
ω
Diff
canalzeichnen
next input

This appendix provides examples of the required format for input text files. The required format consists of all lines shown between the boldfaced option indicators and/or the program names.

Notes:

1. All programs ignore the lines that have the backslash (/) separator. These lines must be given place holders in the input text file. They are included so that the input text file can have labels for each line of data.
2. Italicized comments are for clarification in this appendix and should not be in the input file.
3. All input files must end with a blank line.

D.1 INCIDUNIQUE

MCA Option

Input Filename / Output Filename

filename.txt, filename.csv

γ / R(J/kgK) / L(mm) / X_d/L / d/L / f/L

1.396, 287, 47.36, 0.649, 0.05, 0.061

N / β_g(deg) / P_{c2}(bar) / T_{c2}(K)

74, 41.53, 2.42, 376

Z_2(mm) / R_2(mm) / b_2(mm) / Z_3(mm) / R_3(mm) / b_3(mm)

18, 159.9, 6.813, 18, 165.8, 4.563

n(rpm) / α_2(deg)

20463, 0

Data Option

Input Filename / Output Filename

filename.txt, filename.csv

γ / R(J/kgK) / N / β_g(deg) / P_{c2}(bar) / T_{c2}(bar)

1.396, 287, 74, 41.53, 2.42, 376

Z_2(mm) / R_2(mm) / b_2(mm) / Z_3(mm) / R_3(mm) / b_3(mm)

18, 159.9, 6.813, 18, 165.8, 4.563

n(rpm) / α_2(deg)

20463, 0

80 *No. of xy-coordinate pairs defining each blade surface*

0,0 *xy-coordinates of SS from LE to TE*

0.7134,0.3321...

0,0 *xy-coordinates of PS from LE to TE*

0.7860,-0.0077...

D.2 BOWSHOCK

MCA Option

Input Filename / Output Filename

filename.txt, filename.csv

γ / R(J/kgK) / C_2(m/s) / L(mm) / X_d/L / d/L / f/L

1.396, 287, 200.4, 47.36, 0.649, 0.05, 0.061

N / β_g(deg) / P_{c2}(bar) / T_{c2}(K)

74, 41.53, 2.42, 376

Z_2(mm) / R_2(mm) / b_2(mm) / Z_3(mm) / R_3(mm) / b_3(mm)

18, 159.9, 6.813, 18, 165.8, 4.563

n(rpm) / α_2(deg)

20463, 0

Blade Surface Points

30

Data Option

Input Filename / Output Filename

filename.txt, filename.csv

C_2(m/s) / γ / R(J/kgK) / N / β_g(deg) / P_{c2}(bar) / T_{c2}(bar)

200.4, 1.396, 287, 74, 41.53, 2.42, 376

Z_2(mm) / R_2(mm) / b_2(mm) / Z_3(mm) / R_3(mm) / b_3(mm)

18, 159.9, 6.813, 18, 165.8, 4.563

n(rpm) / α_2(deg)

20463, 0

80 *No. of xy-coordinate pairs defining each blade surface*

0,0 *xy-coordinates of SS from LE to TE*

0.7134,0.3321...

0,0 *xy-coordinates of PS from LE to TE*

0.7860,-0.0077...

D.3 TRANSROTOR

No. of Tubes / γ / C_p(J/kgK) / R(J/kgK) / n(rpm) / N

5, 1.388, 1026.3, 287, 20463, 74

R_{i1}(mm) / R_{i2}(mm) / R_{i3}(mm)

143.5, 146.3, 157.3

R_{e1}(mm) / R_{e2}(mm) / R_{e3}(mm)

177.8, 177.8, 177.8

(1)α_1(deg) / (2)α_1 / (3)α_1 / (4)α_1 / (5)α_1 / (6)α_1 / (7)α_1

0, 0, 0, 0, 0, 0, 0

(1)P_{c1}(bar) / (2)P_{c1} / (3)P_{c1} / (4)P_{c1} / (5)P_{c1} / (6)P_{c1} / (7)P_{c1}

2.42, 2.42, 2.42, 2.42, 2.42, 0, 0

(1)T_{c1}(bar) / (2)T_{c1} / (3)T_{c1} / (4)T_{c1} / (5)T_{c1} / (6)T_{c1} / (7)T_{c1}

378, 376, 376, 378, 383, 0, 0

(1)C_{1n}(m/s) / (2)C_{1n} / (3)C_{1n} / (4)C_{1n} / (5)C_{1n} / (6)C_{1n} / (7)C_{1n}

165.2, 165.2, 165.2, 165.2, 165.2, 0, 0

(1)α_2(deg) / (2)α_2 / (3)α_2 / (4)α_2 / (5)α_2 / (6)α_2 / (7)α_2

0, 0, 0, 0, 0, 0, 0

(1)β_g(deg) / (2)β_g / (3)β_g / (4)β_g / (5)β_g / (6)β_g / (7)β_g

-35.79, -39.42, -41.53, -43.24, -44.24, 0, 0

(1)b_1/B_1 / (2)b_1/B_1 / (3)b_1/B_1 / (4)b_1/B_1 / (5)b_1/B_1 / (6)b_1/B_1 / (7)b_1/B_1

0.2, 0.2, 0.2, 0.2, 0.2, 0, 0

Z_2(mm) / Z_3(mm)

25.1, 18.4

80 *No. of xy-coordinate pairs defining each blade surface*

Streamtube 1 Profile

0,0 *xy-coordinates of SS from LE to TE*

0.6608,0.3659...

0,0 *xy-coordinates of PS from LE to TE*

0.7545,0.0301...

Streamtube 2 Profile...

Bibliography

1. Bölcs, Albin. "Transonic Flow in Turbomachines." Short-course notes. Short-course sponsored by the Compressor Aero Research Laboratory, Wright-Patterson AFB OH, May 1999.

2. Çetin, M., C. Hirsch, G.K. Serovy, and A.S. Üçer. "An Off-Design Loss and Deviation Prediction Study for Transonic Axial Compressors." Paper-ASME 89-GT-324 presented at the Gas Turbine and Aeroengine Congress and Exposition, Toronto, Ontario, Canada, June 1989.

3. Wilson, David G. and Theodosios Korakianitis. *The Design of High-Efficiency Turbomachinery and Gas Turbines.* Upper Saddle River: Prentice-Hall, Inc., 2^{nd} Ed., 1998.

4. Cumpsty, Nicholas A. *Compressor Aerodynamics.* New York: John Wiley & Sons, Inc., 1989.

5. Kerrebrock, Jack L. *Aircraft Engines and Gas Turbines.* Cambridge: The MIT Press, 2^{nd} Ed., 1992.

6. König, W.M., C.K. Hennecke, and L. Fottner. "Improved Blade Profile Loss and Deviation Angle Models for Advanced Transonic Compressor Bladings: Part II - A Model for Supersonic Flow," *ASME Journal of Turbomachinery*, *117*:81–87 (January 1996).

7. Law, C. Herbert. *Design of a 1250 ft/s, Low-Aspect-Ratio, Two-Stage Axial-Flow Compressor: Interim Report,* 1 November 1982-31 January 1983. AFWAL-TR-83-2027, Wright-Patterson AFB OH: Aero Propulsion Laboratory, May 1983.

8. Car, David. Engineer, Compressor Aero Research Laboratory, Wright-Patterson AFB OH. Personal correspondance, January 2000 - March 2001.

9. Law, C. Herbert and Steven L. Puterbaugh. *A Computer Program for Axial Compressor Design (UDO300M): Interim Report,* 1 June 1979-31 April 1982. AFWAL-TR-82-2074, Wright-Patterson AFB OH: Aero Propulsion Laboratory, September 1982.

10. Bölcs, Albin. "User's Guide for the Program 'BOWSHOCK'." Unpublished, June 2000.

11. Bölcs, Albin. "User's Guide for the Program 'INCIDUNIQUE'." Unpublished, June 2000.

12. Bölcs, Albin. "User's Guide for the Program 'TRANSROTOR'." Unpublished, June 2000.

13. Copenhaver, W.W., S.L. Puterbaugh, and C. Hah. "Unsteady Flow and Shock Motion in a Transonic Compressor Rotor." *31st AIAA/ASME/SAE/ASEE Joint Propulsion Conference.* San Diego CA: AIAA, Paper No. 95-2466, 10-12 July 1995.

14. Kerrebrock, Jack L. "Flow in Transonic Compressors," *AIAA Journal*, *19*:4–18 (January 1981).

15. Advisory Group for Aerospace Research and Development. *Through Flow Calculations in Axial Turbomachines*. AGARD Advisory Report No. 175. London: Technical Editing & Reproduction Ltd, October 1981.

16. Anderson, John D. *Modern Compressible Flow*. Boston: McGraw-Hill, 2^{nd} Ed., 1990.

17. König, W.M., C.K. Hennecke, and L. Fottner. "Improved Blade Profile Loss and Deviation Angle Models for Advanced Transonic Compressor Bladings: Part I - A Model for Subsonic Flow," *ASME Journal of Turbomachinery*, *118*:73–80 (January 1996).

18. Johnsen, Irving A. and Robert O. Bullock. *Aerodynamic Design of Axial-Flow Compressors*. NASA SP-36 Report. Cleveland: NASA-Lewis Research Center, 1965.

19. Lieblein, Seymour. "Incidence and Deviation-Angle Correlations for Compressor Cascades," *ASME Journal of Basic Engineering*, 575–587 (September 1960).

20. Koch, C.C. and L.H. Smith. "Loss Sources and Magnitudes in Axial-Flow Compressors," *ASME Journal of Engineering for Power*, 411–424 (July 1976).

21. Lieblein, Seymour. "Loss and Stall Analysis of Compressor Cascades," *ASME Journal of Basic Engineering*, 387–400 (September 1959).

22. Messenger, H.E. and E.E. Kennedy. *Two-Stage Fan, I. Aerodynamic and Mechanical Design*. NASA CR-120859 Report Contract NAS3-13494. Cleveland: NASA-Lewis Research Center, January 1972.

23. Creveling, H.F. and R.H. Carmody. *Axial Flow Compressor Computer Program for Calculating Off-Design Performance (Program IV)*. NASA CR-72427 Report. Contract NAS3-7277. Cleveland: NASA-Lewis Research Center, August 1968.

24. Bölcs, Albin. Professor, École Polytechnique Fédérale de Lausanne, Switzerland. Personal working session, Dayton OH, 10-21 July 2000.

25. Gustafson, B.A. "A Simple Method for Supersonic Compressor Cascading Performance Prediction." Chalmers Univ. of Techn., Dept. for Turbomachinery, 1975.

26. Dixon, Sydney L. *Fluid Mechanics, Thermodynamics of Turbomachinery*. Oxford: Pergamon Press, 3^{rd} Ed., 1978.

Vita

Captain Brian C. McDonald was born in the town of Concord, Massachusetts. He graduated from Concord-Carlisle Regional High School in May 1992. One month after receiving his high school diploma, he entered undergraduate studies at the United States Air Force Academy in Colorado Springs, Colorado. On 29 May 1996, he graduated with a Bachelor of Science Degree in Mechanical Engineering and was commissioned as an officer in the regular Air Force.

Second Lieutenant McDonald's first assignment was with the 418th Flight Test Squadron at Edwards Air Force Base (AFB), California. He served three years there as a C-17A Flight Dynamics Test Engineer. His primary responsibilities included the planning of, conducting of, and reporting on C-17A propulsion- and performance-related developmental test and evaluation projects. While stationed at Edwards AFB, he married his wife in June 1998. In 1999, First Lieutenant McDonald was selected to attend the Air Force Institute of Technology to earn a Master of Science Degree in Aeronautical Engineering. Upon graduation, Captain McDonald will work for the Air Vehicles Laboratory, Air Force Research Laboratory, Wright-Patterson AFB, Ohio.

REPORT DOCUMENTATION PAGE

Form Approved
OMB No. 0704-0188

1. REPORT DATE *(DD-MM-YYYY)*	2. REPORT TYPE	3. DATES COVERED *(From - To)*
20-03-2001	Thesis	Jan 2000 - Mar 2001

4. TITLE AND SUBTITLE
DESKTOP COMPUTER PROGRAMS FOR PRELIMINARY DESIGN OF TRANSONIC COMPRESSOR ROTORS

5a. CONTRACT NUMBER

5b. GRANT NUMBER

5c. PROGRAM ELEMENT NUMBER

6. AUTHOR(S)
Brian C. McDonald, Captain, USAF

5d. PROJECT NUMBER

5e. TASK NUMBER

5f. WORK UNIT NUMBER

7. PERFORMING ORGANIZATION NAME(S) AND ADDRESS(ES)
Air Force Institute of Technology
Graduate School of Engineering and Management (AFIT/EN)
2950 P. Street, Building 640
WPAFB OH 45433-7765

8. PERFORMING ORGANIZATION REPORT NUMBER
AFIT/GAE/ENY/01M-06

9. SPONSORING/MONITORING AGENCY NAME(S) AND ADDRESS(ES)
Air Force Research Laboratory
Compressor Aero Research Laboratory (AFRL/PRTF)
Attn: Dr. William W. Copenhaver
1950 Fifth Street, Building 18
WPAFB OH 45433-7251
(937) 255-7163

10. SPONSOR/MONITOR'S ACRONYM(S)

11. SPONSOR/MONITOR'S REPORT NUMBER(S)

12. DISTRIBUTION/AVAILABILITY STATEMENT
APPROVED FOR PUBLIC RELEASE; DISTRIBUTION UNLIMITED

13. SUPPLEMENTARY NOTES

14. ABSTRACT
A need exist for correlation-based desktop computer programs that predict the flow through transonic compressor rotors with nominal computational time and cost. Modified versions of two desktop computer programs, BOWSHOCK and TRANSROTOR, were used to perform a parametric study on a modern compressor rotor. BOWSHOCK calculates the exit flow properties of a supersonic streamtube through a user-defined compressor rotor. TRANSROTOR calculates flow properties at three stations in a user-defined compressor stage. Modifications to TRANSROTOR included the incorporation of a recently published rotor loss model. Baseline and modified TRANSROTOR versions were run with two modern transonic compressor blades. Results were compared with a Navier-Stokes-based computational fluid dynamics (CFD) code. A parametric study using BOWSHOCK examined the sensitivity of rotor performance to variations in six blade parameters. Both TRANSROTOR versions predicted rotor performance within ten-percent of the CFD results. Computational times were under six minutes.The results of the blade geometry parametric study showed that isentropic efficiency was most sensitive to stagger angle and least sensitive to blade spacing. Total pressure ratio was most sensitive to blade maximum thickness location and least sensitive to blade maximum thickness.

15. SUBJECT TERMS
axial flow compressor blades, compressor rotors, computer programs, correlation, parametric analysis, transonic flow

16. SECURITY CLASSIFICATION OF:			17. LIMITATION OF ABSTRACT	18. NUMBER OF PAGES	19a. NAME OF RESPONSIBLE PERSON
a. REPORT	b. ABSTRACT	c. THIS PAGE			Dr. Paul I. King, ENY E-mail: paul.king@afit.edu
U	U	U	UU	139	19b. TELEPHONE NUMBER *(Include area code)* (937)255-3636 ext. 4628